Flexible Arrival & Departure Runway Allocation

Using Mixed-Integer Linear Programming

A Schiphol Airport Case Study

J.G. Delsen

Delft University of Technology

TU Delft Delft University of Technology

Challenge the future

Flexible Arrival & Departure Runway Allocation

Using Mixed-Integer Linear Programming

A Schiphol Airport Case Study

by

J.G. Delsen

in partial fulfillment of the requirements for the degree of

Master of Science
in Aerospace Engineering

at Delft University of Technology,
to be defended publicly on Thursday April 21, 2016 at 10:00 AM.

Student number:	1369121	
Thesis committee:	Dr. ir. H. G. Visser,	TU Delft
	Ir. P. C. Roling,	TU Delft
	R. ten Hove,	Schiphol Group

TU Delft Delft University of Technology

Summary

This study focuses on research in flexible arrival and departure runway allocation. Currently, the runway usage at Amsterdam Airport Schiphol (AAS) is described by a preference list established by several stakeholders. It makes an important trade-off between minimizing noise exposure to the environment and maximizing capacity. The existing model does not take into account fuel burn and the ensued emissions for the current and future demand in flights. This study tries to address this issue. A model has been developed using Mixed-Integer Linear Programming (MILP) by which flights can be allocated to runways, while optimizing for fuel and noise. The research has the following research question:

Can fuel burn be significantly reduced for aircraft operating at Amsterdam Airport by utilizing a novel flexible arrival and departure runway allocation model, using a predefined set of variables and rules, accounting for noise annoyance, runway capacity and the current and future demand of flights?

In order to engage with this research question an initial look on operations and procedures is given. A basis of understanding of operations, with in specific AAS, is shown in which the complex runway layout is discussed. The currently applied Preference List shows how aircraft are allocated to a runway. Several departure procedures and routes are elaborated on. Each bearing their own characteristics in terms of noise exposure to the surroundings. ICAO-A, ICAO-B, NADP-1 and NADP-2 procedures are in place in AAS operations. An departing aircraft will fly according to these procedures as it continuous its route towards the exit of one of the designated sectors. It is indicated what the approach procedures are. Arriving aircraft will operate on an Initial Approach Fix (IAF), from which it will fly towards the location of the Final Approach Fix (FAF). From this point the aircraft will start its final descent, being a continuous or step-wise descent. These operations indicate the scope for which eventually the runway allocation model will simulate and optimize operations.

The various key drivers of runway capacity and runway usage are carefully evaluated as they are the main elements which shape the runway allocation tool. Different runway dependencies are shown for single- and multi-runway systems. Depending on the layout of the airport, various dependencies exist; converging and diverging runways, intersecting runways, runways in mixed mode operations, parallel runways and finally ground restrictions. Regulations are described in terms of separation regulations and noise- and emission regulations. Separation regulations imply a separation between consecutive aircraft and can be a combination of time- and distance-based separation. Aircraft type and fleet mix is important since different separation minima are applicable for specific combinations of aircraft with Maximum Take-Off Weight (MTOW) classes. Noise and emission regulations are shown to often be set-up locally, in dialogue with different stakeholders. Next to this, global and European policies are in place to reduce noise- and emissions. Furthermore, local conditions might severely restrict runway operations due to wind- or visibility conditions and will play a crucial role in runway allocation. Taxi- and apron capacity is analyzed. Under the assumption that taxi capacity exceeds runway capacity, these factors are not further researched in this study. Additionally, other factors have their impact on capacity, being human factors or the system's state. These fall outside the scope of this research.

In order to develop a runway allocation model which can analyze fuel, noise and emissions, several methodologies are explained. The computations for various runway dependencies are shown. Restrictions on single- or multi-system runways might occur due to runway occupation, jet blast, missed approaches

and other restricting factors when two or more aircraft operate on a runway system. It is shown that these dependencies can be collected in a binary dependency matrix, which works as input feed for the allocation model.

The specifics of Linear Programming are explained. The problem of optimizing fuel and noise has been translated to a Linear Programming problem. The model uses a binary application of MILP in order to optimize for fuel usage and noise exposure. The objective function tries to minimize both fuel and noise exposure to the environment. It takes into account the local surroundings and population density exposed to a certain L_{den} noise limit, as implied by local regulations. The objective function is subject to a variety of constraints. Here the runway dependency constraint incorporates the dependencies from the established dependency matrix. Another important constraint is the Noise Limit Switching constraint. Using this constraint it is possible for the model to make a trade-off for noise exposure to the population. In order to minimize for both fuel and noise, normalization is applied using Weighted Sum normalization. Evaluation can be done through Pareto optimization, which is tested by applying the runway allocation model to several case study scenarios.

The runway allocation model developed for this study is able to assign aircraft to runways based upon an optimization trade-off between fuel usage and noise exposure to the environment. In doing so, a multitude of scenarios may be simulated using the model. Different allocation schemes are tested and the possibilities of potential gains in fuel and noise reduction are researched. Emission outcomes, under the assumption of a linear relation with fuel, are equally researched. Other airports, a larger set of aircraft and aircraft types, different arrival and departure operations can all be added to the model due to the generic characteristics. This is favorable for future academic and industry research in ultimately finding an efficient optimized trade-off between fuel use and noise exposure and possible expansion towards other fields of study.

In order to test the model, a case study has been performed on Amsterdam Airport operations. The case study illustrates how the model works if applied to real airport operations. Actual flight data is used as input for the flight schedule. Fuel, noise and emission computations are applied to the AAS case. Several scenarios are tested and evaluated. These scenarios are based on data for two days. It is shown in which type of scenarios the flexible runway allocation model is most useful. The results are explained in the subsequent sections.

The main goal of this research is to research if fuel burn can significantly be reduced using flexible arrival and departure runway allocation. This is done by addressing a predefined set of variables and rules, accounting for noise annoyance, runway capacity and the current and future demand of flights. It can be concluded from this research that flexible allocation indeed can have significant beneficial impact on fuel usage. Optimization through flexible runway allocation is tested for the Amsterdam Airport Schiphol case study. Conclusions which result from this study are explained in more detail in this section.

The first main conclusion is that fuel usage can be significantly reduced by flexible runway allocation. Under the assumption of a linear relation between fuel usage and emissions, emissions can additionally be reduced. In order to test the potential fuel and emission savings of flexible runway allocation, an optimization tool has been developed. In order to make a comparison, both reference scenarios and optimized scenarios are evaluated. Two scenarios have been established; one scenario for low wind levels resulting in all runways available and one scenario in which operations are restricted by local conditions. For a full day simulation of a low wind scenario a potential fuel increase for multi-objective optimization corresponds to a saving of 157 ton kerosene (9.2%) in fuel consumption. It is shown that for a scenario in which local conditions have their effect on runway availability, savings are equally possible. Due to deteriorated weather conditions, flight operations are restricted to fewer runways. Still some increase in efficiency is observed for the selected multi-objective optimization. For the full day scenario with runway restrictions fuel savings are around 26 ton (1.74%). In both scenarios the noise exposure to the environment is within desirable noise regulation limits.

Secondly, it can be concluded that flexibility and accompanied savings in fuel, noise and emissions, are depended of the time of day and the accompanied peaks in runway demand. Several time of day segmented runs are researched to this end. These are split up in morning, afternoon and evening segments. For the scenario 1 case study with no runway restrictions potential fuel efficiency increase is found. The fuel savings for the morning run are 27 ton (5.19%), the afternoon run shows 58 ton (9.01%) fuel usage decrease and the evening run displays a 38 ton (4.44%) fuel reduction. Even for the scenario 2 case in which several runways are restricted, potential savings are found for the various time of day segments. Morning operations are relatively lower due to high runway demand; 3 ton (0.6%). Afternoon operations indicate 13 ton (1.95%) potential savings. Finally, evening operations show 5 ton (1.92%) in fuel savings. In comparison with Scenario 1 potential efficiency gains are lower due to reduced flexibility since fewer runways are available. The reason for the total fuel savings of cumulative time segments to be smaller then the total of the full day run, is due to increased flexibility of a full day's run. Since the model is able to optimize for a longer time span, more flexibility is obtainable. It is thereby possible to mitigate the noise penalty factors which are apparent in the evening run. By compensation, aircraft in that time segment can be assigned a more profitable runway when full day optimization is performed.

When comparing the different time segments for both scenarios, it is observed that the potential savings for both morning segments are lowest. It can be established that the morning peak has high runway demand. Due to this high demand, capacity is restrained and results in lower flexibility. The afternoon segment is for both scenarios the most profitable. This is due to a reduction in demand of runways, leading to increased flexibility. For the evening simulation it is found that due to a higher demand, flexibility is lower as holds for the morning simulations. Due to penalty factors a different assignment is found when comparing a full day scenario to the evening scenario.

Delaying of aircraft deliberately can have a positive effect on flexibility. Results show that optimization has influence on delay. For a fuel optimized case, often delay is reduced to a minimum in order to put aircraft on the ground as early as possible, hence reducing total fuel consumption. Nevertheless, in some cases it may be possible for the optimization to select a longer total delay duration. Reason behind this, is that an aircraft can hold for a beneficial runway to become available, hence reducing total flight/taxiing time. Runway flexibility is thereby increased.

It can be concluded that annual savings in terms of fuel and emission by flexible runway allocation have significant potential. By looking at potential annual gains, savings in fuel and emissions might be beneficial if the runway allocation model is utilized. Preferably more simulations with different settings have to be researched. The two discussed scenarios give an indication of the potential that flexible allocation might have. The annual efficiency increase in fuel and emission savings can be established to be approximately 4% - 6% or 15,000 - 30,000 tons kerosene under the given assumptions.

A range of optimal noise to fuel ratios exists for multi-objective optimization. From comparison of several scenarios it can be observed that certain optimization settings indicate an optimal noise to fuel ratio range. The established ratio is subject to discussion, but gives an interesting look on the potential savings in airport operations using allocation optimization. A range of optimal α-weights lies approximately between 0.07 and 0.09, which has improved fuel, noise and emission rates with respect to reference scenarios.

In conclusion, using the developed runway allocation tool to flexibly allocate arrival and departure runways can have significant impact on both fuel and emissions savings. Depending on the flexibility of available runways, mainly restricted by separation- and noise regulations, runway demand, local conditions and maintenance, savings are possible. For scenarios where there is plenty of room for flexibility, savings are evident. For restricted scenarios potential savings exist, although to a lesser extend. Due to the level of runway demand, afternoon operations have most flexibility and potential for savings. Annual savings can amount to significant fuel and emission reduction.

Acknowledgments

This report represent the graduate thesis study performed at the faculty of Aerospace Engineering of Delft University of Technology for the MSc track Control & Operations: Air Transport Operations. Hereby I would like to give my thanks to all the people without whom this report would not have been made possible.

First and foremost, I would like to give my thanks to my thesis supervisor, Paul Roling, for his guidance and support. I have always felt welcome to ask questions and I gratefully look back at all the fruitful discussions we had during the thesis project. In supervision, a student cannot ask for anything more, than a door that is always open. I would like to thank Dries Visser for his various input regarding computational and optimization techniques.

Furthermore, I would like to thank Rob ten Hove, Mark Brouwer and Tony Joustra of Schiphol Group for their time, help and feedback during different stages of the research. An extra dimension was given to the research by their industry expertise. I would like to thank Youri Hoppenbrouwers for sharing his experiences as a pilot which proved a valuable contribution.

I would like to thank my parents, for their unconditional support during my studies and for always standing behind the choices I have made. I want to thank my sister Lorraine for showing me how to be strong and never give up.

Last but not least I would like to give my thanks to my fellow students and friends, Bas Ceulemans, Thomas Slijpen, Wieger Vos and Michiel Wolff for their aid and their time to discuss various subjects regarding the thesis work.

Jochem Delsen

March 28, 2016
Amsterdam, The Netherlands

Contents

Summary iii

Acknowledgments vii

List of Figures xiii

List of Tables xvii

List of Abbreviations xix

List of Symbols xxi

1 Introduction 1
- 1.1 Research Question, Scope and Objective . . . 1
- 1.2 Methodology . . . 3
- 1.3 Experimental Set-up . . . 4
- 1.4 Report Structure . . . 4

2 Amsterdam Airport Schiphol 5
- 2.1 Growth Forecast . . . 5
- 2.2 Runway Operations . . . 6
  - 2.2.1 Runway Layout . . . 6
  - 2.2.2 Runway Preference . . . 6
- 2.3 Runway Procedures . . . 7
  - 2.3.1 Departure and Arrival Routes . . . 7
  - 2.3.2 Noise Regulations . . . 9
  - 2.3.3 Peak Handling . . . 10
  - 2.3.4 Runway Incursions . . . 11
- 2.4 Conclusion . . . 11

3 Runway Capacity 13
- 3.1 Definitions of Runway Capacity . . . 13
- 3.2 Capacity Envelopes . . . 14
- 3.3 Capacity Coverage Chart . . . 14
- 3.4 Key Drivers . . . 15
- 3.5 Runway Dependencies . . . 15
  - 3.5.1 Converging and Diverging Runways . . . 16
  - 3.5.2 Intersecting Runways . . . 16
  - 3.5.3 Parallel Runways . . . 16
  - 3.5.4 Mixed Mode . . . 17
  - 3.5.5 Ground Restrictions . . . 17
- 3.6 Regulations . . . 18
  - 3.6.1 Separation Regulations . . . 18
  - 3.6.2 Noise and Emissions Regulations . . . 19

3.7 Fleet Mix . . . 19
3.8 Local Conditions . . . 19
3.8.1 Visibility Conditions . . . 20
3.8.2 Wind Direction and Strength . . . 20
3.9 Taxi and Apron Capacity . . . 20
3.10 Other Factors . . . 21
3.11 Conclusion . . . 21

4 Methodologies **23**
4.1 Methodology Overview . . . 23
4.2 Runway Dependencies . . . 24
4.2.1 Single Runway System . . . 24
4.2.2 Multiple Runway System . . . 26
4.2.3 MTOW Classes . . . 28
4.2.4 Runway Dependency Matrix . . . 28
4.3 Fuel Computations . . . 29
4.3.1 Aircraft and Engine Selection . . . 29
4.3.2 Segment Computations . . . 30
4.3.3 Fuel Flow . . . 32
4.3.4 Fuel Usage . . . 32
4.4 Noise Computations . . . 33
4.4.1 Acoustic Energy Level . . . 33
4.4.2 Integrated Noise Model . . . 35
4.4.3 Noise Coordinate System . . . 35
4.4.4 Runways . . . 36
4.4.5 Flight Tracks . . . 36
4.4.6 Noise Grids . . . 37
4.5 Emission Computations . . . 37

5 Linear Programming **41**
5.1 Mixed-Integer Linear Programming (MILP) . . . 41
5.2 Sets and Indices . . . 42
5.3 Objective Function . . . 43
5.3.1 Decision Variables . . . 43
5.3.2 Fuel Cost Coefficients . . . 43
5.3.3 Population Cost Coefficients . . . 43
5.4 Constraints . . . 44
5.4.1 Equality Constraints . . . 44
5.4.2 Inequality Constraints . . . 44
5.4.3 Noise Limit Switching Constraint . . . 44
5.4.4 Big M Method . . . 45
5.5 Normalization . . . 45
5.5.1 Weighted Sum Method . . . 46
5.5.2 Pareto Optimality . . . 46
5.6 Optimization Algorithms . . . 47
5.6.1 Branch & Bound . . . 47
5.6.2 Dynamic Search . . . 47

6 Runway Allocation Model **49**
6.1 Concept Description . . . 49
6.1.1 Objective . . . 49
6.1.2 Assumptions and Limitations . . . 50
6.2 Model Structure . . . 50
6.2.1 Input . . . 50

6.2.2 Pre-processor . . . 53
6.2.3 Optimizer . . . 54
6.2.4 Post-processor . . . 54
6.3 Computational Performance . . . 56

7 Case Study: Schiphol Airport **57**
7.1 Description . . . 57
7.2 Model Input . . . 57
7.2.1 Assumptions . . . 57
7.2.2 Fuel . . . 58
7.2.3 Noise . . . 58
7.3 Scenarios . . . 59
7.3.1 Set-up . . . 59
7.3.2 Scenario 1 . . . 60
7.3.3 Scenario 2 . . . 66
7.3.4 Scenario 3: Annual operations . . . 72
7.3.5 Scenario Results . . . 73

8 Synthesis **75**
8.1 Verification . . . 75
8.2 Validation . . . 75
8.3 Results . . . 76
8.3.1 Runway Allocation . . . 76
8.3.2 Noise to Fuel Ratio . . . 78

9 Conclusions and Recommendations **81**
9.1 General Conclusion . . . 81
9.2 Limitations . . . 82
9.3 Recommendations . . . 83

Appendices **85**

Appendix A Procedures **85**

Appendix B Airports **89**

Appendix C Scheduling **91**

Appendix D Handhavingspunten **95**

Appendix E Fuel Flow **97**

Appendix F Runway Allocation **99**

Appendix G Noise Grids **105**

Appendix H Runway Dependency Matrices **109**

Bibliography **113**

List of Figures

1.1 Research Framework indicating different stages with their research questions (indicated by numbers) [5]. . . . 3

2.1 Passenger volume and growth at AAS in Millions [10]. . . . 5
2.2 Runway Layout of AAS [4]. . . . 6
2.3 Sectors of in- and outbound traffic at AAS [4]. . . . 8
2.4 Departure Procedure ICAO-A [16]. . . . 9
2.5 Example of Approach Procedure using ILS on AAS Runway 18R [14]. . . . 9
2.6 Average annual noise forecast 2014 [18]. . . . 10
2.7 Example of runway usage using the first runway preference for different peaks at AAS [4]. 11

3.1 Capacity Envelopes [27][32]. . . . 14
3.2 Capacity Coverage Chart for Boston/Logan Airport [27]. . . . 15
3.3 Runway Capacity Key Drivers . . . 15
3.4 Converging and diverging runways [9]. . . . 16
3.5 Intersecting runways [9]. . . . 16
3.6 Parallel operations [21]. . . . 17
3.7 Staggered parallel operations [21]. . . . 17
3.8 Typical classification of weather conditions for a US airport [27]. . . . 20
3.9 Compass rose for preferred runways at AAS [41]. . . . 21

4.1 Methodology components overview. . . . 23
4.2 Final approach for landing with time separation [8]. . . . 25
4.3 Artist impression of a Boeing 737-800 with KLM livery [43]. . . . 30
4.4 Artist impression of a Boeing 777-200ER with KLM livery [43]. . . . 30
4.5 Flight segments for arrivals (not on scale). . . . 31
4.6 Flight segments for departures (not on scale). . . . 31
4.7 Fuel flow Initial phase (1). . . . 32
4.8 Fuel flow Final phase (2). . . . 32
4.9 Fuel flow Take-Off (5). . . . 32
4.10 Fuel flow Climb-Out (6). . . . 32
4.11 Equal-loudness contours [46]. . . . 34
4.12 RIVM population data in INM where darker colors indicate increased population density. 35
4.13 Runway tracks in INM. . . . 36
4.14 Noise contours in INM. . . . 36
4.15 Departure: altitude vs distance. . . . 38
4.16 Approach: altitude vs distance. . . . 38
4.17 Departure: airspeed vs distance. . . . 38
4.18 Approach: airspeed vs distance. . . . 38
4.19 Departure: thrust vs distance. . . . 38
4.20 Approach: thrust vs distance. . . . 38

5.1 Linear Programming components overview. . . . 41

5.2 Pareto front with indication of the feasible region [56]. 46

6.1 Runway Allocation Model Architecture. 51
6.2 User input. 52
6.3 Runway Dependency input (AAS RWY06 example). 53
6.4 Runway Allocation Model output: Example noise grid distribution for a fuel optimized schedule. 55
6.5 Runway Allocation Model output: Example noise grid distribution for a noise optimized schedule. 55
6.6 Computation time performance for the multiple run procedure. 56

7.1 Noise grid with latitude and longitude coordinates: Blue dots indicate population points, green dots indicate the scope for which the runway allocation model calculates and optimizes noise. 59
7.2 Actual morning peak on June 18th 2013, in- and outbound flights have different color [57]. 61
7.3 Noise grid for fuel optimized simulation with exposed population density indicated by the marker size, 24223 houses exposed. 61
7.4 Noise grid for noise optimized simulation with exposed population density indicated by the marker size, 6076 houses exposed. 61
7.5 Runway distribution for a fuel optimized schedule. 62
7.6 Runway distribution for a noise optimized schedule. 62
7.7 Pareto front indicating a set of optimal solutions. The grey dotted line indicates fuel use for the actual reference scenario. 63
7.8 Pareto front zoomed-in, the red marker indicates the selected multi-objective solution. 63
7.9 Emissions for the different optimization settings. 63
7.10 Delay for the different optimization settings. 63
7.11 Runway distribution for a multi-objective optimization. 63
7.12 Actual full day runway allocation during June 18th 2013. 63
7.13 Fuel usage for Multi-objective optimization and Reference Scenario indicating a 9.2% increase in fuel efficiency. 63
7.14 Emissions for Multi-objective optimization and Reference Scenario. 63
7.15 Noise grid for reference simulation with exposed population density indicated by the marker size, 15,274 houses exposed. 64
7.16 Noise grid for multi-objective simulation with exposed population density indicated by the marker size, 9,348 houses exposed. 64
7.17 Pareto front for Scenario 1: Morning run. 64
7.18 Pareto front zoomed for Scenario 1: Morning run. 64
7.19 Fuel efficiency increase of 5.19% for the optimized scenario. 64
7.20 Emission savings for the optimized scenario. 64
7.21 Pareto front for Scenario 1: Afternoon run. 65
7.22 Pareto front zoomed for Scenario 1: Afternoon run. 65
7.23 Fuel efficiency increase of 9.01% for the optimized scenario. 65
7.24 Emission savings for the optimized scenario. 65
7.25 Pareto front for Scenario 1: Evening run. 66
7.26 Pareto front zoomed for Scenario 1: Evening run. 66
7.27 Fuel saving of 4.44% for the optimized scenario. 66
7.28 Emission savings for the optimized scenario. 66
7.29 Actual Morning Peak on June 21th 2013 [57]. 67
7.30 Noise grid for fuel optimized simulation with exposed population density indicated by the marker size, 28,822 houses exposed. 68
7.31 Noise grid for noise optimized simulation with exposed population density indicated by the marker size, 14,729 houses exposed. 68

7.32 Runway distribution for a fuel optimized schedule. . . . 68
7.33 Runway distribution for a noise optimized schedule. . . . 68
7.34 Pareto front. . . . 68
7.35 Pareto front zoomed. . . . 68
7.36 Emissions for fuel, noise and multi-objective optimized operations. . . . 68
7.37 Delay for fuel, noise and multi-objective optimization. . . . 68
7.38 Runway allocation for the multi-objective optimized scenario. . . . 69
7.39 Actual runway allocation during June 21th 2013. . . . 69
7.40 Fuel usage for Multi-objective optimization and Reference Scenario, indicating a fuel saving of 1.74%. . . . 69
7.41 Emissions for Multi-objective optimization and Reference Scenario. . . . 69
7.42 Noise grid for reference scenario with exposed population density indicated by the marker size, 18,839 houses exposed. . . . 69
7.43 Noise grid for multi-objective simulation with exposed population density indicated by the marker size, 20,345 houses exposed. . . . 69
7.44 Pareto front for Scenario 2: Morning run. . . . 70
7.45 Pareto front zoomed for Scenario 2: Morning run. . . . 70
7.46 Fuel usage for Multi-objective optimization and Reference Scenario indicating 0.6% savings in fuel. . . . 70
7.47 Emissions for Multi-objective optimization and Reference Scenario. . . . 70
7.48 Pareto front for Scenario 2: Afternoon run. . . . 71
7.49 Pareto front zoomed for Scenario 2: Afternoon run. . . . 71
7.50 Fuel usage for Multi-objective optimization and Reference Scenario indicating 1.95% savings in fuel. . . . 71
7.51 Emissions for Multi-objective optimization and Reference Scenario. . . . 71
7.52 Pareto front for Scenario 1: Evening run. . . . 71
7.53 Pareto front zoomed for Scenario 1: Evening run. . . . 71
7.54 Fuel usage for Multi-objective optimization and Reference Scenario, indicating fuel saving of 1.92%. . . . 72
7.55 Emissions for Multi-objective optimization and Reference Scenario. . . . 72
7.56 Annual average wind speeds and average maximum windspeeds at Schiphol in 2013 [59]. 73
7.57 Annual wind directions at Schiphol in 2013 [59]. . . . 73

8.1 Selected validation *Handhavings*- locations at AAS indicated by red markers [60]. . . . 76
8.2 Runway allocation schedule by Preference List for actual flights on June 21th 2013. MTOW class is identified by the indicator size. . . . 77
8.3 Runway allocation using the Runway Allocation mode. MTOW class is identified by the indicator size. . . . 77
8.4 Noise to Fuel Ratio; the selected square indicates the range of optimum settings. . . . 79

A.1 SID AAS [14]. . . . 86
A.2 STAR AAS [14]. . . . 87

B.1 Converging/diverging runways: Chicago O'Hare Airport (ORD) . . . 89
B.2 Converging and intersecting runways: Boston Logan Airport (BOS) . . . 89
B.3 Intersecting runways: San Franscico Airport (SFO) . . . 89

B.4 Operated as single runway:
London Gatwick Airport (LGW) 89

D.1 Handhavingspunten AAS [60]. 96

E.1 Fuel flow Boeing 777-200ER Initial phase (1). 97
E.2 Fuel flow 777-200ER Final phase (2). 97
E.3 Fuel flow 777-200ER Take-Off (5). 97
E.4 Fuel flow 777-200ER Climb-Out (6). 97

F.1 Runway allocation for a fuel optimized schedule. 99
F.2 Runway allocation for a noise optimized schedule. 99
F.3 Runway allocation for a multi-objective optimized schedule. 99
F.4 Runway allocation for the reference scenario. 99
F.5 Runway allocation for a fuel optimized schedule. 100
F.6 Runway allocation for a noise optimized schedule. 100
F.7 Runway allocation for a multi-objective optimized schedule. 100
F.8 Runway allocation for the reference scenario. 100
F.9 Runway allocation for a fuel optimized schedule. 100
F.10 Runway allocation for a noise optimized schedule. 100
F.11 Runway allocation for a multi-objective optimized schedule. 101
F.12 Runway allocation for the reference scenario. 101
F.13 Runway allocation for a fuel optimized schedule. 101
F.14 Runway allocation for a noise optimized schedule. 101
F.15 Runway allocation for a multi-objective optimized schedule. 101
F.16 Runway allocation for the reference scenario. 101
F.17 Runway allocation for a fuel optimized schedule. 102
F.18 Runway allocation for a noise optimized schedule. 102
F.19 Runway allocation for a multi-objective optimized schedule. 102
F.20 Runway allocation for the reference scenario. 102
F.21 Runway allocation for a fuel optimized schedule. 102
F.22 Runway allocation for a noise optimized schedule. 102
F.23 Runway allocation for a multi-objective optimized schedule. 103
F.24 Runway allocation for the reference scenario. 103

G.1 Noise Grid Scenario 1: Full Day, fuel optimized. 105
G.2 Noise Grid Scenario 1: Full Day, noise optimized. 105
G.3 Noise Grid Scenario 1: Full Day, multi-objective optimized. 105
G.4 Noise Grid Scenario 1: Full day, Reference Scenario. 105
G.5 Noise Grid Scenario 1: Morning, multi-objective optimized. 106
G.6 Noise Grid Scenario 1: Afternoon, multi-objective optimized. 106
G.7 Noise Grid Scenario 1: Evening, multi-objective optimized. 106
G.8 Noise Grid Scenario 2: Full Day, fuel optimized. 106
G.9 Noise Grid Scenario 2: Full Day, noise optimized. 106
G.10 Noise Grid Scenario 2: Full Day, multi-objective optimized. 107
G.11 Noise Grid Scenario 2: Full day, Reference scenario. 107
G.12 Noise Grid Scenario 2: Morning, multi-objective optimized. 107
G.13 Noise Grid Scenario 2: Afternoon, multi-objective optimized. 107
G.14 Noise Grid Scenario 2: Evening, multi-objective optimized. 107

List of Tables

2.1 Runway preference list at AAS during daytime (06:00 - 23.00) [11]. 7
2.2 Runway preference list at AAS during nighttime (23.00 - 06.00) [11]. 7
2.3 Noise Regulations at AAS [19]. 10

3.1 Wake Turbulence Categories [21]. 18
3.2 Time-based standard separation between consecutive aircraft in seconds [21]. 19
3.3 Distance-based standard radar and wake turbulence separation between consecutive aircraft in Nautical Miles [NM] [21]. 19

4.1 Single runway occupation at event time 80 [s]: a value of 1 indicates runway occupation. 26
4.2 Multiple runway dependency: jet blast starting at event time 80 [s]. 26
4.3 Multiple runway dependency: missed approach contingency starting at event time 80 [s]. Note that ROT is not included in this table. 27
4.4 Multiple runway dependency: intersecting aircraft at event time 80 [s]. 27
4.5 Multiple runway dependency: segregated parallel runways. 28
4.6 Single/multiple runway dependency: opposite direction. 28
4.7 Dependencies for a multi-runway system. 29
4.8 Aircraft & engine specifications for both Medium and Heavy MTOW classes. 29
4.9 Penalty factor for different times of day segments [47]. 34
4.10 Emission data per kilogram of fuel used [49]. 39

6.1 Graphical User Interface input options. 52

7.1 Peak Moments at Schiphol Airport. 58
7.2 Scenario time segments. 59
7.3 Scenario 1: Parameters 60
7.4 Scenario 2: Parameters 66

C.1 AAS Flight Schedule (arrivals excerpt). 92
C.2 Time to Runway overview. SECTOR indicates an outbound flight, hence the time represents the time to runway from the Actual In Block Time (AIBT). All values are expressed in seconds. 93
C.3 Time to taxi, empirically determined. All values are expressed in seconds. 93
C.4 Example of speed limits from AIP charts for AAS [14]. 93

D.1 Validation using *Handhavingspunten* [60]. 95

List of Abbreviations

AAS	Amsterdam Airport Schiphol
AEED	Aircraft Engine Emissions Databank
AEL	Acoustic Energy Level
AIBT	Actual In Block Time
ALDT	Actual Landing Time
ATC	Air Traffic Control
ATM	Air Traffic Management
ATOT	Actual Take-Off Time
BADA	Base of Aircraft Data
BAS	Bewoners Aanspreekpunt Schiphol
BB	Branch & Bound
BMILP	Binary Mixed-Integer Linear Programming
BOS	Boston Logan Airport
CBS	Statistics Netherlands
CCC	Capacity Coverage Chart
CO	Carbon Monoxide
DME	Distance Measurement Equipment
FAA	Federal Aviation Administration
FAF	Final Approach Fix
FCFS	First Come First Serve
GUI	Graphical User Interface
HC	Hydrocarbons
IAF	Initial Approach Fix
IAT	Inter-Arrival Time
ICAO	International Civil Aviation Organization
IDT	Inter-Departure Time
IFR	Instrument Flight Rules
ILP	Integer Linear Programming
ILS	Instrument Landing System
INM	Integrated Noise Model
LGW	London Gatwick Airport
LOS	Level of Service
LVP	Low Visibility Procedures

MAP	Missed Approach Point
MHG	Maximale Hoeveelheid Geluid
MILP	Mixed-Integer Linear Programming
MTC	Maximum Throughput Capacity
MTOW	Maximum Take-Off Weight
NADP	Noise Abatement Departure Procedure
NOx	Nitrogen Oxides
ORD	Chicago O'Hare Airport
PHCAP	Practical Hourly Capacity
PM10	Particulate Matter
RIASS	Runway Incursion Alerting System Schiphol
RIVM	The Netherlands National Institute for Public Health and the Environment
RNAV	Area Navigation
ROT	Runway Occupancy time
SEL	Sound Exposure Level
SFO	San Francisco International Airport
SID	Standard Instrument Departure
SN	Smoke Number
SO	Sulphur Oxide
SPL	Sound Pressure Level
STAR	Standard Terminal Arrival Route
SVFR	Special Visual Flight Rules
UDP	Uniform Daylight Period
VFR	Visual Flight Rules
VOR	VHF Omnidirectional Range
VOS	Volatile Organic Compounds
WTC	Wake Turbulence Category

List of Symbols

Symbol	Description	Dimension
AEL	Acoustic Energy Level	[db(A)]
AEL_{xy}	Acoustic Energy Level for gridpoint xy	[dB(A)]
α	Fuel weights	[-]
β	Noise weights	[-]
$\bar{c}$	Communication buffer	[s]
C	Cost function	[-]
C^F	Fuel cost coefficients	[-]
C^N	Noise cost coefficients	[-]
C^P_{xy}	Population cost coefficients per xy coordinate	[-]
CO	Carbon Monoxide	[g/kg]
D	Distance	[m]
d	Delay step	[-]
D_d	Set of delay steps	[-]
D_{min}	Minimum common approach path distance	[m]
ΔL_A	Corrected frequency band level	[dB(A)]
dt	Time step	[s]
E	Expected average service time	[s]
E_n	Sound exposure	[dB(A)]
E_o	Reference sound exposure	[dB(A)]
F	Following Aircraft	[-]
f	Flights	[-]
F_{dep}	Set of dependent flights	[-]
F_f	Set of flights	[-]
f^{norm}_{fue}	Fuel solution using normalization	[kg]
f^{norm}_{houses}	Houses exposed solution using normalization	[houses]
G_{xy}	Set of grid coordinates	[-]
HC	Hydrocarbons	[g/kg]
IAT	Inter-Arrival Time	[s]
IDT	Inter-Departure Time	[s]
L	Leading Aircraft	[-]
$Lim_{L_{den}}$	Limit L_{den}	[dB(A)]

L_{limit}	Noise limit for considered time period	[dB(A)]
L_A	A-weighted sound level	[dB(A)]
L_{den}	Level day-evening-night	[dB(A)]
L_{night}	Level night	[dB(A)]
m	MTOW class	[-]
M	Big M value	[-]
$\dot{m}_f$	Fuel Mass Flow Rate	[kg/s]
M_m	Set of MTOW classes	[-]
μ	Minimum time separation	[s]
μ_{arr}	Time separation for arrival	[s]
μ_{dep}	Time separation for departure	[s]
μ_{jb}	Time separation due to Jet Blast	[s]
μ_{ma}	Time separation due to Missed Approach	[s]
μ_{mm}	Time separation for mixed mode	[s]
μ_r	Maximum throughput Rate	[aircraft/h]
μ_s	Time safety buffer for mixed mode	[s]
$n^{DM}_{f,m,p,r}$	Binary constant for runway dependencies	[-]
$n_{flights}$	Number of flight movements	[-]
N_{fuel}	Total fuel usage	[kg]
N_{houses}	Houses exposed to noise limit	[houses]
n_f	Normalization factor fuel	[-]
n_n	Normalization factor noise	[-]
NOx	Nitrogen Oxides	[g/kg]
p	Procedure	[-]
p_0	Reference pressure	[Pa]
p_e	Effective free field sound pressure	[Pa]
P_p	Set of procedures	[-]
r	Runway	[-]
R_{dep}	Set of dependent runways	[-]
R_{res}	Set of restricted runways	[-]
R_r	Set of runways	[-]
ROT	Runway Occupancy Time	[s]
s	Parallel runway spacing	[m]
S_{LF}	Minimum separation distance	[m]
SEL	Sound Exposure Level	[dB(A)]
SEP	Regulatory time separation minimum	[s]
SN	Smoke Number	[-]
SPL	Sound Pressure Level	[dB(A)]
t	Time	[s]
T	Time	[s]
T_{den}	Considered time period	[s]

t_{lineup}	Time to line-up aircraft	[s]
τ	Reference time of one second	[s]
TFU	Total Fuel Used	[kg]
V_{TAS}	True Airspeed	[m/s]
V_A	Airspeed approaching aircraft	[m/s]
V_F	Airspeed following aircraft	[m/s]
V_L	Airspeed leading aircraft	[m/s]
w_n	Time of day penalty factor	[-]
x	Decision variable	[-]
xy	Coordinates	[-]
$\mathbb{Z}$	Integers	[-]

Chapter 1

Introduction

The aviation industry is continually growing with a rapid pace, nevertheless consistent profitability is an elusive matter. Constant changes in aircraft movement, mix of aircraft fleet, routes and procedures are in play to address the growing demand of air transportation. Runway capacity at airports and especially at hubs, plays a vital role in this ever changing environment.

In 1973 the Federal Aviation Administration (FAA) established the following definition on runway capacity, being "the maximum number of aircraft operations that an airfield can accommodate during an hour when there is a continuous demand for service" [1]. This runway capacity is dependent on several factors. Runway system layout, demand characteristics, operational constraints and local conditions all have their effect on the total performance of an airport's capacity [2]. More efficient utilization of available infrastructure at airports could address the growing demand for capacity [3]. Amsterdam Airport Schiphol (AAS), being a complex airport, may benefit from optimizing their runway performance. Currently, the runway usage is described by a preference list established by several stakeholders. It makes an important trade-off between minimizing noise exposure to the environment and maximizing capacity [4]. The existing model does not take into account fuel burn and the ensued emissions for the current and future demand in flights. The research focuses on the development of an optimization model to include these factors with respect to runway allocation. This research, which is performed as a MSc thesis, has the following research question:

> *Can fuel burn be significantly reduced for aircraft operating at Amsterdam Airport by utilizing a novel flexible arrival and departure runway allocation model, using a predefined set of variables and rules, accounting for noise annoyance, runway capacity and the current and future demand of flights?*

This study focuses on research in flexible arrival and departure allocation. A model has been developed by which flights can be allocated to runways, while optimizing for fuel and noise. The report will explain fundamental knowledge on these subjects and the allocation model itself will be discussed. In the subsequent sections of this chapter, the research questions will be further discussed. Methodologies are briefly discussed, which prove to be a ground basis of the developed runway allocation model. The case-study used in this research will be briefly discussed in the section on experimental set-up. Finally, this chapter will conclude with an overview of the report structure.

1.1 Research Question, Scope and Objective

This section identifies the research questions and sub-questions. It is build up in such a way, that when each sub-questions is answered, inherently the main research questions can be answered. The main research topic is split up into several questions. Each question has its sub-questions as is indicated below. The research questions is developed using the SMART (Specific, Measureable, Attainable, Relevant, Time-bound) principle. It is indicated that not every sub-question is established using the SMART principle, but in total the mutually exclusive and collectively exhaustive list of sub-questions adds up to a SMART defined research question. The main research questions has been introduced. It is split up in

several additional questions from which the sub-questions follow as indicated below:

1. What is the current situation at Schiphol Airport?
   (a) How is the AAS build up in terms of runway layout and configuration?
   (b) What are the current arrival and departure procedures at AAS?
   (c) What airside capacity systems are currently available?
   (d) What is the current demand of flights?
   (e) What data is available from AAS?
2. What are AAS' objectives for handling demand and emissions?
   (a) Which factors are important and how are they prioritized?
   (b) What are the prospects for future demand and future emission regulations?
3. What are influencing factors of Runway Capacity?
   (a) What are the current (separation) regulations?
   (b) How are runway dependencies correlated?
   (c) How does the fleet mix have influence on runway capacity?
   (d) Which local conditions are important for runway capacity?
   (e) How do taxi and apron capabilities influence runway capacity?
   (f) What are other influencing factors on runway capacity?
4. Which methods are most suitable to solve the runway allocation problem?
   (a) Which methods are currently available and which ones are primarily used?
   (b) What are the shortcomings of existing capacity methods?
   (c) Which methods or combinations of methods are most suitable for the AAS runway allocation case?
5. What are the variables and drivers of the model?
   (a) What is the scope of the runway allocation model?
   (b) What input variables are needed for the model?
   (c) What data is needed regarding AAS?
   (d) What is the preferred output method?
6. What will be the results of the model?
   (a) How does the model perform in terms of computation time, feasible results?
   (b) How can the model be verificated?
   (c) What is the model's validity and what data is needed?
   (d) What is the development time of the model?
7. How can the model be implemented/compared in existing models/systems?
   (a) How can the model and its results be implemented?
   (b) How can the model be utilized with respect to further research?
   (c) What are other utilizations or implementations options for the model?

The research questions are important as they together address the research objective. The questions are answered in different stages of the research progress. This is indicated in Figure 1.1, in which the research framework is displayed. The framework indicates at which stage answers are researched. The research framework and research questions together give the structure on the study on runway allocation.

The scope of the research has been defined in a literature study [6] prior to this thesis research. Important in this scope are two factors being the current body of knowledge on the subject and the current industry standards in runway allocation. It has been assessed that current capacity models exist, with a wide variety of optimization methods in order to optimize operations. The specific combination of constraints, while optimizing for fuel burn and noise exposure is a novel approach. Using linear programming the optimization model tries to find an optimum trade-off between fuel and noise while adhering to unique runway dependency constraints. In the literature study the current body of knowledge on these subjects has been researched. In the review of this previous research, a combination was made between several types of algorithm in order to compute and optimize the result for specific scenarios. An uniform model is not yet available, since airports are often restricted by local constraints. Solutions have to be tailored to these constraints. This is where a gap in current knowledge exists and where this

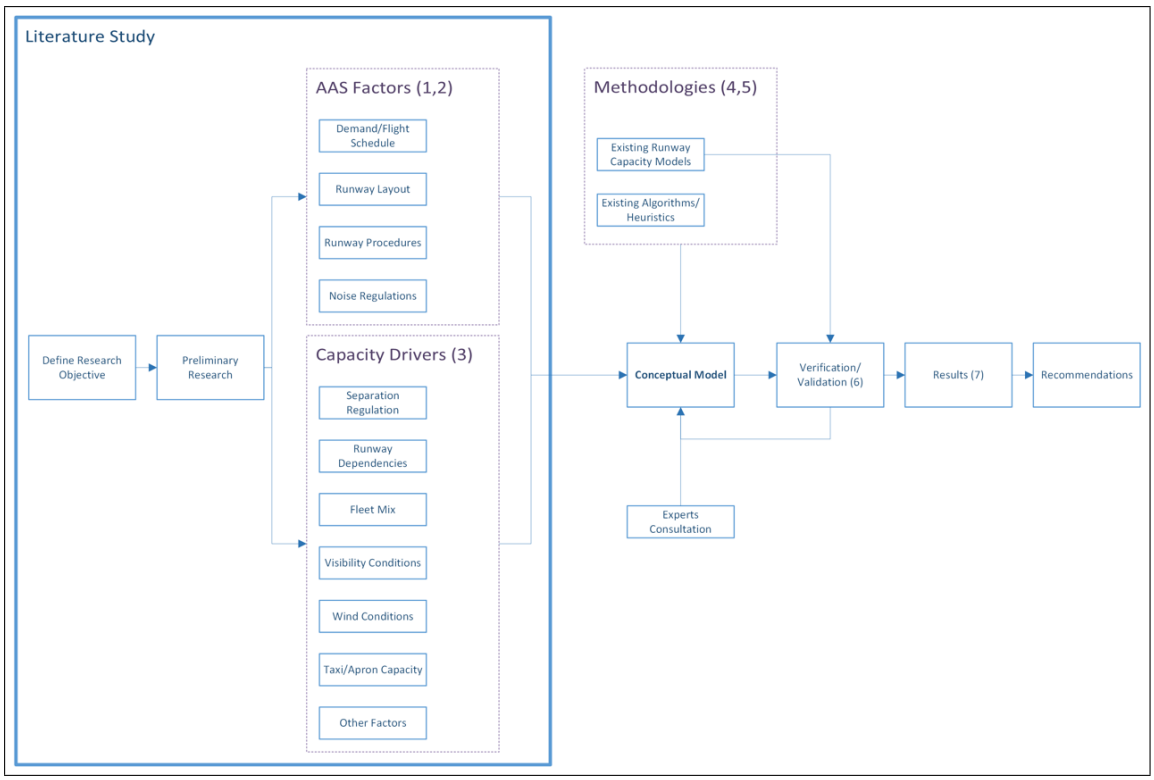

Figure 1.1: Research Framework indicating different stages with their research questions (indicated by numbers) [5].

research tries to add. By researching possibilities of methods of flexible runway allocation, it is possible to combine previous research in a new model and find possibilities of reducing fuel burn at airports which are currently constraint by runway preference lists and other local conditions. This research will focus on implementing the possibility of including fuel burn optimization, while addressing external effects of noise exposure and emissions.

1.2 Methodology

In order to optimize runway capacity while addressing an optimal trade-off between fuel burn and noise exposure, a runway capacity model is developed during this research. Several methodologies are in place, which eventually are brought together in the development of the model. Fuel computations are shown, where aircraft characteristics, flight segments and fuel flow prove important. Noise computations, which are partially computed using the Integrated Noise Model (INM), are elaborated on. Emission computations are discussed to identify emissions. It is assumed that there is a linear connection between fuel usage and emissions. Runway dependencies are proved to be of crucial importance in airport operations. The methodologies in order to identify these dependencies are discussed.

Several methods applicable to the runway allocation problem are identified from the literature study. Initially, Blumstein [7] started with an analytical allocation model, which provided a sound basis for additional research. MACAD as established by Stamatopoulos [8] was further used in a Schiphol Airport Case Study by Klugt [9]. Based upon this research, further analysis is done in defining capacity at AAS. This is combined with research in other fields in which various other allocation methods are applied.

Current research is based on an optimization problem type, in which an objective function is subject to several constraints. A frequent used procedure for optimization problems is Mixed-Integer Linear Programming (MILP), using binary states of matrices to identify allocation possibilities. It has to be noted that different other methods are available. A next step is to find the optimal solution. Here

several methods are possible. First Come First Serve (FCFS) in combination with a local Branch & Bound (BB) algorithm are proven methods to identify the optimal solution of optimization problems.

The developed runway allocation model uses several methodologies necessary to establish the optimization problem. Fuel, noise and emissions have their separate computation method. Additionally, the linear programming model will be discussed. This study applies the methodologies and resulting optimization model to the Amsterdam Airport Schiphol case study. The workings of experimental conceptual model are explained in the next section.

1.3 Experimental Set-up

In order to develop and test if fuel burn can be minimized using a novel allocation method, an experimental model has been developed. This model will test for the AAS system specific scenarios of runway allocation in order to try to find optimal fuel burn runway allocation settings. The model enables the identification of several questions and sub-questions as indicted in Figure 1.1.

The simulation model is build up from combining several separate blocks. This improves the generic ability, by which it will be possible to use the model in different airport scenarios. It has been identified that runway allocation and capacity depend on several influencing factors, as seen in Section 1.2.

The developed runway allocation model takes into account the key drivers of runway capacity; runway dependencies, regulations, fleet mix, wind- and visibility conditions and other factors. The model tries to address these factors. The optimization is performed by converting the problem into a Linear Programming problem. Thereby making it possible to optimize for fuel usage and noise exposure. The model then is tested on several scenarios. It is explained how the model works in detail. Next to this, potential gains in fuel efficiency and noise reduction will be displayed by applying the runway allocation tool to scenarios and comparing them to reference scenarios.

The model is verificated by checking every code block separately and by tested if the output of the single blocks contains errors. Validation is done using existing Schiphol Airport data from 2013 and so-called *Handhavingspunten*. This is done so the output data of the simulation model can be compared to real data, to give an idea of the feasibility of the results with respect to the main research question.

1.4 Report Structure

This study focuses on research in flexible arrival and departure allocation. A model has been developed by which flights can be allocated to runways. The allocation is done by optimizing for fuel and the external factor of noise. The report will explain fundamental knowledge on these subjects and the allocation model itself will be discussed. The research questions, scope and objectives are discussed in Chapter 1. Here a brief overview of the methodologies, experimental set-up and report structure is given. In Chapter 2 operations and procedures at Schiphol Airport are discussed. The topic of runway capacity is elaborated on in Chapter 3. Key drivers behind capacity are explained, as they will prove to be of importance for the runway capacity model. The used methodologies for fuel, noise, emissions and runway dependencies will be discussed in Chapter 4. The methodology for linear programming approach is demonstrated in Chapter 5. The workings of the runway allocation model are explained in Chapter 6. A case study in which the allocation model applied is treated in Chapter 7. Here several scenarios are set up in order to test the model. Results are discussed in Chapter 8. Here verification, validation and sensitivity analyses is performed. The report will conclude with Chapter 9 on conclusions, recommendations and future research proposals.

Chapter 2

Amsterdam Airport Schiphol

The topic of this research regards runway capacity as it occurs at Amsterdam Airport Schiphol. Before any further analysis of the research on runway capacity is done, it is important to provide a basis of understanding of Schiphol Airport. As it will become clear in subsequent chapters, capacity is determined by several airport specific factors. Therefore, an initial look on the operations at AAS is given in this section.

2.1 Growth Forecast

Within a growing aviation industry, Schiphol Airport managed to grow its number of passengers transported and the amount of cargo handled in 2014. Schiphol transported 55 million passengers, an increase of 4.6% versus 2010, mainly caused by strong growth from the Middle-East (+13.7%) and from Europe (+6.3%), visualized in Figure 2.1 [10]. The volume of cargo handled in amounted to 1.6 million tonnes, which is an increase of 6.7% compared to 2013. The increase in average flight movements in the period 2016-2018 is forecasted to be 1.5-2% [4]. In order to accommodate this growth, Schiphol is continuously investing in optimizing operating capacity to be able to accommodate the forecasted growth in passengers and cargo numbers.

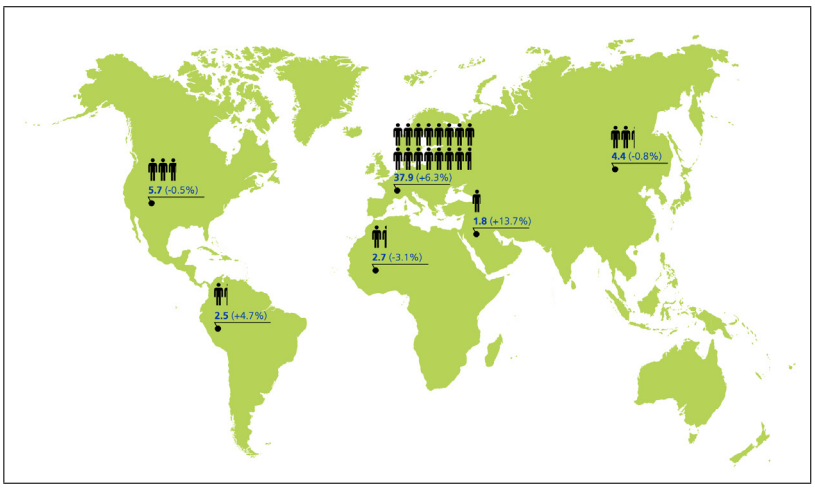

Figure 2.1: Passenger volume and growth at AAS in Millions [10].

2.2 Runway Operations

In this section the runway operations at AAS are discussed. In order to provide the scope for this research, key elements of airport- and runway operations are highlighted in this section. In terms of runway capacity, Schiphol Airport is restricted to use its six runways. The runway layout, runway preference list and the different departure and arrival procedures and routes are elaborated on.

2.2.1 Runway Layout

Runway layout is of key importance in understanding runway capacity. AAS has a complex runway system with a total of six runways. The layout is depicted in Figure 2.2 [4]. As indicated by the red marks, the Polderbaan and the Aalsmeerbaan are only used in one direction. The Oostbaan is primarily used for small general aviation. The preference of the runway allocation is explained in the following section.

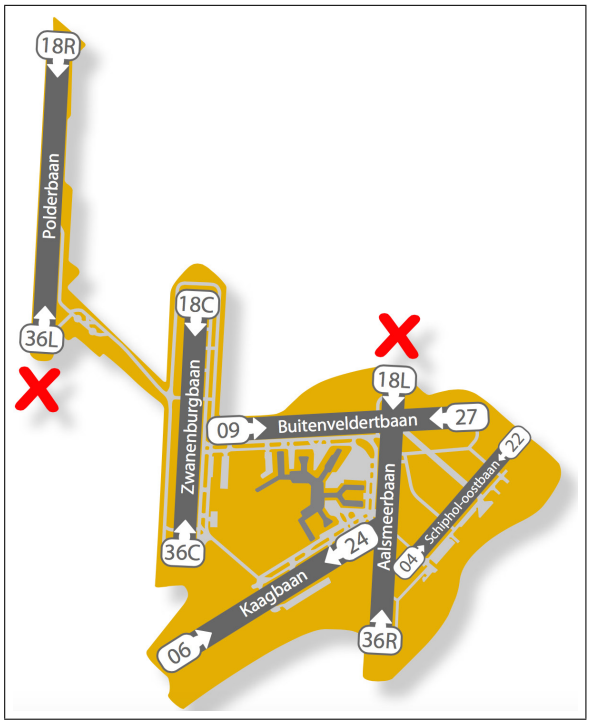

Figure 2.2: Runway Layout of AAS [4].

2.2.2 Runway Preference

Currently, runway assignment is done via a runway preference list as seen in Table 2.1 and Table 2.2 [11], for day and night operations, respectively. L stands for Landing, whereas S stands for Starting. Runway preference has been established by stakeholders, identified by the *Alderstafel*[1], in order to reduce the environmental impact, such as noise exposure and emissions. The preference list is primarily dependend on several external factors, which are: visibility, wind conditions, cloud base, precipitation, Uniform Daylight Period (UDP), peak periods, runway availability and anticipation of peak periods, while maintaining safety and efficient handling of the aircraft flow [13].

[1]The Alderstafel consists of the involved management, aviation sector, local residents and the government [12]

Table 2.1: Runway preference list at AAS during daytime (06:00 - 23.00) [11].

Visibility	**Preference**	**L1**	**L2**	**S1**	**S2**
Good	1	06	(36R)	36L	(36C)
Visibility $>$ 5,000 m	2	18R	(18C)	24	(18L)
Cloud base $>$ 1,000 ft	3	06	(36R)	09	(36L)
Within UDP	4	27	(18R)	24	(18L)
Good or marginal	5a	36R	(36C)	36L	(36C)
Visibility $>$ 1,500 m	5b	18R	(18C)	18L	(18C)
Cloud base $>$ 300 ft	6a	36R	(36C)	36L	(09)
	6b	18R	(18C)	18L	(24)

Table 2.2: Runway preference list at AAS during nighttime (23.00 - 06.00) [11].

Preference	**Landing**	**Take-off**
1	06	36L
2	18R	24
3	36C	36L
4	18R	18C

2.3 Runway Procedures

Next to the aforementioned preference list regulations, Schiphol has several procedures in place in order to regulate air traffic for arrivals and departures. In this section these procedures are described and explained. Important noise regulations applicable to Schiphol Airport are given. Subsequently, peak handling and runway incursion procedures are introduced. More general procedures regarding separation regulations and their specifics are discussed in Chapter 3.4.

2.3.1 Departure and Arrival Routes

Departure and Arrival operations are of major impact with respect to fuel and noise. Different operations can potentially lead to savings in fuel usage and noise exposure. The conventional routes are discussed in this section. Flights departing from and approaching AAS are assigned to a sector depending on their direction of destination or origin, respectively. In Figure 2.3 the different sectors for departing (blue) and approaching aircraft (yellow) are visualized. The outbound flights can be allocated one of five sectors using a Standard Instrument Departure (SID) route, whereas inbound flights are allocated to three sectors using Initial Approach Fix (IAF) indications. Both departure and approach operations may use Area Navigation (RNAV) which is a method of Instrument Flight Rules (IFR) navigation. It allows an aircraft to navigate using a predefined set of routes.

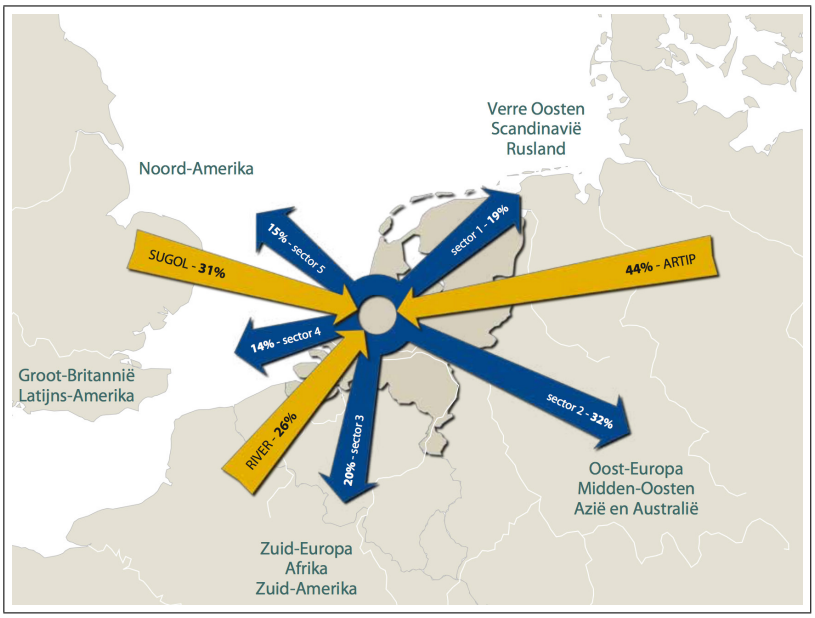

Figure 2.3: Sectors of in- and outbound traffic at AAS [4].

2.3.1.1 Departure Routes

SIDs indicate waypoints for outbound flights, as indicated in the Standard Departure Chart [14] in Appendix A.1. For every runway these waypoints provide means for navigation. These SIDs lead to one of the five outbound sectors from Figure 2.3. Two other sectors as seen in the Appendix are for military use. Another sector indicates the AAS airspace. The SID which is appropriate for a given flight is chosen on basis of the runway configuration in use, hence the preference list. As capacity may exceed single SID capacity, two SIDs are in place per runway-sector combination. Occasionally, it is allowed to use the military sectors, in order to reduce flight time [15].

Several types of departure exist as established by International Civil Aviation Organization (ICAO). Commonly, ICAO-A, ICAO-B, NADP-1 and NADP-2 procedures are used. An example of ICAO-A departure operation can be observed in Figure 2.4. The ICAO procedures are found in DOC 8168 [16]. In the work of Kim et al. [17] explanation is given on the differences between both NADP-1 and NADP-2 procedures. A difference exists between ICAO-A and NADP-1 being both close-in noise abatement procedures, versus ICAO-B and NADP-2, which are distant noise abatement procedures. The difference lies in the fact that the latter type of procedures reduces noise impact to the surroundings further away from the airport.

2.3.1.2 Arrival Routes

Inbound air traffic is allocated to three sectors, indicated by IAF identifiers. For Schiphol Airport these are entitled as SUGOL, ARTIP and RIVER. The predefined routes are indicated by a Standard Terminal Arrival Route (STAR) of which a chart of Amsterdam Airport's STARs is added to Appendix A.2. From this chart the three IAFs are clearly distinguished. The procedure is to fly from the IAF location to the Final Approach Fix (FAF). The final phase is the descent, in which the glide path is followed towards the runway. An example of an approach phase starting at the FAF is indicated in Figure 2.5. At the Missed Approach Point (MAP), the missed approach procedure may be enacted when the landing cannot be proceeded [9]. Several technologies which enable navigation guidance at AAS are Instrument Landing System (ILS), VHF Omnidirectional Range (VOR) and Distance Measurement Equipment (DME). Throughout this process Air Traffic Control (ATC) is continually ensuring that separation regulations are obeyed.

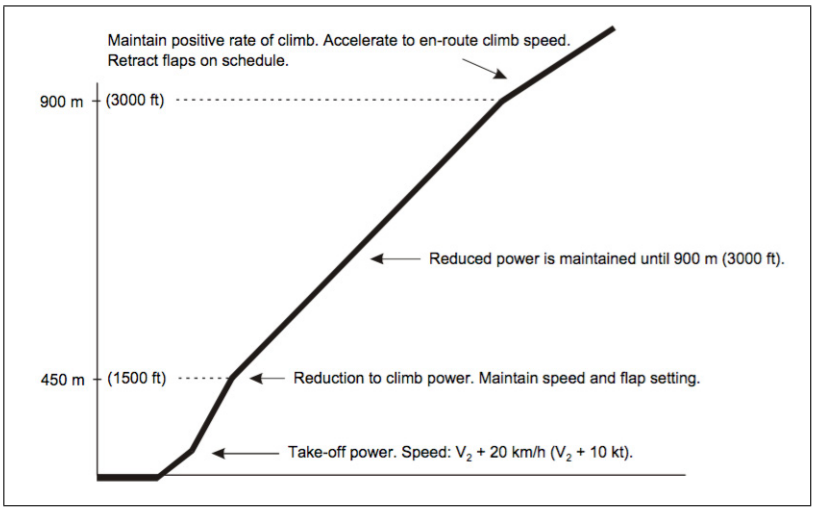

Figure 2.4: Departure Procedure ICAO-A [16].

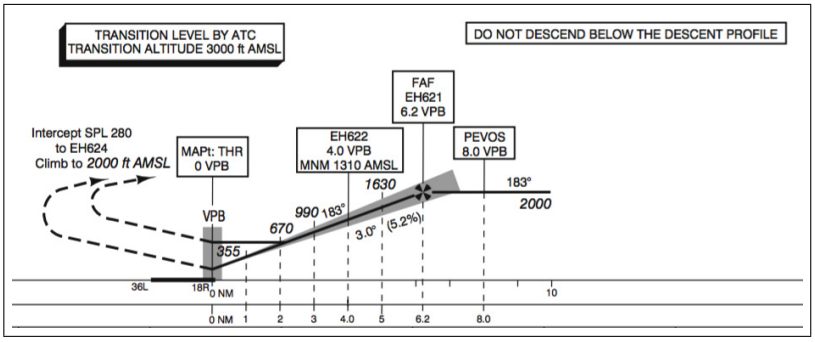

Figure 2.5: Example of Approach Procedure using ILS on AAS Runway 18R [14].

2.3.2 Noise Regulations

For air traffic at Schiphol Airport strict regulations are in place. The discussed preference list from Table 2.1 and 2.2 has been established with taking into account minimizing environmental impact. Noise plays a key factor. In Table 2.3 the regulations for noise hindrance are observed [4]. The criteria focus on the amount of aircraft movements as well as the noise hindrance to the environment. The average noise load during a 24 hour period from 00.00h to 24.00h is described by L_{den}. The average noise load during a night period from 23.00h to 07.00h is described by L_{night}. Both parameters are used to indicate the noise hindrance measured from an observer's location during a one year period. For calculations of L_{den} the movements are multiplied by a given penalty value. By taking the summation of the noise load of individual observer points, with corresponding aircraft movements, results in the average noise load. In Figure 2.6a the annual noise forecast per day is seen, in Figure 2.6b this is observed for night time.

An important novel element of noise restrictions on AAS is the Maximale Hoeveelheid Geluid (MHG). The MHG for 2016 is calculated to be 60.45 dB(A) as annual average for full day operations. It is a maximum allowable cumulative measure for noise produced within the boundaries of equivalence criteria. Together with the equivalence criteria and the preference list for runway allocation, the total noise hindrance on the environment is regulated.

(a) L_{den} (b) L_{night}

Figure 2.6: Average annual noise forecast 2014 [18].

Table 2.3: Noise Regulations at AAS [19].

Aspect	**Agreement**
Air traffic movements criteria	Until 2020 max. 510,000 aircraft movements annually, of which max 32,000 between 23.00h and 07.00h
Equivalence criteria[2]	The use of AAS needs to meet criteria for equal protection of the environment: - max. 12,800 houses with noise hindrance of 58 dB(A) L_{den} or more - max. 180,000 severe noise hindrance of 48 dB(A) L_{den} or more - max. 11,100 houses with noise hindrance of 48 dB(A) L_{night} or more - max 49,500 severe sleep disturbances with noise hindrance of 40 dB(A) L_{night} or more

2.3.3 Peak Handling

Schiphol airport is subject to inbound and outbound peak hours of which there are approximately six every day [9]. If these peaks follow each other in a short time span, there is possible overlap on runway assignment (due to congestion). In order to handle the traffic in such occasions, two arrival- and departure runways are used simultaneously. This is depicted in Figure 2.7 [4]. Adhering to the first preference, the Aalsmeerbaan (landing 36R) and Zwanenburgbaan (start 36C), are respectively used as first- and second take-off runway. If the total traffic volume and its distribution over a day period is at a low level, it may suffice to use only one departure and one arrival runway. For the first preference, the Kaagbaan (L06) and Polderbaan (S36L) are then in use. The procedures for runway track preference and assignment on the occasion if one or more of the six runways is inoperable is readily available and for brevity is not discussed in this report. This material on runway procedures can be found via Bewoners Aanspreekpunt Schiphol (BAS) [20].

[2]Based on variations in weather a factor called *Meteotoeslag* is applied in determining equivalence criteria [19].

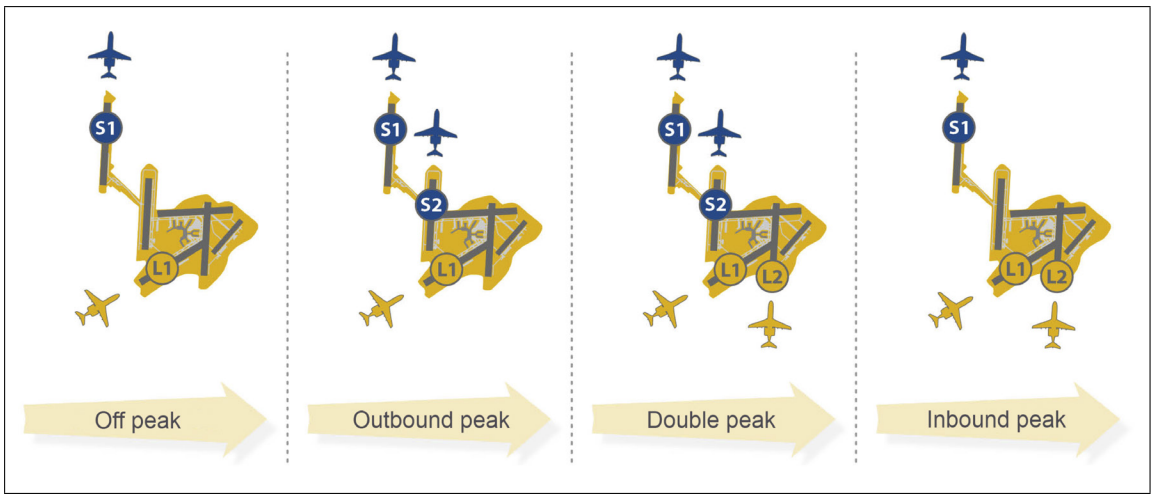

Figure 2.7: Example of runway usage using the first runway preference for different peaks at AAS [4].

2.3.4 Runway Incursions

Worldwide runway incursions are noted as one of the main topics in aviation safety. The definition of runway incursion as given by ICAO is the following: "Any occurrence at an aerodrome involving the incorrect presence of an aircraft, vehicle or person on the protected area of a surface designated for the landing and take-off of aircraft" [21]. ATC has several technical procedural possibilities which can warn if an incursion is imminent. At Schiphol Airport the Runway Incursion Alerting System Schiphol (RIASS) [22] is active. The complex infrastructure of the runway systems is one of the main causes of incursions [22]. Resultantly, it is an important aspect in research on runway allocation.

2.4 Conclusion

In conclusion, a basis of understanding of operations and procedures at AAS has been provided. It was seen that Schiphol is partaking in a growing aviation market, in which capacity plays a major role in order to be competitive. The layout of the airport has been explained, which indicated the complexity of multiple runways. The currently used Preference List has been explained by which aircraft are assigned to a runway. Furthermore, the departure and arrival procedures and routes have been discussed. Commonly, different operations for aircraft taking-off at AAS are ICAO-A, ICAO-B, NADP-1 and NADP-2, which have their own characteristics in terms of noise exposure to the environment. It was shown that the arrival phase is split up in a section from an Initial Approach Fix towards a Final Approach fix, from which the final descent starts. Additionally, the current noise regulations have been highlighted which will play a major role in the subsequent chapters. The next chapter will further explain the details of runway capacity and its key drivers.

Chapter 3

Runway Capacity

Runway capacity is a complex matter as it consist of numerous influencing factors. Together these factors determine the total capacity of a system. In order to further engage with this subject, an introduction of the basic principles will be established. Next to this, the influencing factors are elaborated on in this chapter. By treating all the aspects, the subject of runway capacity becomes clear and more comprehensible, aiding the development of a runway allocation tool.

3.1 Definitions of Runway Capacity

This section will describe several definitions of runway capacity as used in the aviation industry. Capacity provides an estimate on the number of aircraft arrival and departures per time unit which can be achieved on a particular set of runways. Typically, this is done in operations per hour [23]. Idris et al. [24][25] indicated in their work that the runway is the main flow constraint in a runway system. Depending on dominant factors influencing capacity, different concepts of capacity exist. As indicated by Janic [26], there can be operational, economic and environmental factors. They may coexist, but often only one type is dominant and determines airport capacity under given circumstances. In the following, operational capacity is used unless otherwise stated. Some important parameters crucial to runway capacity are given below.

Maximum-Throughput Rate: This is the average number of demands a server can process per unit of time when always busy [27]. In the following formula μ_r is Maximum throughput rate and E(t) is the expected average service time.

$$\mu_r = \frac{1}{E(t))} \tag{3.1}$$

Level of Service: This is the number of demands processed per unit of time while meeting specified Level of Service (LOS) standards.

Several types of capacity exist. These different types will be briefly discussed below. Here maximum throughput- and practical capacity are the most widely applied types of capacity in research [23][27][28][29] and by the FAA [30]. These two concepts are ideally meant for planning purposes. Two other methods are most widely used to describe reasonable capabilities of existing systems. Declared capacity is widely used for airport benchmarking, although there are many different understandings of declared capacity which sometimes leads to inconsistency in comparison.

- **Maximum Throughput Capacity:** Maximum Throughput Capacity (MTC) or otherwise known as saturation capacity or ultimate capacity, is explained as the total number of movements which can be performed in one hour on a given set of runways, while obeying Air Traffic Management (ATM) regulations. Runway capacity can be calculated for its maximum potential given the

assumption of constant aircraft demand. This type of capacity does not make use of any LOS requirements.

- **Practical Hourly Capacity:** Originally proposed by the FAA in the early 1960's, it is defined as the expected number of movements that can be performed in 1 hour on a runway system, with an average delay per movement of 4 minutes. The runway system reaches its capacity when this threshold is exceeded. As a rule of thumb, the Practical Hourly Capacity (PHCAP) of a runway system is approximately equal to 80-90% of its MTC, depending on the specific conditions at hand.
- **Sustained Capacity:** Sustained capacity of a runway system is defined as the number of movements per hour that can be reasonably sustained over a period of several hours. Maximum performance often cannot be sustained in practice for a period of more than one or two consecutive hours. Sustained capacity is a more realistic target than maximum throughput capacity when it comes to operations over a period of several hours or an entire day of air traffic activity.
- **Declared Capacity:** Declared capacity is defined as the number of aircraft movements per hour that an airport can accommodate at a reasonable LOS. Delay is used as the chief indicator of LOS. There is no accepted definition of declared capacity and no standard methodology for setting it. In most instances, the declared capacity is set at approximately 85-90% of the MTC of the runway system.

The term runway capacity will be used further on in the rapport. From now on runway capacity is defined as maximum throughput capacity.

3.2 Capacity Envelopes

Runway capacity can be computed by mathematical models on a probabilistic basis. The principal output of such models can be in the form of a runway capacity envelope [31]. Examples of such runway envelopes are found in Figure 3.1 [27]. It shows a boundary indicating the maximum throughput condition for a variety of arrival and departure mixtures. The figure indicates the different boundaries for different runways or runway systems. It is be noted that any point within the boundary is a feasible solution.

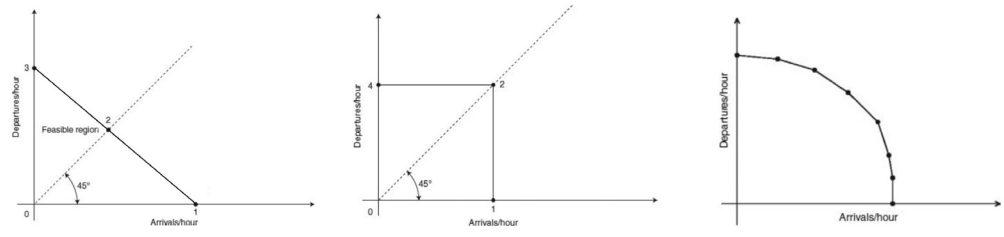

(a) Single runway: alternating arrivals and departures

(b) Two parallel runways: 1 arrival, 1 departure

(c) Multi-runway system

Figure 3.1: Capacity Envelopes [27][32].

3.3 Capacity Coverage Chart

A way to display the capacity of runways is by using the Capacity Coverage Chart (CCC). It indicate the statistical airside capacity over a year. It is influenced by wind direction and strength as well as visibility and ceiling and runway configurations [32]. It is a widely used method to indicate capacity at airports.

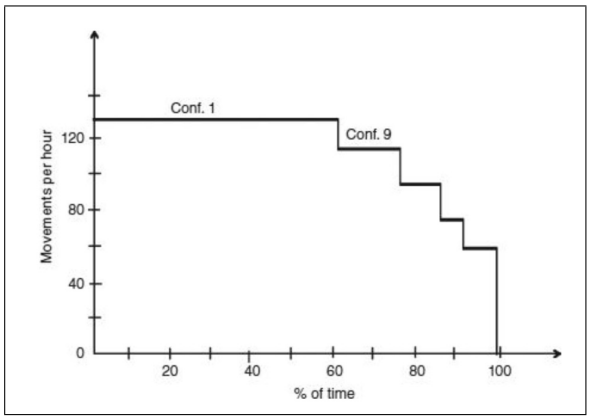

Figure 3.2: Capacity Coverage Chart for Boston/Logan Airport [27].

3.4 Key Drivers

Runway capacity consists of a range of influencing factors. After an introduction of the basics of runway capacity, this chapter will provide a more in-depth look on the factors determining the runway capacity [27]. Initially single runway systems are discussed. Thereafter, complex systems will be elaborated on, of which AAS is a clear example. Additionally, regulations, local conditions, taxi- and apron systems and other factors will be elaborated on. Figure 3.3 shows an overview of all key drivers of runway capacity as will be discussed in this section.

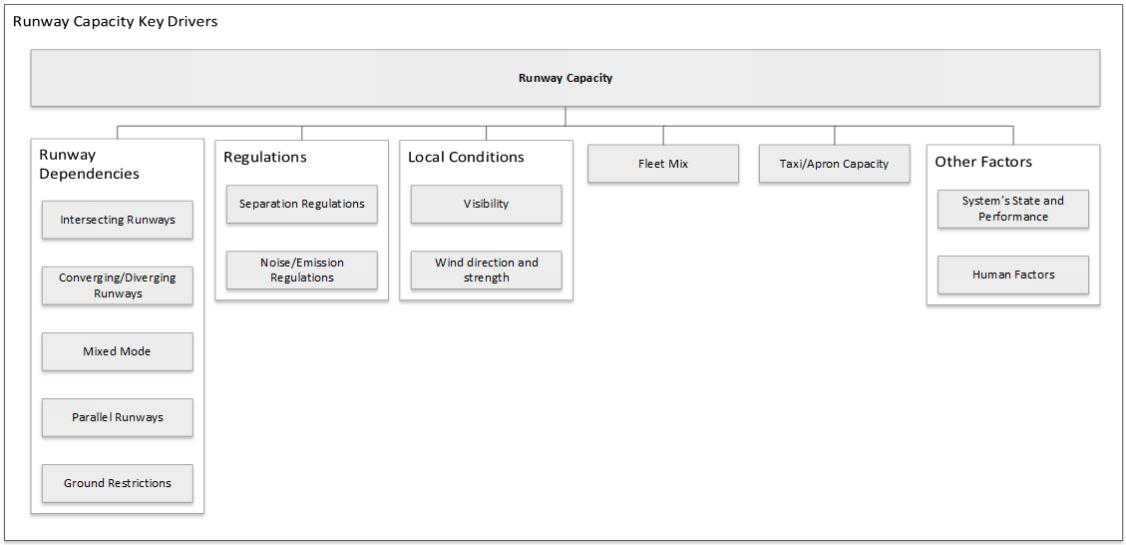

Figure 3.3: Runway Capacity Key Drivers

3.5 Runway Dependencies

Runway layout is an important factor in determining capacity. Runway dependencies are the results of this layout, since correlation may exists between runways. It is possible that aircraft are constrained in their operations due to these factors. Multiple dependencies exists based on the runway configuration. Based on previous work five different categories of dependencies are identified [9][13][21]:

- Converging and diverging runways
- Intersecting runways
- Mixed mode
- Parallel runways
- Ground restrictions

3.5.1 Converging and Diverging Runways

Runways which do not physically cross, but are converging towards each other have an intersection at their projected centerlines. They are otherwise known as 'Open V' runways. An example is found at Chicago O'Hare Airport (ORD), of which the layout is found in the Appendix in Figure B.1. In Figure 3.4 an example is given on the dependencies applicable to the converging or diverging situation. Jet blast and wake turbulence are active constraints as the flight paths intersect, as well as a possible interference on the ground may occur when an aircraft is starting its take-off role. Next to this, missed approaches for arrivals can be potentially hazardous due to the same reason as for intersecting centerlines.

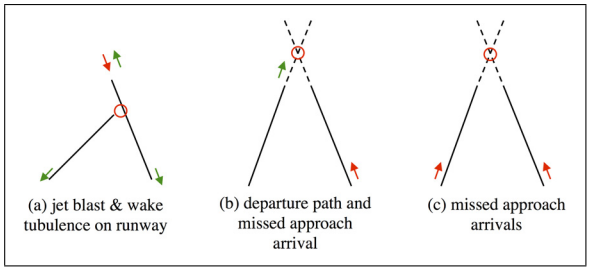

Figure 3.4: Converging and diverging runways [9].

3.5.2 Intersecting Runways

With intersecting runways, as indicated in Figure 3.5, there are different dependencies occurring. Jet blast and wake turbulence are one type of dependencies, while the other type of dependencies results from the point of runway intersection. The runways can be used for different mix of arrival and departures. Depending on wake turbulence and runway occupation a certain separation between airplanes has to be applied in order to maintain safety. Examples are Boston Logan Airport (BOS) and San Francisco International Airport (SFO), which both have multiple intersections in their runway system. The runway layout is added to the Appendix in Figures B.2 and B.3.

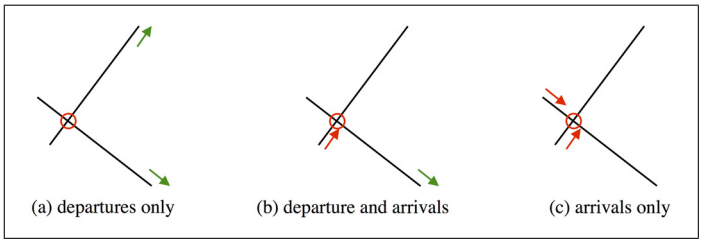

Figure 3.5: Intersecting runways [9].

3.5.3 Parallel Runways

Many major airports operate parallel runways. In Europe most airports in the vicinity of large capitals (e.g. Schiphol and Heathrow Airport) operate parallel runways [33]. It indicates that runways are placed in parallel or in staggered position. There are four parallel runways modes [21]:

- Independent parallel instrument approaches
- Dependent parallel instrument approaches
- Independent parallel instrument departures
- Segregated operations on parallel runways

The first two modes are parallel approaches. For the first mode there are no separation minima in place, for the second mode there are certain dependencies. The first three modes are operated in parallel as indicated by Figure 3.6. As seen from the figure there is a minimum distance between runways of 760 meter. If the distance is smaller, then the combined system is operated as a single runway. An example of segregated operations is given in Figure 3.7. Other forms are semi-mixed parallel operations where one runway is exclusively used for either approaches or departures. Mixed-mode parallel operations may also be applicable if one runway is used for both landing and take-off.

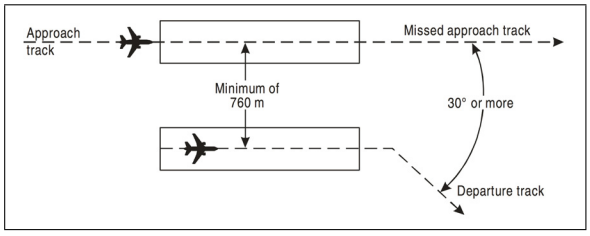

Figure 3.6: Parallel operations [21].

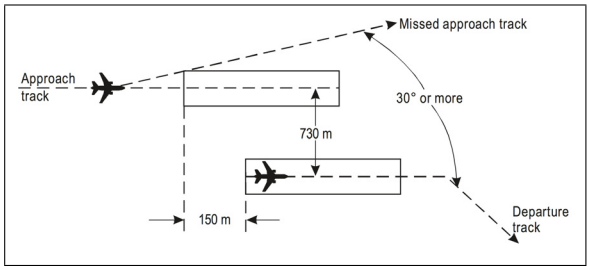

Figure 3.7: Staggered parallel operations [21].

3.5.4 Mixed Mode

Arriving and departing aircraft share a common runway if this runway is operated in mixed-mode. Sufficiently large gaps have to exist in between two different consecutive aircraft. An active input is needed from ATC, hence often resulting in a large workload on the controllers as routine is harder to build up. This procedure is often operated at single runway airports, for example London Gatwick Airport (LGW) which is observed in Figure B.4.

3.5.5 Ground Restrictions

Another type of dependency between runways is ground restriction. During taxiing it may occur that an aircraft crosses an active runway [34]. This active runway crossing impedes the primary purpose of take-off and landing. Next to this, it diverts resources of the ATC from their main tasks. Wake turbulence separation distance may result in large gaps on the runway, which may allow one or more aircraft to cross while taxiing. It may also occur that such a gap is too small, hence increasing time interval between landing and take-off. A mitigating solution might be to implement multiple runway crossing sections or high-speed taxiways.

3.6 Regulations

This section will elaborate on the regulations applicable to the case of runway capacity of departing and arriving air traffic. An important set of regulations is the one regarding separation regulations. Secondly, some further clarification on noise and emission regulations is given in the subsequent section.

3.6.1 Separation Regulations

Separation regulations are in place in order to maintain safety and simultaneously making optimum use of airspace [35]. Minimum separation distances are established to reduce risk of mid-air collisions. ATC is responsible for application of these regulations. The regulations are internationally established by ICAO as well as locally. ICAO doc. 4444 PANS-ATM is an important document stating minimum separation distances. In order to apply these separation conditions, three types of flight rules exist. Visual Flight Rules (VFR), Special Visual Flight Rules (SVFR) and IFR. The first two are 'fly by sight' rules where pilot has responsibility, while the latter one is 'fly by instruments'. Separation is mainly based upon wake turbulence, but radar separation may additionally indicate a minimum distance.

3.6.1.1 Wake Turbulence

Wake turbulence is created by two counter-rotating air masses, otherwise known as vortices [36]. Lift is generated by a pressure difference over the wing's surface. The pressure at the surface of the upper side of the wing is low, while the pressure at the surface under the wing is highest. This difference in pressure creates a roll of the air at the aft position of the wing. Resultantly, the air is now in a spinning motion downstream of the wing. The wake turbulence created is depended on the aircraft size. Since these wake turbulences may potentially have an impact on safety, regulations are in place. A Wake Turbulence Category (WTC) displays the degree of impact of this turbulence. They are set up by ICAO [21] and indicated by a single character per Maximum Take-Off Weight (MTOW) category. The distribution over different MTOW classes is seen in Table 3.1.

Table 3.1: Wake Turbulence Categories [21].

WTC	Description	MTOW
J	Super Heavy	MTOW $\sim$ 560,000 kg
H	Heavy	136,000 kg $\leq$ MTOW
M	Medium	7,000 $<$ MTOW $<$ 136,000 kg
L	Light	MTOW $\leq$ 7,000 kg

EUROCONTROL has developed a new method to categorize wake turbulence minima. It is named RECAT-EU and will be an alternative to ICAO PANS-ATM categories as indicated above. It will be put in use in 2016. Presumably, this method will have a positive effect on safety and capacity and reduce airport delays [37].

Exceptions to the standard separation rules apply in the case of parallel landings [13]. Amsterdam Schiphol Airport, for example, has three parallel runways, known as the Polderbaan (18R), the Zwanenburgbaan (18C) and the Aalsmeerbaan (18L). Two aircraft on simultaneous approaches to 18R and 18C respectively will breach the normal separation minima because of the distance between these runways, but are permitted to do so as long as they are on the designated approach path and are using the runway's specific ILS.

3.6.1.2 Time-based and Distance-based Separation

For successive departures and arivals two types of separation exist. These are time-based and distance-based separation. Wake turbulence is the main influencing factor for these types of separation [33]. To give an overview of these important restrictions Table 3.2 and Table 3.3 indicate the time- and distance-based separation, respectively. The distance-based separation indicates the minimum radar

separation which is regulatory. The values in parentheses are not based on wake vortex separation but are indicated by minimum radar separation which is in most cases equal to 3 NM, but can also be 2.5 NM under certain circumstances.

Table 3.2: Time-based standard separation between consecutive aircraft in seconds [21].

Following Aircraft	Light	Medium	Heavy	Super
Light	60	120	120	180
Medium	60	60	120	180
Heavy	60	60	90	120
Super	60	60	60	

Table 3.3: Distance-based standard radar and wake turbulence separation between consecutive aircraft in Nautical Miles [NM] [21].

Following Aircraft	Light	Medium	Heavy	Super
Light	(3)	5	6	8
Medium	(3)	(3)	5	7
Heavy	(3)	(3)	4	6
Super	(3)	(3)		

3.6.2 Noise and Emissions Regulations

Noise and emissions regulations are often determined locally by different stakeholders in the vicinity of an airport. Next to this there are global and European policies applicable to noise and emission in the aviation sector. For runway capacity this can be a restricting factors as was seen in Section 2.3.2 at Schiphol Airport.

A Noise Abatement Departure Procedure (NADP), as defined by ICAO and FAA, may be in place in order to minimize noise load in the vicinity of an airport. ICAO-A focuses on mitigating noise load in close vicinity, whereas ICAO-B uses a different measure and focuses on environmental noise load further away from the airport. Veerbeek and Brouwer [38] analyzed NADP-1 and NADP-2 procedures at Schiphol airport. It proved that a possible fuel reduction using the NADP-2 procedure is feasible.

The FAA standard tool for determining the predicted noise impact around airport is INM. It can be used for regulatory purposes. This model is able to calculate the noise impact and is used in computing noise levels and runway allocation capacity due to the noise impact [39].

3.7 Fleet Mix

Fleet mix is an important aspect of runway capacity. As was seen in Section 3.6.1, wake turbulence categories are based upon MTOW. In order to model runway capacity these wake vortex categories characterize the aircraft fleet mix and have their impact on the capacity [33]. In their research Chandrasekar and Hwang [40] used several other classifications in order to identify an algorithm for arrival and departure sequencing. Wingspan, (approach) speed class and size of an aircraft is needed for their runway capacity proposition. As indicated by Mirkovic [2] mean inter-arrival time depends on the fleet mix and is an integral part of most runway capacity simulation models.

3.8 Local Conditions

Local condition are of utmost importance in airport operations. Runway capacity is partially determined by the local conditions at hand. These conditions can vary from visibility, cloud base, precipitation to local wind conditions.

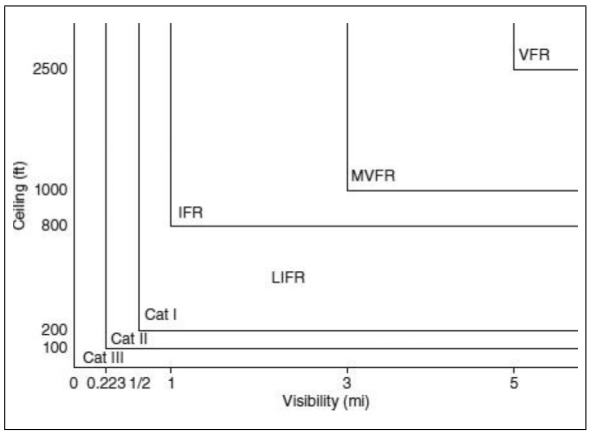

Figure 3.8: Typical classification of weather conditions for a US airport [27].

3.8.1 Visibility Conditions

Criteria apply for maintaining safety at certain visibility conditions. In the Netherlands, for all airports and airfields the following conditions apply [11]:

- If visibility is greater than 5 km and the ceiling higher than 1,000 ft, no special precautions are required.
- If visibility is between 1.5 km and 5 km and/or the ceiling is between 300 and 1,000 ft, special precautions are implemented. Visual approaches are not permitted and specific procedures apply to dependent (parallel) runways.
- If visibility is less than 1.5 km and the ceiling lower than 300 ft, so-called Low Visibility Procedures (LVP) take effect. Neither the pilot nor the air traffic controller is able to observe aircraft movements effectively. Under LVP, a number of additional safety precautions are applied: runways are protected with stop bar lights at their entrances and exits; aircraft separation is increased; runway usage and capacity are adjusted; work in the maneuvering area is restricted or stopped altogether; and taxiing aircraft are actively supervised.

Different visibility categories are in place. The typical classification is displayed in Figure 3.8. Each classification comes with specific constraints on runway use and are heavily dependent on local weather conditions.

3.8.2 Wind Direction and Strength

A runway can only be used if the crosswinds acting on the runway are within prescribed limits. Hence the orientation and availability in given weather conditions is crucial for runway capacity. In Figure 3.9 a wind compass rose is given as used at Schiphol Airport [41]. The preferred runway for an outbound peak is shown.

3.9 Taxi and Apron Capacity

According to De Neufville and Odoni [27] the taxiway system at major airports is often designed to provide capacity exceeding the capacity of the runway system. For this study it is assumed not to be a limiting factor on airport capacity. Still local constraints can be identified at for example taxiway intersections, where active runway crossing may occur or on locations where high speed exits coincide with the taxiway. In these situations, airports may operate close to maximum capacity. Taxiway capacity is thus depending on airport specific configurations and local conditions [2]. Accordingly, apron areas can be viewed as airport specific as well. For Amsterdam Airport Schiphol a case study has been

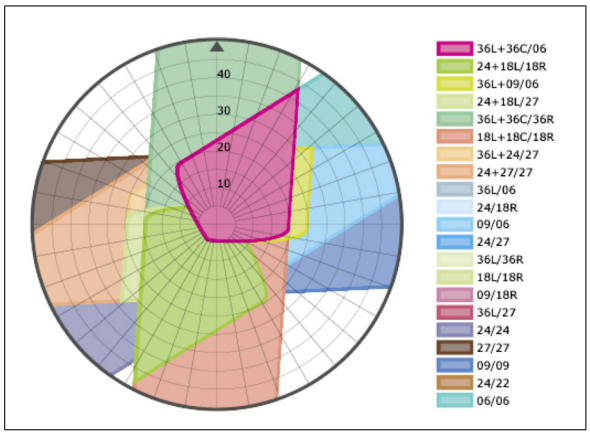

Figure 3.9: Compass rose for preferred runways at AAS [41].

done on airport surface traffic planning optimization on a complex system [42]. Here simulation and optimization of the routing of aircraft on taxiways has been performed.

3.10 Other Factors

Other factors of influence are various. Human factors, such as pilot and controllers can have impact on the system to certain degree. ATM system's state and performance also plays a role. A safety buffer is occasionally in place on the minimum separations between consecutive airplanes to account for imperfections in the ATC communication system. A buffer of up to 10 seconds between each aircraft is in such scenarios added [27].

3.11 Conclusion

All factors which have their impact on runway capacity have been discussed in this chapter. Runway allocation is restricted by runway dependencies, regulations, local conditions, fleet mix, taxi capacity and other factors. Runway dependencies have been identified to be unique for a given runway combination. Next to this, regulations and local conditions give rise to additional restrictions on capacity. Aircraft type and fleet mix proved to be important since the Wake Vortex category may have impact on capacity. Taxi and apron capacity proved important aspects, but will not be further researched in this study. Finally, human factors and system state may have effect in changes in capacity. Apart from a the described communication buffer, these factors will not be treated in this study. The runway allocation model is primarily based on the influence of these key runway capacity drivers. The following chapters will incorporate these factors in eventually the design of the runway allocation model.

Chapter 4

Methodologies

This chapter will discuss in detail the methodologies used for the research and preparation of the Runway Allocation Tool. A fundamental basis for the needed methodology components is provided. It is started with an overview of the used methodologies. Thereafter, runway dependency methodologies are treated in Section 3.5. Fuel computations will be discussed in the subsequent section. In the section on noise computations, all properties of noise calculations are elaborated on. This will include a detailed overview on the Integrated Noise Model. Finally, emission computations are discussed in Section 4.5. The computational basis in this chapter provides the constituents necessary for development of the runway allocation tool.

4.1 Methodology Overview

This section gives an overview of the methodologies brought forward in the remainder of this chapter. It follows from Figure 4.1 that five main components are considered. Together they provide the necessary periphery of the designed runway allocation tool. Runway dependencies are split up in several sections identifying all possible dependencies as they may occur in a single- or multi-runway system. Fuel computations, as will be discussed further on in the chapter, consists of a part on segments, fuel usage per segment and total fuel. The noise methodologies include the Integrated Noise Model and other noise computations. Emission computations is dealt up in four parts each representing an emission product. The methodology regarding Linear Programming is discussed separately in Chapter 5.

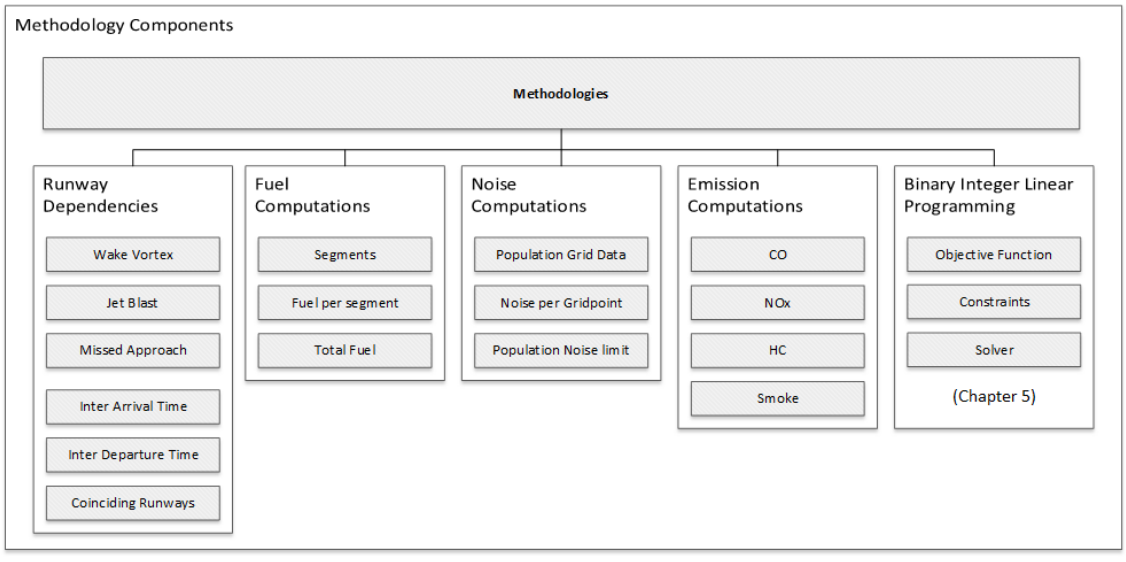

Figure 4.1: Methodology components overview.

4.2 Runway Dependencies

In Section 3.5 a multitude of runway dependencies has been discussed. In this section, further explanation is provided on the methodologies of computing these dependencies. The type of aircraft and type of operation in terms of Arrival-Departure (AD), or Departure-Arrival (DA) or additional combinations (AA, DD), will have its influence on dependencies between runways. This section explains dependencies in a generic way. In the existing body of knowledge, a uniform breakdown of runway dependencies has been established by ICAO [21], Stamatapolous [8], Joey van der Klugt [9], et al. This research will build further upon that breakdown. Runway dependencies serve as an input for the Runway Allocation Model. In order to integrate the dependencies, they are consolidated in a binary dependency matrix.

4.2.1 Single Runway System

As discussed in Section 3.5, several dependencies between runways exist in an airport environment. In order to implement these dependencies in an allocation model, they are rewritten to constraints as will be seen in the subsequent sections. A runway dependency matrix for a multi-runway system is developed at the end of this section, which articulates in the runway capacity and dependency constraints. A dependency has influence on the flight- or grounds paths of leading aircraft followed by a trailing aircraft. The result is a difference in minimum time in aircraft spacing. Several factors can cause these dependencies, being wake vortices, jet blast and missed approach procedures. The following section will explain the Inter-Arrival Time (IAT) and Inter-Departure Time (IDT), respectively, for single runway operations.

4.2.1.1 Inter-Arrival Time

Separation constraints consist of time-based and distance-based separation. As explained in Section 3.6.1 there exist predetermined separation standards. These are listed in Table 3.2 and 3.3. In this section it is explained how this separation minimum is used in computations and which assumptions are in place for a single runway operation with multiple aircraft. Two regulations are in place to address the separation minima. These are Radar- and Wake Vortex Separation and Runway Occupancy time (ROT).

Radar- and Wake Vortex Separation As observed in Figure 4.2 two consecutive aircraft are separated by a space μ, which is the time separation imposed by the air traffic controller. Here D is the length of the common approach path. S_{LF} is the minimum separation distance requirement for a leading aircraft L and following aircraft F. Under the assumption that speed of the leading aircraft is equal to the speed of the trailing aircraft ($V_L = V_F$) on the same common approach path, the following equation holds for the minimum time separation:

$$\mu_1 = S_{LF}/V_F \tag{4.1}$$

Runway Occupancy Time This is the time a runway is occupied by a single aircraft. It depends on the type of aircraft and its speed. The runway length and availability of high-speed taxiways are also important aspects. Under the assumption that airspeed of the trailing and leading aircraft are equal, the formula for runway occupancy now becomes:

$$\mu_2 = ROT_L \tag{4.2}$$

Finally the largest of both μ_1 and μ_2 will function as the new final separation minimum. IAT is now be computed using the following computations:

$$\mu = max(\mu_1, \mu_2) \tag{4.3}$$

$$IAT_{LF} = \mu \tag{4.4}$$

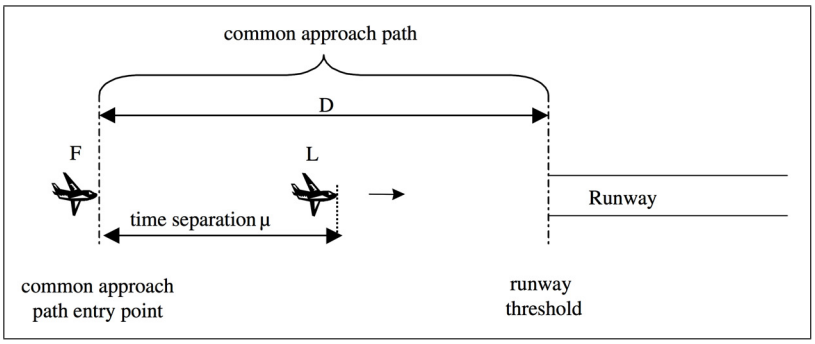

Figure 4.2: Final approach for landing with time separation [8].

4.2.1.2 Inter-Departure Time

For departures, Inter-Departure Time can be computed under the same assumptions as applied to Inter-Arrival Time. IDT is equated identically, where ROT_L is the runway occupancy time of the leading aircraft, and SEP_{LF} the time separation minima as seen before in Table 3.2. From the following equations the final separation time if found:

$$\begin{aligned} \mu_1 &= SEP_{LF} \\ \mu_2 &= ROT_L \\ \mu &= max(\mu_1, \mu_2) \end{aligned} \tag{4.5}$$

It is noted that $\bar{c}$ is the mean of the normal random variable c, indicating a communication time delay in departures. The value of c acts as a buffer for the duration of radio communication. Now the final Inter-Departure Time will become:

$$IDT_{LF} = \mu + \bar{c} \tag{4.6}$$

In development of a runway allocation model in which these methodologies are applied another assumption is made; the time-based separation distances are equal to or larger than the runway occupancy time. This is shown in equation 4.7. Hereby, the separation conditions are defined by the official time based separation regulations.

$$SEP_{LF} \geq ROT_F \tag{4.7}$$

For calculations where the common departure path and variable airspeed for the leading and trailing aircraft are taken into account, another aspect comes to play. Radar and wake turbulence separation plays are role when departing aircraft fly on a longer common departure path. Additionally, distance based separation on the complete common departure path changes [9]. This will explicitly not be part of this study but has potential for future studies as will be discussed in Chapter 9. It is noted that the assumption of equal speed is in many real world cases not valid, e.g. due to different aircraft types and variable wind conditions.

4.2.1.3 Dependencies in Matrix Form

Inter-Departure and Inter-Arrival Time have now been established. In order to be implemented, as will be explained Chapter 6, these separation minima are translated to a generic matrix format, serving as input for further computations. An example is given in Table 4.1. In this example an aircraft touches down at the runway at Event Time $dt = 0$. This indicates the runway at that specific moment in time is occupied by an aircraft, and is assigned a number 1 in the table. For this scenario the IATs are computed using the method explained in the previous paragraph. The extracted time-based separation data form Table 3.2, is assumed to be 60 seconds for this particular operation of two consecutive Medium MTOW aircraft. It is observed that consecutive time steps $dt = 20$ and $dt = 40$ are equally assigned a value

of 1. This value indicates that this time-runway combination is occupied. The occupation being the IAT has a duration of 60 seconds, indicated by the three time steps of which are assigned value 1. On the first hand counter-intuitively, other aircraft are only allowed to land on time-runway combinations where a zero is assigned in the matrix. Hence indicating this spot is open for additional operations by other aircraft.

Table 4.1: Single runway occupation at event time 80 [s]: a value of 1 indicates runway occupation.

Time [s]	20	40	60	80	100	120	140
dt [s]	-60	-40	-20	0	20	40	60
Runway	0	0	0	1	1	1	0

4.2.2 Multiple Runway System

For multiple runways it is evident that there are several combinations of procedures at hand. Consecutive arrivals or consecutive departures are possible. Departures following arrivals and vice versa. In the following these will be described by AA, DD, AD and DA, respectively.

4.2.2.1 Converging/Diverging Runways

In the situation of converging or diverging runways, two important dependencies exist. Namely, jet blast and missed approach procedures. In this section aforementioned dependencies will be discussed. Finally, a dependency matrix will be displayed, incorporating both dependencies. This matrix will operate as an input feed for the allocation tool.

Jet blast Jet blast as discussed in Section 3.5 is created when a jet engine produces air movement particularly during high thrust settings at take-off. This potentially results in a dependency with other runways. The formula below indicates how this jet blast is anticipated for. Here μ_{jb} is the minimum time of the next departure after the start of the take-off roll of the departure on the other runway. ROT_L is the departure ROT until the intersection/convergence point, t_{lineup} is the line-up time of the departing aircraft, and $\bar{c}$ is the communication buffer between departure clearance and the actual start of the departure roll.

$$\mu_{jb} = ROT_L + t_{lineup} + \bar{c} \tag{4.8}$$

In Table 4.2 it is observed how this results in a dependency matrix. Here two runways are seen, where on runway 1 a departing aircraft induces a jet blast constraint on runway 2. The result is a blockage on the second runway for two time steps of in total 40 seconds. Depending on the configuration of runways, this separation time may vary. Arriving and departing aircraft are both constrained by jet blast constraints therefore the dependency matrix differs for different operations of consecutive aircraft.

Table 4.2: Multiple runway dependency: jet blast starting at event time 80 [s].

Time [s]	20	40	60	80	100	120	140
dt [s]	-60	-40	-20	0	20	40	60
Runway 1	0	0	0	1	1	0	0
Runway 2	0	0	0	1	1	0	0

Missed Approach Another dependency between runways is the Missed Approach dependency. Missed approach procedures are listed in the Aeronautical Information Publication (AIP) Netherlands report EHAM-Amsterdam/Schiphol [14] for the airport Schiphol case. Other airports have identical regulations on how to respond during a missed approach. This type of runway dependency imposes additional constraints on runway availability when a missed approach path intersects with a flight path of another flight. The following equation displays how the separation time for a missed approach occurrence is calculated.

$$\mu_{ma} = \frac{D_{min}}{V_A} + \bar{c} \tag{4.9}$$

Here μ_{ma} is the time spacing needed, D_{min} is the maximum distance of the approaching aircraft with flight speed V_A to the runway, for which another flight may be given clearance. When the missed approach path of an arriving aircraft is intersecting with the projected flight path of a departure these two movements need to be sufficiently separated. A communication buffer is given by $\bar{c}$. How this dependency translates into a dependency matrix with fixed time steps of 20 seconds, is shown in Table 4.3. An aircraft operating at runway 1 will presumably occupy runway 1 at time step 80. To mitigate the risk of collision during a missed approach, runway 2 is blocked from time 60 until time 120, a timespan of $4 \cdot 20 = 80$ seconds. Depending on the specific airport layout, these values may differ. Note that ROT is not included in the table below. The final runway dependency matrix will be a combination of several (potentially overlapping) dependencies.

Table 4.3: Multiple runway dependency: missed approach contingency starting at event time 80 [s]. Note that ROT is not included in this table.

Time [s]	20	40	60	80	100	120	140
dt [s]	-60	-40	-20	0	20	40	60
Runway 1	0	0	0	1	1	1	0
Runway 2	0	0	1	1	1	1	0

4.2.2.2 Intersecting Runways

The specifics of intersecting runways have been discussed in Section 3.5. The dependencies show similarities with converging and diverging dependencies although some differences exist when a different mix of arrivals or departures occurs. For arriving aircraft the following equations holds, which is identical to converging and diverging operations:

$$\mu_{arr} = \frac{D_{min}}{V_A} + \bar{c} \tag{4.10}$$

When a departing aircraft obstructs the runway the following constraint is active, where ROT_{dep} is the runway occupancy time of the departing aircraft.

$$\mu_{dep} = ROT_{dep} + \bar{c} \tag{4.11}$$

The translation into a generic dependency matrix is shown in Table 4.4. Here it is observed that an aircraft arriving at time 80 poses restrictions on another runway in earlier steps in time. For the intersecting aircraft a large enough separation minimum is in place to mitigate the risk of collisions.

Table 4.4: Multiple runway dependency: intersecting aircraft at event time 80 [s].

Time [s]	20	40	60	80	100	120	140
dt [s]	-60	-40	-20	0	20	40	60
Runway 1	0	0	0	1	1	0	0
Runway 2	0	1	1	1	1	0	0

4.2.2.3 Parallel Runways

As explained in Section 3.5 different forms of operations on parallel runways may occur. If parallel runway are spaced by a distance $s < 760m$, the same separations are in place as for a single runway from Section 4.2.1 for the two runways combined. The standard separation minima are used in that case, since wake vortices may originate from aircraft in this dependent parallel runway configuration. For a spacing of $s > 760m$, runways are considered independent. Here normal Inter-Departure and Inter-Arrival Time calculations apply.

Segregated operations The fundamentals of segregated runways have been explained in the Chapter 3. For dependency calculations segregated runways are similar to parallel runways. There is a difference in the minimum of consecutive flights if the runways are spaced closely enough.

Table 4.5: Multiple runway dependency: segregated parallel runways.

Time [s]	20	40	60	80	100	120	140
dt [s]	-60	-40	-20	0	20	40	60
Runway 1	0	0	0	1	1	0	0
Runway 2	0	1	1	1	1	0	0

Opposite Directions Operations in opposite direction can have increased risk, certainly in case of missed approaches if parallel runways are closely spaced or if a single runway is considered. Therefore, extra safety factors are in place with respect to normal parallel operations. The missed approach dependency gives rise to additional spacing between aircraft operations. This is displayed in Table 4.6, where one runway is operated from runway end a and b.

Table 4.6: Single/multiple runway dependency: opposite direction.

Time [s]	20	40	60	80	100	120	140
dt [s]	-60	-40	-20	0	20	40	60
Runway 1 (end a)	0	0	0	1	1	1	1
Runway 1 (end b)	1	1	1	1	1	1	1

4.2.2.4 Mixed Mode Operations

Mixed mode operations exist when arrivals and departures are operating on a single runway. It may pose a significant risk with respect to safety, thereby increasing workload for ATC. Operations should therefor always be investigated on a per runway configuration basis. In this research, as will be elaborated on further in the chapter regarding the case study, additional safety measure are taken. A safety factor is applied in order to create a large enough distance between consecutive operations on a single runway. Single runway separation minima are in place as seen in Section 4.2.1. Next to this a safety factory μ_s is applied, as seen in the formula below:

$$\mu_{mm} = ROT_{dep} + \mu_s + \bar{c} \tag{4.12}$$

4.2.2.5 Ground Operations

Ground restrictions, e.g. crossing of taxi or apron tracks, are not incorporated in this research in terms of dependencies. This is done under the assumption of De Neufville and Odoni [27] that taxiway system provide capacity exceeding the capacity of the runway system. It will be further addressed as recommendation for future studies in Section 9.3.

4.2.3 MTOW Classes

In the aforementioned dependencies, airspeed, runway occupancy time and official separation regulations are combined to form runway dependency matrices. These factors are dependent on the type of aircraft. As a result a dependency matrix may differ for different MTOW classes under the same operations. In the remainder of this study different dependency matrices are used for consecutive aircraft of different MTOW classes.

4.2.4 Runway Dependency Matrix

As conclusion to the section on runway dependencies an overview of a multi-runway system with different constraints is given in Table 4.7. This example is for an aircraft with Runway 1 as arrival destination. Here runway 1 has two runway ends, 1a and 1b which lie opposite of each other. In Appendix H, an overview is given for the runway dependency matrices as used for the case study on Amsterdam Airport Schiphol. This will be discussed in the subsequent chapters.

Table 4.7: Dependencies for a multi-runway system.

Time [s]	20	40	60	80	100	120	140	Type of
dt [s]	-60	-40	-20	0	20	40	60	Dependency
Runway 1 (end a)	0	0	0	1	1	1	0	Used runway
Runway 1 (end b)	1	1	1	1	1	1	1	Opposite direction
Runway 2	0	0	0	0	0	0	0	[-]
Runway 3	0	0	1	1	1	1	0	Intersecting
Runway 4	0	0	1	1	1	1	0	Parallel
Runway 5	0	0	0	0	0	0	0	[-]

4.3 Fuel Computations

Fuel computations play a crucial role in this study on flexible arrival and departure runway allocation. If a trade-off is anticipated between fuel and noise, computations in these areas have major impact on the final outcome. Fuel usage is expressed as kilogram of kerosene used for a particular operation. In order to identify fuel usage, several factors are evaluated. Firstly, an aircraft and engine configuration is selected. Once an aircraft type is chosen, flight segments are set up. These segments indicate the track distance and time an aircraft will be situated on a certain segment. Since in every segment different thrust settings are applied, the engine fuel flow will similarly differ per segment. The methodology discussed here is under a assumption; per segment a fixed fuel flow rate can be identified. This section will discuss the computations on fuel. Important aspects discussed are segments, fuel flow and total fuel consumption per segment.

Table 4.8: Aircraft & engine specifications for both Medium and Heavy MTOW classes.

Component	**Aircraft**	**Aircraft**
Manufacturer	Boeing	Boeing
Aircraft	737-800	777-200ER
MTOW Class	Medium	Heavy
Engine Type	High-by pass	High-by pass
Noise Stage	Stage 3	Stage 3
Max Gross Takeoff Weight	79016 [kg]	297557 [kg]
Max Gross Landing Weight	66361 [kg]	213188 [kg]
Engine Manufacturer	CFM	General Electric
Engine	CFM56-7B26	GE90-90B
Number of engines	2	2
Entry into service	1998	1995
Fuel	Jet-A kerosene	Jet A kerosene

4.3.1 Aircraft and Engine Selection

After observation and analysis of multiple aircraft, a trade-off is performed in order to select an aircraft for scenario testing in terms of fuel, noise and emission operations. For this study two types of aircraft are selected for both Medium and Heavy MTOW classes. This is done under the assumption of the aircraft being representative for a set of flights as may occur at an airport. For the Amsterdam Airport Schiphol case, analyzing of the aircraft types operating on two consecutive days has been done. For the medium MTOW class the Boeing 737-800, Figure 4.3, proved not only the most occurring aircraft, it also proved having a representative maximum take-off weight for its class after analyzing the average MTOW of all medium aircraft. For the Heavy or Large MTOW class the Boeing 777-200ER, Figure 4.4, is selected as being representative for the heavy class based upon analyzing the average MTOW of all heavies operating on AAS for both days. The Light MTOW class is underrepresented and therefore neglected from further research in this report. In terms of fuel burn and noise generation, engines play a vital role. In Table 4.8 an overview is given of both aircraft and engine specifications for the selected

aircraft.

Figure 4.3: Artist impression of a Boeing 737-800 with KLM livery [43].

Figure 4.4: Artist impression of a Boeing 777-200ER with KLM livery [43].

4.3.2 Segment Computations

A next step in determining fuel consumption is done by defining flight segments. Fuel flow is dependent on the net thrust an airplane produces in different flight segments. For this reason, a set of flight segments is identified. These are split up in three segments for arriving aircraft and three segments for departing aircraft as can be seen in Figure 4.5 and Figure 4.6, respectively.

4.3.2.1 Descent: Initial Approach Fix

The scope of this study is bounded to the moment an arriving aircraft passes the Initial Approach Fix until it descents, reaches the gate, and eventually departs via an outgoing Sector, as has been discussed in Section 2.3. The first segment identified is the segment from the Initial Approach Fix until the Final Approach Fix. For this research these are found in the EHAM AIP, other similar documents prescribing airport operations exist. In order to determine the length of such a path, careful analyzing is done of the Standard Arrival Charts. Consultation of experts, for this case a pilot was interviewed, indicated that it is hard to identify one fixed distance, since pilots fly according to waypoints as indicated by ATC, but have a certain degree of freedom on how to approach these waypoints, i.e. some deviation is possible. In this study the length of segments has been evaluated using measurements of the AIP charts, under the assumption of fixed lengths. Deviation or changes in trajectory are not considered. This is done as indicated in the STAR figure in Appendix A.

4.3.2.2 Descent: Final Approach Fix

In order to establish segment length starting at the Final Approach Fix location until end of runway location, observation and analysis of the flight charts in the AIP is performed. It is defined what the

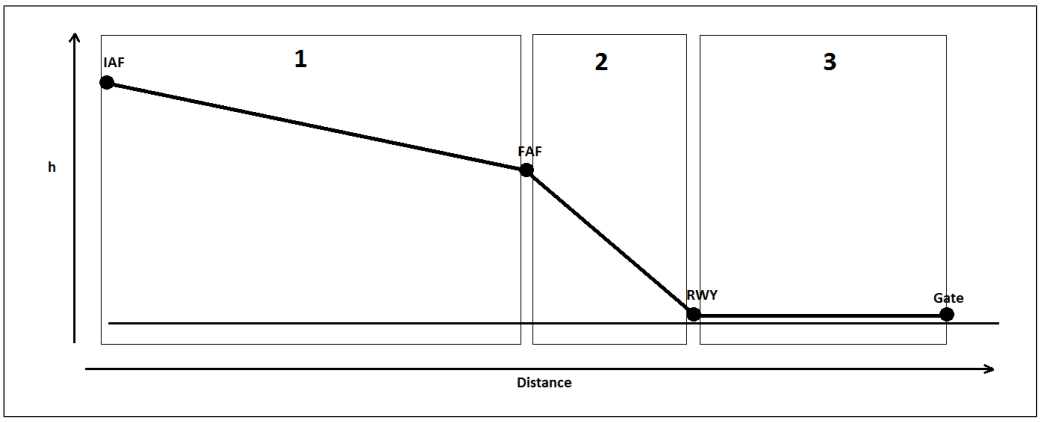

Figure 4.5: Flight segments for arrivals (not on scale).

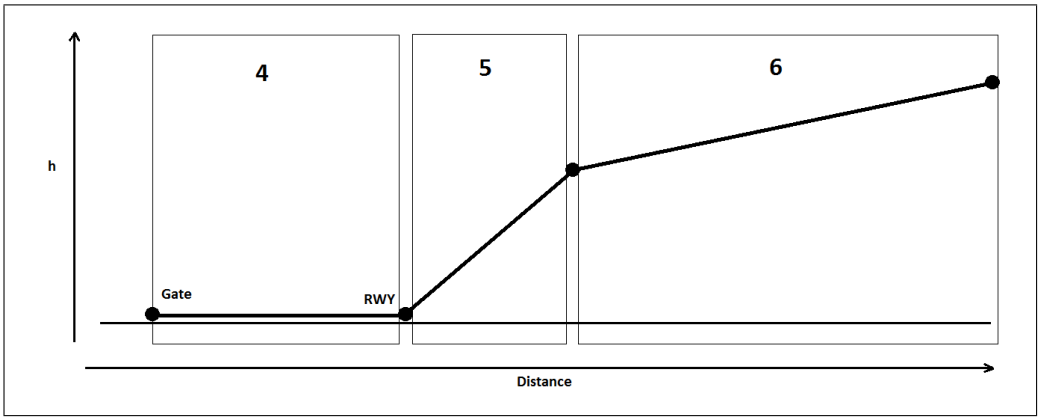

Figure 4.6: Flight segments for departures (not on scale).

exact lengths are per flight segment. There exist different approach operations, which have been briefly explained in Chapter 2. The methodology explained here focuses on ILS procedures. The Arrival Charts indicate length for this type of operation for runway. With respect to generic aspects of this methodology, it is assumed that these distances are readily available for most airports and operations.

4.3.2.3 Taxi: Arrivals and Departures

The methodology for taxi times is based on empirical analysis of existing data. In the scope of this research taxi capacity is assumed to be larger then runway capacity. Based on this assumption, taxi times are independent to factors like flight origin or destination. For this reason, an estimation of average taxi times per runway-gate combination is performed. The method applied in order to estimate taxi times, is by empirically analyzing existing data. 2556 flights have been evaluated operating at Amsterdam Airport Schiphol. From this data, an average runway to gate time is established. Additionally, taxi times can be research based on origin and destination dependency by including this information in the workings of the model. More on this topic is discussed in Chapter 9. An overview of the taxi times is found in Appendix C.3.

4.3.2.4 Departure: Take-Off and Climb-Out

Take-off operations are equated similarly to descent operations. AIP charts indicate the distance from a runway to sector. The same method as for Final Approach Fix measurements has been applied. The charts used for this study are found in the figure with SIDs in Appendix A.

4.3.3 Fuel Flow

Apart from distance measurements, another factor is necessary in order to compute fuel usage. Per segment fuel flow or fuel burn characteristics are extrapolated using Base of Aircraft Data (BADA) from EUROCONTROL. From this database aircraft performance specifics can be extracted. By inserting different criteria as variables in BADA, segments can be plotted. From this data the fuel flow per segment and condition can be evaluated. In the figures below the fuel flow is displayed with respect to altitude for the Boeing 737-800. These computations are also performed for the Heavy MTOW class. Fuel flow for the taxi phase is estimated on 7% of total thrust, which is commonly used by ICAO and other studies in taxiing operations [44]. The results are added to Appendix E. Here the numbers in the caption indicate the flight segment as observed in Figure 4.5 and 4.6.

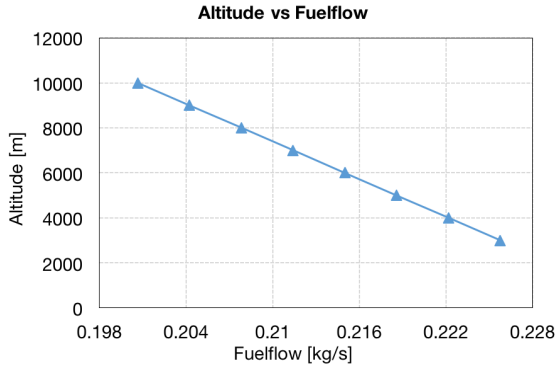

Figure 4.7: Fuel flow Initial phase (1).

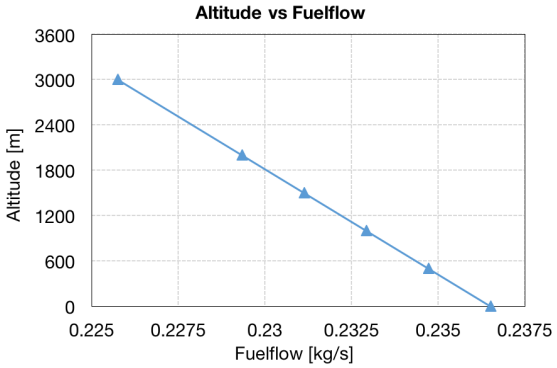

Figure 4.8: Fuel flow Final phase (2).

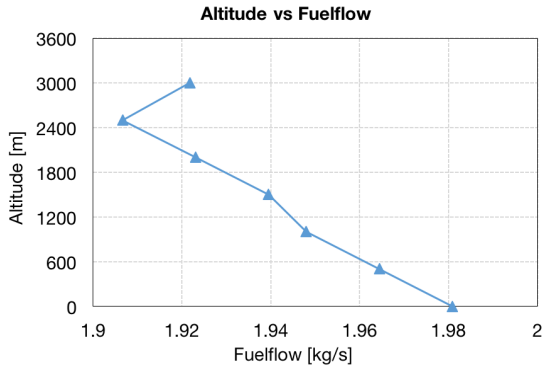

Figure 4.9: Fuel flow Take-Off (5).

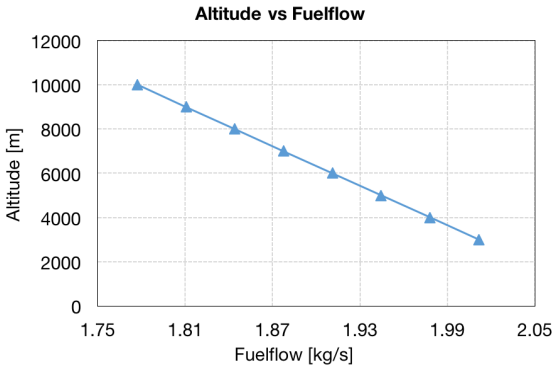

Figure 4.10: Fuel flow Climb-Out (6).

4.3.4 Fuel Usage

In the previous sections several flight segments have been addressed. Each segment has its own characteristics in terms of distance and altitude. Also indicated are the different fuel burn specifics per segment. Using these variables as input, final fuel cost per segment can be equated using the formulas below:

$$D = \text{Distance} \quad [m] \tag{4.13}$$

$$V_{TAS} = \text{True airspeed} \quad [m/s] \tag{4.14}$$

$$T = \text{Time} \quad [s] \tag{4.15}$$

$$\dot{m}_f = \text{Fuel Mass Flow Rate} \quad [kg/s] \tag{4.16}$$

$$\text{TFU} = \text{Total Fuel Used} \quad [kg] \tag{4.17}$$

In order to find the total fuel used per segment the following computation is solved using dimensional analysis.

$$\text{TFU} = \frac{D \cdot \dot{m}_f}{V_{TAS}} = \frac{m \cdot \frac{kg}{s}}{\frac{m}{s}} \quad [kg] \tag{4.18}$$

Here the distance is the actual distance as flown by the aircraft. The true airspeed can be evaluated from local regulation procedure speeds indicated in aeronautical charts, for AAS an these are given in Table C.4. Using the aforementioned computations, the total fuel can now be calculated. This is done by determining the segment distance and setting the airspeed for that segment. Now the total time for which an aircraft flies on a segment is found. Combining the time per segment with the fuel flow kg/s, a total value for fuel usage is found per segment.

If an aircraft experiences delay on a certain flight segment, this results in a longer distance flown at equal airspeed. Although total fuel usage is therefore increased, the assumption is made that it has no effect on the flight path in terms of noise calculations. In other words, fuel use is increased during delay, noise exposure remains constant.

4.4 Noise Computations

This section will explain all noise-related methods used to compute aircraft noise and the exposure to the environment. A fundamental basis is provided for noise calculations. The INM is discussed, as it plays a vital role in the establishment of noise levels. The resulting noise levels are used in the runway allocation model, as will be explained in Chapter 6.

4.4.1 Acoustic Energy Level

Exposure of noise as it occurs at a single event is described by the Sound Exposure Level (SEL). For SEL it holds that the one-second long steady level contains as much energy as the varying level over the full event [45]. In this section the analytically basis to compute SEL is explained from which the Acoustic Energy Level (AEL) is derived.

The Sound Pressure Level (SPL) reflects the actual sound as received by an observer on ground. Since the human ear is more susceptible to certain frequencies a weighting factor is applied to this SPL. This is called the A-weighting filter. It reduces the impact of frequencies which are less annoying to the human ear. The A-weighted sound level relates to the SPL by, $L_A(i) = \text{SPL}(i) + \Delta L_A(i)$, where $\Delta L_A(i)$ is the corrected frequency band level. This is observed in Figure 4.11. The formulas for SPL and overall L_A are displayed below. Here p_e is the effective free field sound pressure. p_0 is the reference pressure.

$$\text{SPL} = 10 \cdot \log \left[\frac{p_e^2}{p_0^2} \right] \tag{4.19}$$

$$L_A(i) = \text{SPL}(i) + \Delta L_A(i) \tag{4.20}$$

$$L_A = 10 \cdot \log \sum 10^{\frac{L_A(i)}{10}} \quad [\text{dB(A)}] \tag{4.21}$$

A noise event as induced by aircraft noise is given by a function of time. The longer an observer is exposed to noise, the more annoyance due to noise will be experienced. The SEL accounts for this time dependency by the formula below. Here t_f is the total exposure time in seconds, τ is a reference time of one second.

$$\text{SEL} = 10 \cdot \log \left[\frac{1}{\tau} \int_0^{t_f} 10^{\frac{L_A(i)}{10}} dt \right] \quad [\text{dB(A)}] \tag{4.22}$$

SEL addresses single event noise. In order to account for multi-event noise, another parameter is introduced; L_{den} is a cumulative noise level for multiple events. A summation is made for each individual SEL value over a given period of time. The L_{den} is a specific day-evening-night metric which takes into

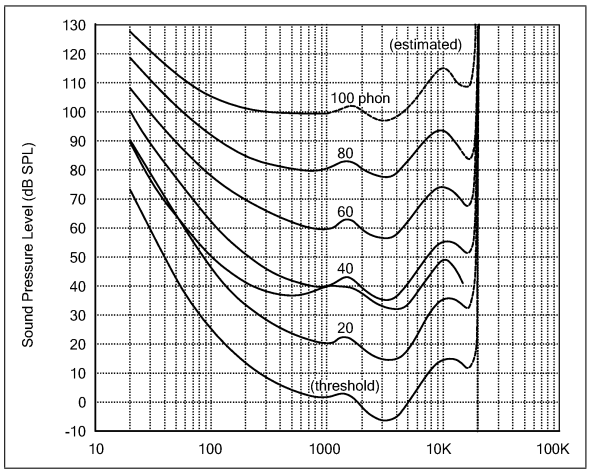

Figure 4.11: Equal-loudness contours [46].

account a complete 24 hour day. This measure is widely used in noise measurements and regulations [47].

$$L_{den} = 10 \cdot log\left[\sum_{n=1}^{n_{flights}} w_n 10^{\frac{\text{SEL}_n}{10}}\right] - 10 \cdot log\left[\frac{T_{den}}{\tau}\right] \quad \text{[dB(A)]} \tag{4.23}$$

In the above formula τ is a reference period indicator of one second. T_{den} is the time of the considered time period [3]. w_n is a penalizing factor for different times of day. The penalty factors for a complete day are given in Table 4.9.

Table 4.9: Penalty factor for different times of day segments [47].

Segment	**Start**	**End**	**Penalty** (w_n)
Day	07:00	19:00	1
Evening	19:00	23:00	3.162
Night	23:00	07:00	10

The value of L_{den} plays a major role in restricting airports in their operations as it poses a noise exposure limit. As seen in Section 2.3.2, an example of L_{den} restrictions is given for Amsterdam Airport Schiphol. In order to use this limit in computations for runway allocation an adjustment has to be made due to the logarithmic implications of the formula. In linear optimization, as will be discussed in subsequent chapters, logarithmic equations have first to be converted to a linear function by considering the AEL or sound exposure ratio. This is done by converting the SEL as shown in the formula below. Here E_0 is a reference sound exposure.

$$\text{AEL} = \frac{E_n}{E_0} = 10^{\frac{\text{SEL}_n}{10}} \tag{4.24}$$

This new AEL can be inserted in the L_{den} function:

$$L_{den} = 10 \cdot log\left[\sum_{n=1}^{n_{flights}} w_n \frac{E_n}{E_0}\right] - 10 \cdot log\left[\frac{T_{den}}{\tau}\right] \tag{4.25}$$

Now the following equation is used for cumulative noise calculations. This relation will be used in the

[3] The reference time period T_{den} is the product of number of seconds of the part of day the descriptor is defined for. For a complete day this value is 86,400 [s] [47].

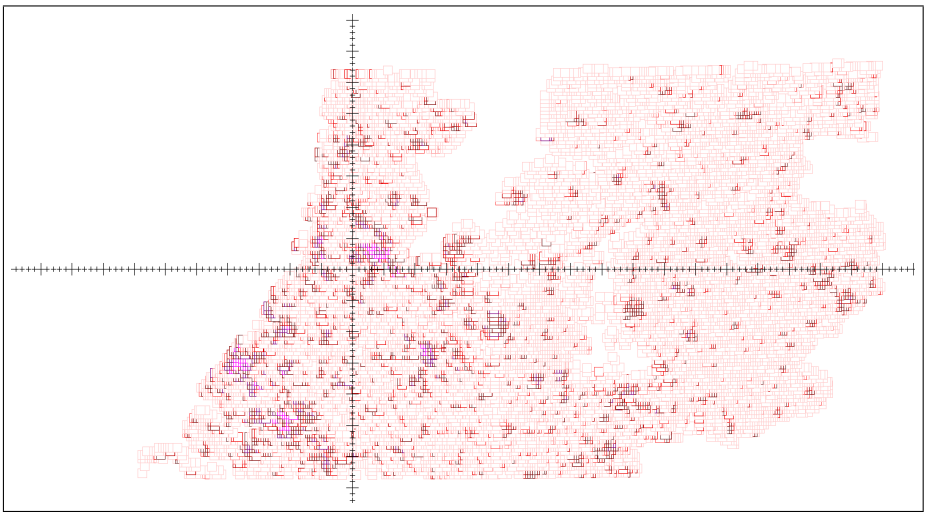

Figure 4.12: RIVM population data in INM where darker colors indicate increased population density.

runway allocation model as will be explained in Chapter 6.

$$\sum_{n=1}^{n_{flights}} w_n \frac{E_n}{E_0} \tag{4.26}$$

4.4.2 Integrated Noise Model

The INM is a software tool designed by the FAA. It has been designed to evaluate aircraft noise impacts in the vicinity of airports and heliports. The INM model is able to calculate SEL for a set of aircraft operations, defined by user input. Aircraft data, airport configuration, flight tracks, grid area and population data can be inserted or selected from existing data within the software model. This generic approach makes it possible to process a wide variety of airports and their specifics. The single event noise exposure can be computed within a pre-established grid. Schiphol Airport has been simulated in terms of runway layout, arrival and departure tracks. Population data is imported in INM for this study. This will be discussed in the following section. For further information on the computations and workings of the Integrated Noise Model, the reader is referred to the INM Technical Manual [48].

4.4.3 Noise Coordinate System

In assessing the noise regulations and limits at airports it is important to know the population specifics of the surrounding areas. Current operations at airports are often restricted for the total amount of people exposed to a certain noise level. It is of key importance to determine population density. Next to this, it has to be researched to what extend noise levels affect the airport surroundings. In this study use is made of the population data provided by Statistics Netherlands (CBS). An official population file of 2008 is used publicized by The Netherlands National Institute for Public Health and the Environment (RIVM). This file represents the situation as it occurred in 2005, when regulations for noise restrictions were established. It consists of *Rijksdriehoek* coordinates; a set of geographic coordinates with population density data. For the study on AAS, this data is used as input for the INM noise model. Figure 4.12 indicates the population density, with Schiphol Airport being the reference point. Different colors indicate a different population density per location point. As will be discussed in the subsequent sections, noise contours can be plotted using INM. Using the noise contours, INM is able to compute the sound exposure at each location point for a set of aircraft operations.

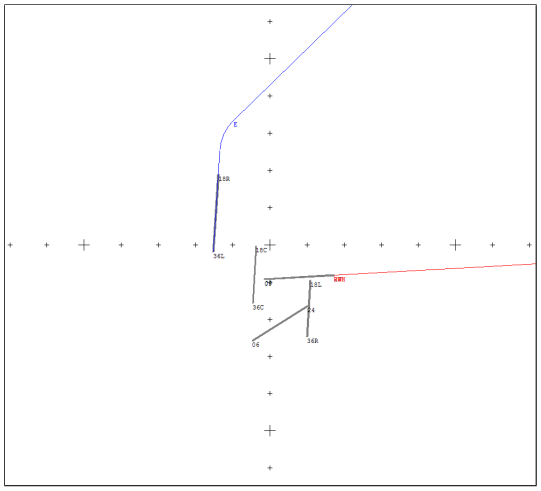

Figure 4.13: Runway tracks in INM.

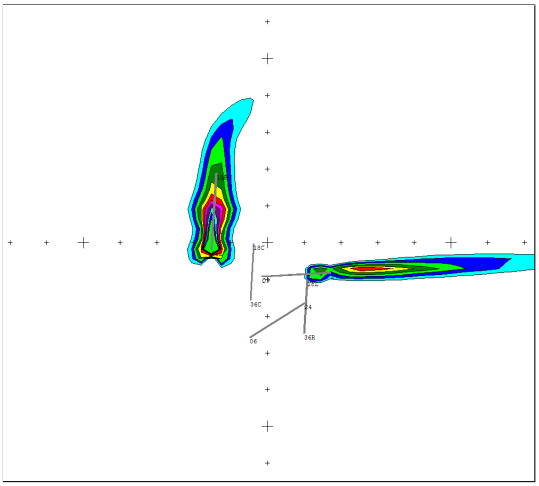

Figure 4.14: Noise contours in INM.

4.4.4 Runways

Flight segments for noise calculations are divided in arrivals and departing operations. Using the Integrated Noise Model, a simulation for departing and arriving aircraft can be processed. Before aircraft can be assigned to an operation, the specific aircraft flight path or otherwise called track has to be defined. If the simulation includes an airport, in this study being Schiphol Airport, first runways have to be entered into INM. In Figure 4.13 it is shown how 5 runways are implemented in the INM model[4]. Here an example is given of runway layout as situated at Schiphol Airport. The crosses correspond to the cross marks in Figure 4.12 and are located at the center of Schiphol Airport.

4.4.5 Flight Tracks

After creating an airport in INM, the next step is to create tracks. In order to display the method applied, this section illustrates flight operations as used in INM. For the departure case, as well as the arrival case examples are given on how the procedures are used in order to establish the flight track and compute noise exposure. The demonstrative examples in this section are simulated using a Boeing 737-800 as aircraft. The configured runways are displayed in Figure 4.13, to represent AAS. Tracks have been added for departure (blue) and arrival (red) operations on runway 36L and runway 27, respectively. Further specifics of these tracks are discussed in the next sections for departures and arrivals.

4.4.5.1 Departures

Figure 4.15 indicates the altitude after an ICAO-A departure on runway 36L. As anticipated, this flight track has identical altitude characteristics as the ICAO-A departure procedure as observed in Figure 2.4. In Figure 4.17 the airspeed is observed. After accelerating for take-off at full thrust, a cutback is performed to the climb thrust level until 3,000 ft is reached. At 3,000 ft the aircraft will fly at 250 kts until the climb-out trajectory reaches 10,000 ft. This is also observed in Figure 4.19, where thrust is highest during take-off.

4.4.5.2 Arrivals

For arrivals different approaches exist as discussed in Section 2.3. For the approach procedure in this example step-wise descent is selected for an operation on runway 27. Figure 4.16 indicates the altitude for an aircraft originating from an IAF location. A brief horizontal segment indicates the transition

[4]In the simulation of the runway layout of AAS the Schiphol-Oostbaan is not incorporated. This runway is only used for smaller aviation or at rarely occurring wind conditions [13].

towards the FAF[5], after which the final descent phase is entered. Airspeed is indicated in Figure 4.18. It is observed that the x-axis represents the distance to runway. At $x = 0$ the start of the runway is reached. After this moment the airplane decelerates significantly. In Figure 4.20 it is observed that during the final phase additional thrust is given in order to keep the aircraft from stalling. Upon reaching the runway tarmac, reversed thrust is applied. This is indicated by the brief leap in thrust displayed by the movement of the blue line.

4.4.6 Noise Grids

After simulating the airport, creating flight tracks, selecting aircraft and assigning arrival or departure operations, the INM model can now calculate sound exposure levels at the inserted population grid points. An example of the noise contours generated by the simulation is shown in Figure 4.14. These are the results for 200 departures and 200 arrivals on the selected runways by aircraft type Boeing 737-800. The AEL can be computed at every gridpoint. For this research the grid points represent longitudinal and latitudinal coordinates with population density. From the following formula it is seen how each gridpoint with coordinates xy is exposed to an energy level, indicated by cost C^N_{xy}. The latter equation is used in the runway allocation linear program, as will be discussed in Section 5.4.3. Here AEL_{xy} is the energy level for gridpoint xy.

$$\text{AEL} = \frac{E_n}{E_0} = 10^{\frac{\text{SEL}_n}{10}} \tag{4.27}$$

$$\text{AEL}_{xy} = C^N_{xy} \tag{4.28}$$

4.5 Emission Computations

Emissions in aircraft operations can be the results of incomplete combustion in aircraft jet engines or are otherwise a product of the combustion process. The fuel flow through the engines is therefore of importance in the calculation of emissions. In several airport regulations, emission of gaseous pollutants is bounded by limits. An example is Airport Schiphol, where governmental regulations are in place to restrict environmental pollution. This study investigates emissions by consulting the ICAO Aircraft Engine Emissions Databank (AEED) [49]. The main assumption here is that emissions are researched only for a given throttle or fuel flow setting, thereby neglecting atmospheric conditions. As recommendation, different methods, e.g. Boeing 2 Method, which include these atmospheric conditions, are given in Chapter 9. In determining emissions several pollutants are considered. These are listed below. Sulphur Oxide (SO), Volatile Organic Compounds (VOS) and Particulate Matter (PM10) are not taken into consideration in this study.

- Carbon Monoxide (CO)
- Nitrogen Oxides (NOx)
- Hydrocarbons (HC)
- Smoke Number (SN)

Data is extracted from AEED[6]. For a multitude of engines, the emissions are given for different flight segments. In Table 4.10 an example is given for the Boeing 737-800 engine, CFM56-7B26. The dimensions are given in gram per kilogram of fuel used. For the Smoke Number, a dimensionless term quantifies the smoke emissions. The Smoke Number is calculated from the reflection of a filter paper measured before and after being exposed to the emitting gas of an aircraft engine. In subsequent chapters the runway allocation model will be further explained with respect to emissions. The emission data is used for two MTOW classes; Medium and Heavy. For each different engine engines and emission data has been evaluated.

[5]For some AAS runways the start of the FAF segment is at altitude 3000 ft, for others this is at 2000 ft. These different altitudes are accounted for in the noise and fuel computations of the Runway Allocation Model.

[6]In this research the ICAO Emissions Databank v21b has been used.

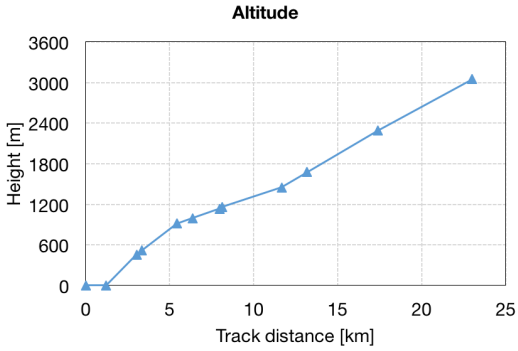

Figure 4.15: Departure: altitude vs distance.

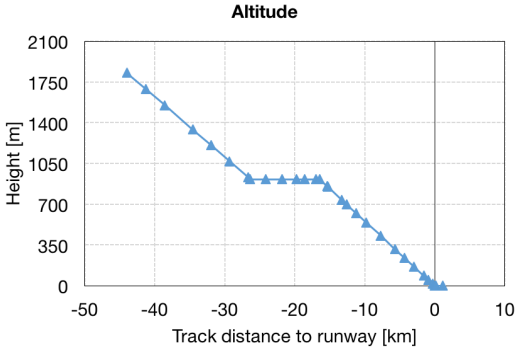

Figure 4.16: Approach: altitude vs distance.

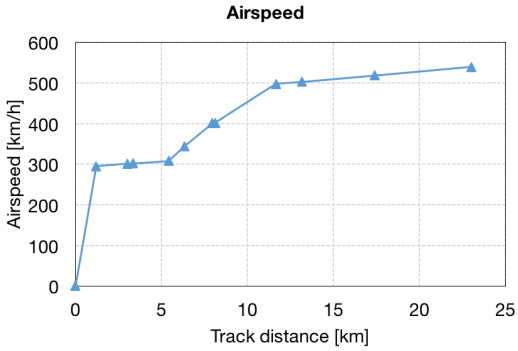

Figure 4.17: Departure: airspeed vs distance.

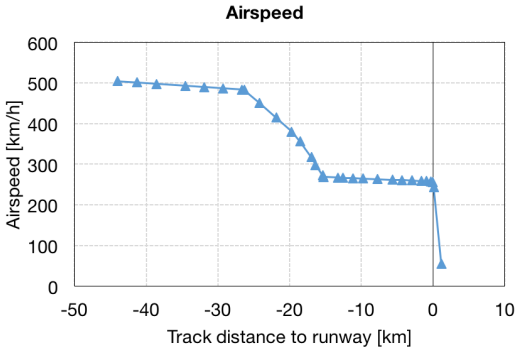

Figure 4.18: Approach: airspeed vs distance.

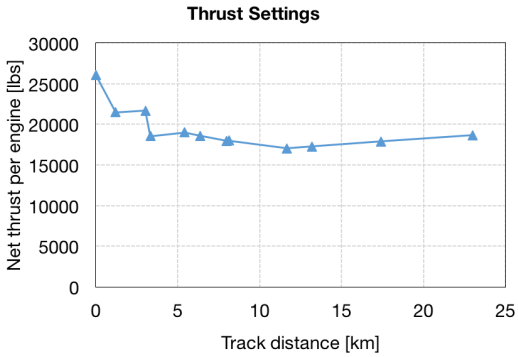

Figure 4.19: Departure: thrust vs distance.

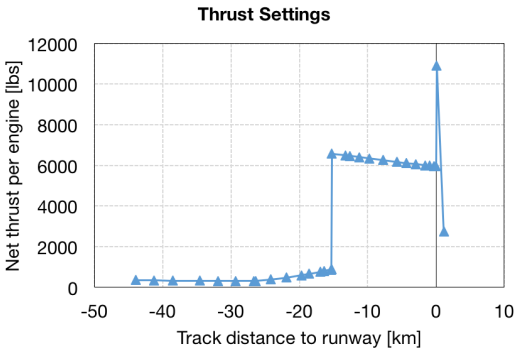

Figure 4.20: Approach: thrust vs distance.

Table 4.10: Emission data per kilogram of fuel used [49].

Emission	Segment	Value	Dimension
CO	Take-Off	0.20	g/kg
	Climb-Out	0.16	g/kg
	Approach	3.07	g/kg
	Idle	30.94	g/kg
NOx	Take-Off	21.79	g/kg
	Climb-Out	17.08	g/kg
	Approach	8.93	g/kg
	Idle	4.27	g/kg
HC	Take-Off	0.02	g/kg
	Climb-Out	0.02	g/kg
	Approach	0.05	g/kg
	Idle	1.75	g/kg
SN	Take-Off	13.10	[-]
	Climb-Out	9.80	[-]
	Approach	2.10	[-]
	Idle	2.10	[-]

Chapter 5

Linear Programming

This chapter explains the optimization problem as to be solved by the runway allocation model. It incorporates the constraining factors as discussed in the previous chapters, such as runway dependencies. It is explained how fuel and noise cost coefficients are inserted and dealt with in an optimization problem. The goal of the objective function is to find an optimum (in this case minimum) for total fuel usage and noise exposure levels, while adhering to the established constraints. The model uses a binary application of Mixed-Integer Linear Programming (MILP) in order to optimize the value for fuel burn and noise. Specifics of such linear programming problem are explained in the first section. Thereafter, the characteristics of the linear programming as used in the runway allocation tool are discussed where important theorems are provided. Finally, optimization solving methods are discussed.

5.1 Mixed-Integer Linear Programming (MILP)

Linear programming is a method used to mathematically find an optimal solution (maximum or minimum) to a problem. The requirements of such mathematical optimization are build on linear relationships. Various fields of study use this method of optimization. While it is widely used in operations research in business and economics, it has a proven track record in engineering and a plurality of other fields. It is often applied in modeling optimization problems in planning, routing, scheduling, assignment and design [50]. The various components of a linear programming model as established for this study are shown in Figure 5.1.

In linear programming a single objective function is optimized. This function is subject to constraints, which may be either of the inequality or equality genus. Variations with multi-objective optimization exist as will be seen in remainder of this chapter. Linear programming optimizes for points at the

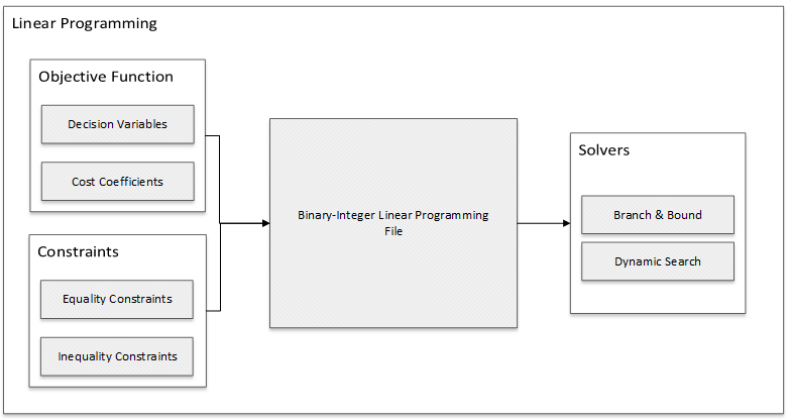

Figure 5.1: Linear Programming components overview.

extreme of a feasible area. It consists of a convex set of points, in which a convex curve shapes the boundary at these extremes. Outside of this feasible area lies the infeasible area for which no solutions exist.

A standard linear problem is formulated in canonical form as follows:

$$\text{Maximize:} \quad C^T x \tag{5.1}$$

$$\text{subject to:} \quad Ax \leq b \tag{5.2}$$

$$\text{And:} \quad x \geq 0 \tag{5.3}$$

In the above equation $C^T x$ is the objective function to be maximized. Here x is a vector indicating the so-called decision variables. In finding an optimum this vector will represent the set of optimum solutions. A cost coefficient is presented by C which is transposed. A is a pre-established matrix and together with b indicate the constraints of the linear problem.

If the problem to be optimized consists of integers, which is often the case in scheduling quantities for whole numbers, the type of problem is called Integer Linear Programming (ILP). These types of problems are often harder to solve than standard linear problems due to the integer nature. The following equation is added to the standard canonical form, indicating the integer characteristics of x. Here $\mathbb{Z}$ is the mathematical symbol representing integers.

$$\forall x_i \in \mathbb{Z} \tag{5.4}$$

Another special case of Integer Linear Programming occurs if both integers and continuous variables coexist. This type of problem is referred to as Mixed-Integer-Linear programming. For the special case that all variables are integer and restricted to be binary (0 or 1), this type of problem is called Binary Mixed-Integer Linear Programming (BMILP) or BILP [51]. The following relation replaces the equations for x_i when a BMILP problem is optimized, here x_i can be either 0 or 1. This type is used for the runway allocation model developed in this study.

$$\forall x_i \in \{0, 1\} \tag{5.5}$$

5.2 Sets and Indices

In this section the sets used to establish the linear problem are defined. Each set consists of parameters or coefficients bearing the characteristics of the set. An overview of the sets is given in the list below. The set of flights F_f has index f for flights and is related to the list of aircraft and represented by the flight number (e.g. KL0612). The set of MTOW classes is defined by M_m in which m may be either Medium or Heavy MTOW class; other classes will not be addressed in this study. Due to the generic nature of the model it is possible for future studies to incorporate other classes using fairly straightforward operations. P_p is the set of aircraft procedures and consists of Arrivals and Departures indicated by index p. It is noted that a flight f always has a predefined and dependent MTOW class m and procedure p. The set of runways is displayed by R_r, where r is the unique runway identification description. The delay steps for which an aircraft can delay are given by set D_d, in which index $d = \{d_0 ... d_{max}\}$ can have the values of $d = \{0, 20, 40, 60\}$ [s] as will be applied in the runway allocation model. T_t is the set of time steps t, indicating the time window for which simulation runs. Finally, $G_x y$ is the set of coordinates for a grid x and y. For the runway allocation model these are converted to longitudinal and latitudinal coordinates.

F_f = Set of flights

M_m = Set of MTOW classes

P_p = Set of procedures

R_r = Set of runways

D_d = Set of delay steps

T_t = Set of time steps

G_{xy} = Set of grid coordinates

5.3 Objective Function

As explained in Section 5.1, a linear problem has an objective function. The optimization model for runway allocation tries to find a optimum value for fuel and noise, in this case a minimum. The following objective function Z is defined which is used in the optimization of the runway allocation problem:

$$\text{Minimize:} \quad Z = \alpha \cdot n_f \sum_{f \in F} \sum_{r \in R} \sum_{d \in D} C^F_{f,r,d} \cdot x_{f,r,d} + \beta \cdot n_n \sum_{xy \in G} C^P_{xy} \cdot G_{xy} \tag{5.6}$$

The decision variables $x_{f,r,d}$ and G_{xy} are explained in the subsequent section. Thereafter, the cost coefficients $C^F_{f,r,d}$ and C^P_{xy} are discussed. It is observed that α and β precede the decision variables. These factors indicate the weighting of fuel and noise respectively and are discussed in Section 5.5. The normalization factors n_f and n_n are equally discussed in that section.

5.3.1 Decision Variables

The following decision variable indicates an aircraft with origin f assigned to runway r and delay d. Flight specifics are given by a flight dependent m, being the MTOW class, and a flight dependent p being the procedure of either arrival or departure.

$$x_{f,r,d} \tag{5.7}$$

$$G_{xy} \tag{5.8}$$

It holds that $x_{f,r,d} = 1$ if flight f with appointed runway r, with delay d is selected, otherwise $x_{f,r,d} = 0$. The decision variable G_{xy} holds information for the longitudinal and latitudinal coordinates. It has a value of 1 if a certain noise limit is crossed, otherwise it has a value of 0. This switching procedure will be explained in the section on constraints. The statements indicating the binary nature are displayed by adding the following lines to the linear problem:

$$\forall x_{f,r,d} \in \{0, 1\} \tag{5.9}$$

$$\forall G_{xy} \in \{0, 1\} \tag{5.10}$$

5.3.2 Fuel Cost Coefficients

The cost coefficients for fuel identify the cost for a given flight. For the arrival case this is done for the segment starting at an IAF location to a runway. For the departing case this is done for the segment of the runway up to leaving the sector perimeter. The cost is expressed in kilograms of kerosene used for the given flight. How the values for this cost function are established is discussed in Section 4.3. As indicated below, the fuel coefficients are depended of flight, MTOW class, procedure, runway and delay.

$$\text{Fuel cost coefficient:} \qquad C^F_{f,r,d} \tag{5.11}$$

5.3.3 Population Cost Coefficients

The cost coefficient for population is indicated by C^P_{xy}. The value indicates the amount of people or houses within a grid G_{xy}. It states the number of houses or persons exposed to a certain noise level at a certain longitude and latitude coordinate. The data on population density as extracted from population data by CBS, consists of inhabitants per gridpoint. In order to convert this measure to houses per gridpoint the official conversion rate of 2.2 persons per residence [52] is used[7].

$$\text{Population cost coefficient:} \qquad C^P_{xy} \tag{5.12}$$

[7] The conversion is done since Amsterdam Airport official noise exposure limits are defined by sound exposure for a maximum amount of private residences [10].

5.4 Constraints

The minimization function is subject to several constraints. The constraining factors are the elements which influence the allocation and flight trajectories of the operating aircraft. They are split up in two different types of constraints; inequality and equality constraints. One of the inequality constraint which acts as a switching function is discussed separately in Section 5.4.3.

5.4.1 Equality Constraints

The first constraint is the Always Assign Flight constraint. This constraint makes sure that whenever an aircraft is selected by the solving algorithm, it is always assigned to a runway. Omitting this constraint would result in unassigned airplanes and that would therefore go lost in the process. An airplane can only be assigned if it has the possibility of actually reaching the runway r in a given time frame and within a given delay d.

$$\text{Always Assign Flight AAS}_f: \quad \sum_{r\in R}\sum_{d\in D} x_{f,r,d} = 1 \qquad \forall f \in F \tag{5.13}$$

Using the same method of equality, runways can be omitted from being assigned to. This Runway Restriction constraint may occur when a runway is under maintenance, and aircraft are prohibited to use this runway. Another possibility is the restriction of certain runways due to local conditions, such as wind and visibility. Other possibilities of simulating restrictions may prove beneficial if simulations are desired with a specific set of runways available. The constraint which restricts certain runway operations is given below, where R_{res} is the set of restricted runways:

$$\text{Runway Restriction RR}_r: \quad \sum_{f\in F}\sum_{d\in D} x_{f,r,d} = 0 \qquad \forall r \in R_{res} \tag{5.14}$$

5.4.2 Inequality Constraints

As opposed to equality constraints, inequality constraints are defined by inequality signs. Runway dependencies are implemented using these types of constraints. The Runway Occupation constraint is a constraint set in order to have not more than one aircraft per location via an inequality constraint. Here R_{dep} indicates the time-dependent runways from the dependency matrix. The flights in F_{dep} within a certain time window are affected by the runway dependencies.. For all given runway dependencies from Chapter 4, constraints are established in the following form, where $n^{DM}_{f,r,t}$ is a binary constant resulting from the dependency matrices indicating if the dependency becomes active (1) or inactive (0):

$$\text{Runway Occupation RO}_{r,t}: \quad \sum_{f\in F_{dep}}\sum_{d\in D} n^{DM}_{f,r,t}\cdot x_{f,r,d} \leqslant 1 \qquad \forall r \in R_{dep},\ \forall t \in T \tag{5.15}$$

5.4.3 Noise Limit Switching Constraint

The noise limit switching constraint uses a logical function to check if a noise limit L_{limit} is reached[8] at a certain gridpoint xy. If indeed a limit is reached a value of 1 is assigned to G_{xy}. This occurs for example when to many aircraft passing the same location point, hence generating more noise than allowed. In total not more than a given amount of houses may be exposed to this limit in the case of Schiphol Airport, as was showed in Section 2.3.2. M stands for a very large number and is part of the

[8]For Schiphol Airport the noise limit is identified to be 58 dB(A) L_{den} for annual operations [19].

Big M method. The theorem behind the Big M method is explained in the subsequent section. The Noise Limit Switching constrained is indicated by the following function:

$$\text{NLSC}_{xy}: \quad \sum_{f\in F}\sum_{r\in R}\sum_{d\in D} C^{N}_{xy_{(f,r,d)}} \cdot x_{f,r,d} - M \cdot G_{xy} \leq L_{limit} \qquad \forall xy \in G \tag{5.16}$$

The cost coefficients for the noise grid $C^{N}_{xy_{(f,r,d)}}$ indicate AELs as found through INM for every gridpoint xy as discussed in Section 4.4.6. L_{limit} consists of the local noise limit and the time averaging factor and depends on the considered time period as was observed in Section 4.4. The limit is illustrated in the formula below. Here $Lim_{L_{den}}$ is the L_{den} limit for an airport expressed in dB(A) . T_{den} is the time period considered, τ is a reference time of 1 second.

$$Lim_{L_{den}} = 10^{\frac{L_{den}}{10}} \tag{5.17}$$

$$L_{limit} = L_{L_{den}} \cdot \frac{T_{den}}{\tau} \tag{5.18}$$

5.4.4 Big M Method

The Big M theorem is applied as a switching function. A logical condition and indicator variables are used to impose conditional restrictions. Here the fundamental basics of this method are explained. The Big M method is used in the Noise Limit Switching Constraint in order to apply a switch if a certain noise level is exceeded. A distinction is made between hard constraints as seen in the previous section, which are constraints that cannot be violated and on the other hand soft constraints. These latter constraints can be violated but at the cost of a penalty [53]. For the Big M method this penalty is expressed as a large number.

In the following set of equations, a nonzero value in a group of variables (X) could potentially imply a nonzero in another group of variables (Y). If this occurs, a switch is used. By this switching technique a group of variables may change value.

$$\sum X_i - M \cdot Z_k < L \tag{5.19}$$

$$X_i \geq 0 \tag{5.20}$$

$$Z_k = 0 \text{ or } 1 \tag{5.21}$$

Z is a binary value of either 0 or 1. M is a very large number. In this example when Z = 0, X has to be smaller then L, hence fulfilling the constraint. If X is larger then L, the value of M is needed to satisfy the equation. Resultantly, when X crosses the limit of a value L, Z will change value from 0 to 1. Hence a switch is now in function. Z is an indicator variable indicating whether any X_i has been assigned to change. The value of M should exceed the value of the maximum attainable summation of all i in X_i. For the Noise Limit Switching Constraint the value of M is established by the summation if were all binary values of $x_{f,r,d}$ equal to 1.

5.5 Normalization

In this section the normalization technique is explained; for which several variants and procedures exist. This section explains the rationale for selecting the weighted sum normalization method, in which a Pareto front is created.

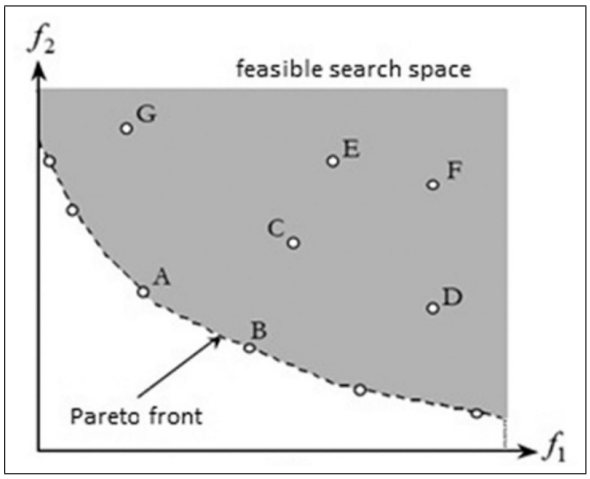

Figure 5.2: Pareto front with indication of the feasible region [56].

5.5.1 Weighted Sum Method

The weighted sum method is chosen as the most suitable normalization method for this type of problem. It allows the multi-objective optimization problem to be equated as a single-objective problem [54]. Other methods exist such as Cascaded Weighted Sum, hierarchical or ε-constraint methods. Due to their complexity they were deemed inappropriate for the linear problem for this research. The Weighted Sum Method consists of a sum of the objective functions to be optimized multiplied by a weighting coefficient α or β. Ideally these coefficients are normalized to have a sum of 1. Using this method, the weighting can be adjust to fully optimize for fuel or for noise, or any other trade-off combination. The following formula shows that α and β have the following relation and range from 0 to 1:

$$\alpha = 1 - \beta \tag{5.22}$$

Since both objectives, fuel and noise, have different dimensions, normalization has to be applied. It is now possible to get a Pareto optimal solution which is consistent with the weights of α and β assigned. It is chosen to set the normalization as a range of the minimal and maximal solution for both fuel and noise results. By selecting this range a dimensionless trade-off can be performed. This is shown in the formulas below for fuel and noise, respectively:

$$n_f = \frac{1}{f_{fuel}^{norm}} = \frac{1}{max(f_{fuel}^{noiseoptimized}) - min(f_{fuel}^{fueloptimized})} \tag{5.23}$$

$$n_n = \frac{1}{f_{houses}^{norm}} = \frac{1}{max(f_{houses}^{fueloptimized}) - min(f_{houses}^{noiseoptimized})} \tag{5.24}$$

5.5.2 Pareto Optimality

The optimal solutions which are found by applying appropriate weights using the Weighted Sum method form a so called Pareto optimal set [55]. The points which correspond to this optimal set are named Pareto points. The curve which connects these optimal points is called a Pareto curve or Pareto front. This is clearly depicted in Figure 5.2. The feasible area consists of all possible solutions, whereas the Pareto front is the set of optimal solutions, which are determined in this study. These are indicated as A and B in the figure. f_1 and f_2 indicate both objectives. In order to optimize the objective function, several optimization methods exist to determine the optimal Pareto solutions.

5.6 Optimization Algorithms

Several optimization algorithms exist. The optimization software used in this study is CPLEX. It is able to compute a linear problem as explained in this chapter. CPLEX can apply various methods of optimization. Most commonly used are the Branch & Bound algorithm and the Dynamic Search algorithm. Both are successful in optimizing the problem as stated. The methods are briefly discussed below.

5.6.1 Branch & Bound

Branch & Bound (BB) is often used for NP-hard problems. A set of potential solutions is established as a tree, were the root indicates the total set. The algorithm looks at branches of the tree; Upper and lower bounds are compared to a previously found solution. If the new solution is words then found solution, the branch is discarded. CPLEX uses advanced BB operations, cutting planes and heuristics to find integer solutions.

5.6.2 Dynamic Search

For a variety of models, dynamic search locates feasible and optimal solutions faster than conventional branch & cut procedures. CPLEX has an advanced algorithm which finds optimal solutions for Mixed-Integer Linear Programming problems faster than its peer algorithms. After comparing several methods for their accuracy and speed, this method was selected for the optimization in the runway allocation model.

Chapter 6

Runway Allocation Model

This chapter will elaborate more on the developed runway allocation model. A concept description, objectives and assumptions are listed. The models decision variables, minimization function and constraints were discussed in the previous chapter. Their implementation in the actual model is explained in this chapter. Additionally, an overview of the model structure is presented. The final section will discuss computational performance.

6.1 Concept Description

The runway allocation model developed for this study is able to assign aircraft to runways based upon an optimization trade-off between fuel usage and noise exposure to the environment. In doing so, a multitude of scenarios may be simulated using the model. Different allocation schemes can be tested and the possibilities of potential gains in fuel and noise reduction are researched. Emission outcomes, since taken linear to fuel, are equally researched. The model has been developed[9] generically so that scaling up of the problem size is possible. Other airports, a larger set of aircraft and aircraft types, different arrival and departure operations can all be added to the model due to the generic characteristics. This is favorable for future academic and industry research in ultimately finding an efficient optimized trade-off between fuel use and noise exposure and possible expansion towards other fields of study. This section describes requirements and important assumptions made.

6.1.1 Objective

In order to address the objective of reducing fuel burn and optimizing noise exposure using a novel runway allocation model, the following requirements are established:

- Minimize total fuel burn.
- Delay is kept within pre-established limits.
- Desirable runway throughput capacity is maintained.
- An actual flight schedule can be used as input.
- Aircraft can be divided in 2 MTOW categories: Medium and Heavy.
- Model is applicable to the Schiphol Airport runway configuration and other airport configurations.
- Runway configuration can be altered (e.g. maintenance on 1 or more runways).
- Runway dependencies and separation constraints can be generically incorporated.
- Comparison with currently used Preference List has to be possible.
- Results can be reviewed and compared on their noise hindrance impact.
- Computing time has to be within acceptable bounds.
- The model is generic and can be applied to a wide variety of airports, aircraft and procedures.

[9] The Runway Allocation Model has been developed using MATLAB R2015b.

6.1.2 Assumptions and Limitations

During the development several assumptions have been made. These may be the result of limitations with respect to the available data. The most significant assumptions in developing the model are listed below:

- A linear relation between fuel consumption and emission discharge per flight segment is assumed.
- Flight and taxi distance determines the fuel cost per route. This distance is found through extraction of AIP information charts and is therefore an approximation of reality.
- It is assumed that there is no distinction between step wise or continuous decent in terms of fuel consumption.
- Aircraft per category are assumed to fly at same $V_{approach}$. Therefore there is no distinction between the opening and closing case of consecutive approaching aircraft.
- Arrival times at IAFs are assumed fixed as a result of the flight schedule. Possible different time of arrival at IAF due to delay upstream is not taken into account.
- For increased delay a penalty is added to the fuel costs. Delay is not incorporated within the noise computations through INM.
- An average wind speed and direction is assumed; only 1 wind-vector per scenario run is selected based on annual expectations.
- Visibility is assumed constant during the day, posing possible restrictions on runways. Additional separation distance due to visibility is not taken into account.

6.2 Model Structure

In order to establish a functional runway allocation model, several components are needed to interact. In the previous chapters the different methodologies have been discussed for runway dependencies, fuel, noise, emissions and linear programming. The runway allocation model combines these. A framework is given in Figure 6.1 where the interaction of different parts is illustrated. A script has been developed in which all separate functions are called and is identified as `RunwayAllocationTool`. The different functions and elements are explained is this section.

6.2.1 Input

The model demands several sets of input. User input is given to define the appropriate scenario. A flight schedule is loaded into the model. Additionally, an airport specific dependency matrix is inserted. These are individually explained in this section.

6.2.1.1 User Input

User input is handled by the `input_userinput` function. It is important in defining the scenario. As will be shown in the following chapter for the AAS case study, scenario settings can be changed according to the user's preference. By changing the input parameters a multitude of scenarios can be computed. In Figure 6.2 the Graphical User Interface (GUI) is displayed of which the specifics are explained in Table 6.1. An important aspect of the user interface is the possibility to choose a procedure for single or for multiple runs. By selecting multiple runs (option 2), the allocation tool will consecutively simulate scenarios with a range of different noise and fuel weights (α and β). This is done using the `write_weightedfunctions` function. Automatically a set of runs will be combined in order to find a set of Pareto optimal points, indicating the Pareto front. In order to set up the normalization factors and initial run is needed to determine the maximum and minimum ranges. This will be further analyzed in Chapter 7. Next to the user input through the GUI, other parameters have been set within the model. Some examples are the noise penalties for operations during day, evening, night, noise limits, population limit, and other airport specific factors.

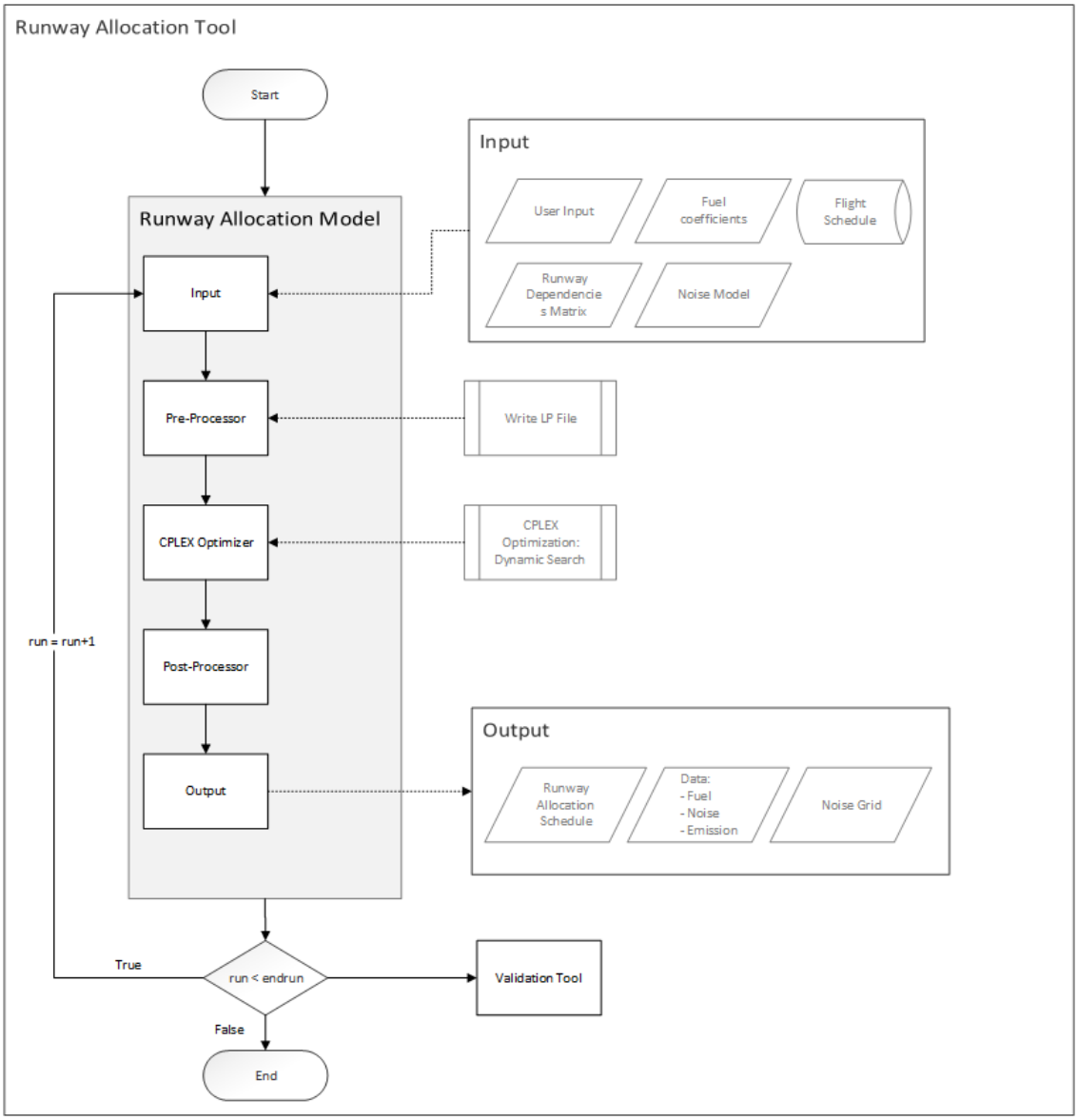

Figure 6.1: Runway Allocation Model Architecture.

Table 6.1: Graphical User Interface input options.

Input Parameter	**Description**
Enter run	Give run a unique ID.
Scenario Day	Choose scenario day 1 or scenario day 2.
Procedure	Choose procedure 1 for a single run.
	Choose procedure 2 for multiple normalized runs.
	Choose procedure 3 for reference scenario runs.
Enter time start	Enter starting time, starting from 06:00 AM.
Enter time duration	Enter the run duration time window.
Runways unavailable	Enter the runways to exclude (due to local conditions or maintenance).
Departures only	Enter runways where arrivals are prohibited.
	E.g. under certain local conditions such as wind and visibility.
Arrivals only	Enter runways where departures are prohibited.
Maximum delay	Enter the maximum delay an aircraft may experience.
Fuel Weights: α	Enter the weights for fuel from 0 to 1 (β is always converted to 1 - α).
Normalization factor: n_f	Enter the normalization factor for fuel computations.
Normalization factor: n_n	Enter the normalization factor for noise computations.

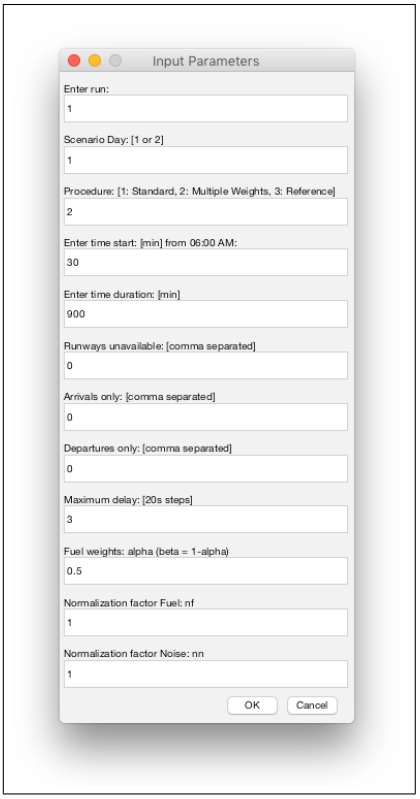

Figure 6.2: User input.

6.2.1.2 Schedule

The runway allocation model works with an input feed of a flight schedule via the `input_schedule` function. This schedule consists of actual flight data of arriving and departing aircraft. An excerpt of such a flight schedule is found in Appendix C. Several important elements are extracted from this flight schedule which are summarized below. The schedule used in the model is an augmented version of the actual flight schedule. For this research the arrival time at the Initial Approach Fix is needed for arriving aircraft. Accordingly, the Actual Landing Time is adapted to find the time at IAF using a

Time to Runway matrix. An overview of this matrix is found in Appendix C.2. Once the time at IAF is known, it can be calculated at which times the aircraft can potentially arrive at all runways within the given runway set.

- Aircraft ID
- Actual Landing Time (ALDT)
- Actual Take-Off Time (ATOT)
- Aircraft MTOW category
- IAF for arrivals
- SECTOR for departures

6.2.1.3 Airport Specific Dependency Matrix

Runway dependencies are handled by the `input_dependencies` function. Runway dependencies have been elaborately discussed in Section 3.5. Correlation between runways plays a major role in restricting runways and therefore has a significant impact on runway capacity. The runway dependency matrices have been established generically, meaning they are provided separately from the model itself and can be easily adapted to any preferred scenario. Pivoting to other airports or implementing additional dependencies is possible. An overview of the dependency matrices used in the runway allocation model is found in Appendix H. An example of a runway dependency for a Medium MTOW aircraft, in arrival operation on runway 06 of Amsterdam Airport Schiphol is displayed in Figure 6.3. A runway dependency matrix is specified by the following characteristics:

- Runway
- MTOW class
- Type of operation: Arrival or Departure
- Consecutive flight operation: AD/DA/AA/DD

R06 - Medium - Arrival														Dependency
nr	1	2	3	4	5	6	7	8	9	10	11	12	13	
Time	-120	-100	-80	-60	-40	-20	0	20	40	60	80	100	120	
Steps	-6	-5	-4	-3	-2	-1	0	1	2	3	4	5	6	
R06	0	0	0	0	0	1	1	1	1	1	0	0	0	ROT
R09	0	0	0	0	0	0	0	0	0	0	0	0	0	
R18C	0	0	0	0	1	1	1	0	0	0	0	0	0	Missed Approach
R18R	0	0	0	0	0	0	0	0	0	0	0	0	0	
R24	0	0	0	1	1	1	1	1	1	1	1	0	0	Opposite
R27	0	0	0	0	0	0	0	0	0	0	0	0	0	
R36C	0	0	0	0	1	1	1	1	1	0	0	0	0	Intersecting
R36R	0	0	0	0	0	0	1	1	1	1	0	0	0	Missed Approach
R18L	0	0	0	0	0	0	1	1	1	1	0	0	0	Missed Approach
R36L	0	0	0	0	0	0	0	0	0	0	0	0	0	

Figure 6.3: Runway Dependency input (AAS RWY06 example).

6.2.2 Pre-processor

The pre-processor has the function of writing an LP-file (linear programming). This is needed as the subsequent part in the model, the optimizer, has to be feeded an LP format file. The objective of the pre-processor is to transform the various inputs into a readable linear programming problem file. Another feature is reducing the computational process time needed by the optimizer through discarding infeasible solutions. The output of the pre-processor is a file defining objective function, constraints and bounds. The Integrated Noise Model is used as input for apriori calculations. The INM model has been demonstrated in Section 4.4.2.

6.2.2.1 Decision Variables

Decision variables are written using the `write_DV` function. In order to simulate allocation operations using linear programming decision variables form the basis of further computations. The results after

optimization has been applied will consists of decision variables in binary vector format. This vector will be further processed in the post-processor.

6.2.2.2 Fuel Costs

Fuel costs are established using the `write_costsFuel` function. The fuel cost coefficients are collected and processed for the selected flights. Here the previously discussed fuel computations are applied. Fuel usage is dependent on MTOW class. For every class a different set of fuel coefficients is equated and stored in a fuel coefficient matrix.

6.2.2.3 Noise Costs

Noise costs are processed in the `write_costsNoise` function. This function makes use of the output of the values from the Integrated Noise model as explained by the methodologies in Section 4.4. Several important steps are performed to establish a noise coefficient matrix.

- Cut off value: A cut off value is applied to the raw data of Acoustic Energy Levels for all gridpoints. By applying this procedure all insignificant energy levels are discarded. These values have a negligible impact on the noise exposure on the environment. Performance is drastically improved.
- Grid reduction: After applying a cut off value for individual energy levels, further reduction of the total longitudinal and latitudinal grid is applied. Reducing the grid size is done by eliminating points which, for a full day of flight, never reach the noise limit. Since the problem is NP-hard, as seen in Section 5.1, the problem increases rapidly when the size of the problem grows. By reducing the number of gridpoints a significant increase in efficiency is gained.
- MTOW: Different MTOW classes produce different noise contours for a given flight segment. For this reason Medium and Heavy aircraft classes are processed separately. The noise costs are therefore dependent on MTOW.
- Noise penalty: Noise penalties are given for operations during the evening and night. The was previously summarized in Table 4.9 from Section 4.4.

6.2.2.4 Linear Programming File

The function `write_LP2file` writes the optimization problem in linear programming form. The input from the user, flight schedule and runway dependency matrix has now been processed in the pre-processor. Cost functions for fuel and noise have been established. The next step is to aggregate these elements and form the linear programming problem. This done using the function `write2LP`. By writing the linear problem to an exterior LP file, computational performance is increased.

6.2.3 Optimizer

Use is made of the IBM ILOG CPLEX Optimization Studio 12.6 optimizer. It makes use of optimization algorithms as discussed in Section 5.6. The CPLEX optimizer uses the LP-file as produced in the pre-processor as input. The CPLEX optimizer now finds the optimal solution for the optimization problem. The output is passed to the post-processor. The computation time of the CPLEX solver is important as it take up the lion's share of total computation time. Certain parameter settings can be adjusted to improved the performance of the solver. The time limit parameter is adjusted so the solver gives the optimal solution it found at the moment of reaching the time limit.

6.2.4 Post-processor

The post-processor extracts the optimization results. Here the decision variables are of primary importance. These have to be displayed in a readable manner, hence transforming the decision variables back to a readable schedule. The post-processor is used to generate a graphical representation of the new runway allocation per runway. The output as generated by the post-processor contains the following factors.

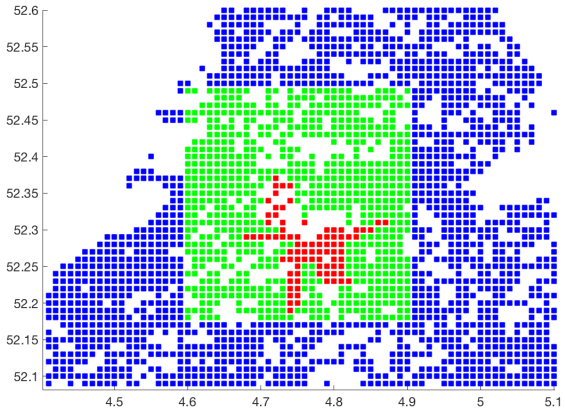

Figure 6.4: Runway Allocation Model output: Example noise grid distribution for a fuel optimized schedule.

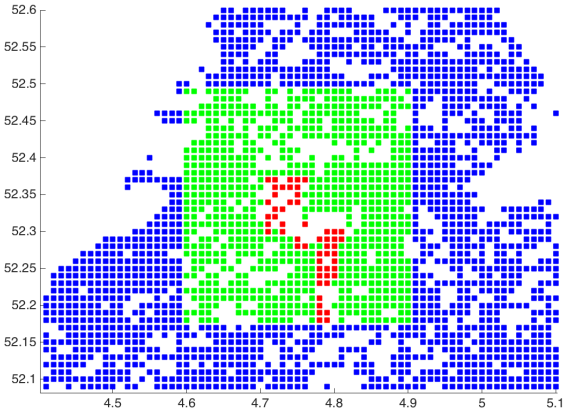

Figure 6.5: Runway Allocation Model output: Example noise grid distribution for a noise optimized schedule.

- New runway allocation overview
- Fuel burn (emissions/cost) result
- Noise Grid
- Emissions
- Runway usage intensity
- Delay

6.2.4.1 Allocation Schedule

The optimized runway allocation schedule is processed through the `output_plotresults` function. It gives an overview of all flights assigned to their optimized runway. This will be discussed in Chapter 8, where an example will be given and compared to the conventional runway allocation schedule.

6.2.4.2 Fuel

Fuel usage is computed by the `output_fuelusage` function. The new runway destinations of all the assigned aircraft are known after optimizing. This function finds the resulting fuel usage per segment. The total fuel used is dependent of the IAF to runway segment for arrivals, and the runway to Sector segment for departures. In this fuel computation delay is accounted for.

6.2.4.3 Noise

Noise exposure to the environment is made graphically visible using the `output_plotresultsGrid` function. In Chapter 7, this is observed by the various noise grid plots. The algorithm which computes the noise exposure first defines all the existing population grid points in longitudinal and latitudinal coordinates. Thereafter it computes the selected grid window in which measurements are performed. Finally, it computes the longitudinal and latitudinal locations for which a given noise limit is exceeded. In Figure 6.4 and 6.5 examples are given for a fuel and noise optimal scenario. Here the grid consists of population gridpoints indicated by blue. The selected grid for which optimization is performed is indicated by green squares. If a noise limit is exceeded for a certain gridpoint, a red square will be displayed. Every gridpoint has a value for population density expressed in number of residential houses attributed to it.

6.2.4.4 Delay

Delay per flight is equated via the `output_delay` function. Every flight is assigned a value for delay, $d = \{0, 20, 40, 60\}$ [s]. The algorithm computes the total delay per runway to an indication of how

delay is handle by the runway allocation model. An output is given in which the total airplanes per delay step are displayed. Next to this the total delay for the complete schedule is visualized.

6.2.4.5 Emissions

Emissions are handled by the `output_emissions` function. The output is given for four gaseous pollutant, as was elaborated on in Section 4.5. The total emissions are given in kilogram for the complete simulated schedule. The results are given for every flight segment; approach, taxi and departure.

6.3 Computational Performance

Performance of the model in terms of computation time is important. It is desirable to achieve results within a reasonable period in order to compile a complete Pareto Front. In the Industry it is beneficial if computation times are within a given amount of time. Possibilities of including a live flight schedule are eminent. In order to work with a real time schedule, and be able to calculate optimum allocation slots, the scenarios should be run in reasonable time. Two elements are computationally most time expensive, as computation benchmarks using the Matlab Profiler indicated:

- `write_LP2file`: Since the linear program LP-file can consist of up to a hundred-thousands lines of code, it takes time to write the complete file. This is mitigated by storing the constraints in a separate file. This way the largest part of the LP-file has to be created only once for the multiple run procedure (2); per run only the objective function part is rewritten.
- `CPLEX optimizer`: The CPLEX optimizer uses complex algorithms to find optimal solutions. For large problems the optimizer only slowly converges towards a predefined minimum gap before an optimal solution is indicated. To mitigate this time consuming process, a time limit can be applied. It has to be noted that the solution deteriorates, the shorter this computational time window is set. The time limit is chosen to be 300 seconds for a single optimization run. This value is selected after multiple tests with different time limits. On average the solution reached an adequate gap tolerance for a proven optimized integer feasible solution of 0.10% within this time limit. From Figure 6.6 is it observed that the CPLEX solver takes up most time with respect total computation time. For run 1, 3 and 4 the solver has found an optimal solution within the time gap, indicated by a lower height of the stacked bar.

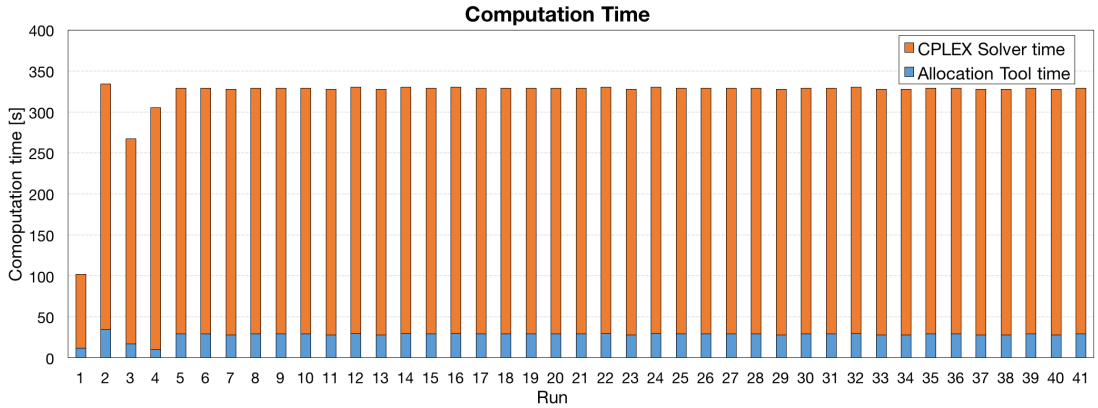

Figure 6.6: Computation time performance for the multiple run procedure.

Chapter 7

Case Study: Schiphol Airport

In this chapter the runway allocation model will be applied to the Amsterdam Airport Schiphol case. The case study will show how the model works if applied to real airport operations. Actual flight data is used as input for the flight schedule. Fuel, noise and emission computations which have been explained in the previous chapters are applied to the AAS case. In this study several scenarios will be tested. These scenarios are based on data for two days. In the subsequent chapter, results of the scenarios will be discussed more elaborately. In order to investigate the results, the two scenario days are split up in different day segments, being morning, afternoon and evening operations at Schiphol Airport.

7.1 Description

As discussed in Chapter 2, Schiphol Airport is compared to other airports an interesting and complex airport due to its runway layout. Operations on several runways incur restrictions on other runways as has been explained in Section 3.5. It has been observed that currently a runway preference list is in play in order to allocate arriving and departing aircraft to runways. By flexible allocation, inherently deviating from this so called preference list, may result in fuel and noise savings. Due to the complex structure of the runway layout, the level of flexibility is therefore higher at AAS in comparisons to airports with solely single- or dual-runway layout.

What this case study tries to establish is to compare the existing standard preference list operations with the novel method explained in previous chapters. It is identified to which extend fuel and noise may be optimized, in order to save on total fuel usage, while maintaining noise regulation limits as discussed in Section 2.3.2. Emissions are evaluated under the assumption of having a linear relation with fuel use per segment.

7.2 Model Input

It was explained in Chapter 6 that the input variables for the runway allocation model are the following; fuel coefficients, noise coefficients, runway dependencies, regulations and flight schedule. These are briefly discussed in this section in their relation to Schiphol. Firstly, several key assumptions are listed.

7.2.1 Assumptions

Although the runway allocation model tries to simulate runway operations as occurring at airports, it is important to highlight that it is a mere simulation of reality. To make this research and case study experiment reproducible for future studies, several assumptions are explained below. The assumptions made in developing the model are the following:

- Time segments are established based on peak moments in air traffic from Table 7.1.
- Flight schedule is based on actual data made available by Schiphol Group.
- Only 2 aircraft MTOW types are taken into account; Heavy and Medium.

Table 7.1: Peak Moments at Schiphol Airport.

Movement	Time start	Time end
Inbound	8:00	9:30
Outbound	9:45	11:15
Inbound	12:00	13:30
Outbound	13:45	15:00
Inbound	15:00	15:45
Outbound	16:00	16:45
Inbound	17:00	18:30
Outbound	19:00	20:30

- Wind speed and direction is averaged, only 1 wind vector based on annual expectations is taken into account per scenario.
- Wind- and visibility conditions are assumed constant during the day.
- Runway dependencies are computed using previously established methods and associated assumptions.
- For Scenario 1 wind factors are neglected due to low level of wind speeds.
- For Scenario 2 wind factors are accounted for by restriction of operations on a set of runways.

7.2.2 Fuel

In Section 4.3, the generic methodology in order to calculate fuel coefficients has been explained. It was displayed how optimization coefficient for fuel are researched and inserted for the AAS case. Here the flight tracks or segments are unique for Schiphol. Fuel calculations are performed for the Boeing 737-800 (Medium MTOW class) and Boeing 777-200ER (Heavy MTOW class).

7.2.2.1 Segments

A key element for fuel coefficients is the distance an aircraft will fly on a certain segment. This segment is for arrivals the distance between a point of entry, being the location of an Initial Approach Fix, and the gate. For departures, the segment starts at the gate and has its end point when a flight leaves a certain Sector. This is readily discussed in previous Section 4.3.2. In the Schiphol case study these segments are identified from AIP charts, Appendix A. For the Schiphol scenario fuel calculations, the assumption has been made that one aircraft per MTOW class is modeled for the total aircraft fleet. Although this is a simplification of reality, the scenario setup will evaluate preference list allocation and new flexible allocation with respect to each other. Relative improvements will therefore be found for the the discussed segments. Fuel data computed in this scenario does not necessarily represent actual fuel data, notwithstanding, the percentage difference with respect to the reference scenario gives a reasonable indication of the potential gains on the given segments.

7.2.3 Noise

The methodologies used for noise computations are discussed in Section 4.4. Using the Integrated Noise Model for the AAS case, noise impact can be calculated for a given grid. By using the population data in longitudinal and latitudinal coordinates, a grid is established. The optimization model will analyze the selected grid, as is observed by Figure 7.1. A map of the Netherlands is shown in which blue markers are the population points available from CBS data [52]. Here the green square indicates the location points for which the algorithm computes noise. Further on in this chapter it will be shown that whenever a noise limit is exceeded at a given point, this will be indicated in the noise grid.

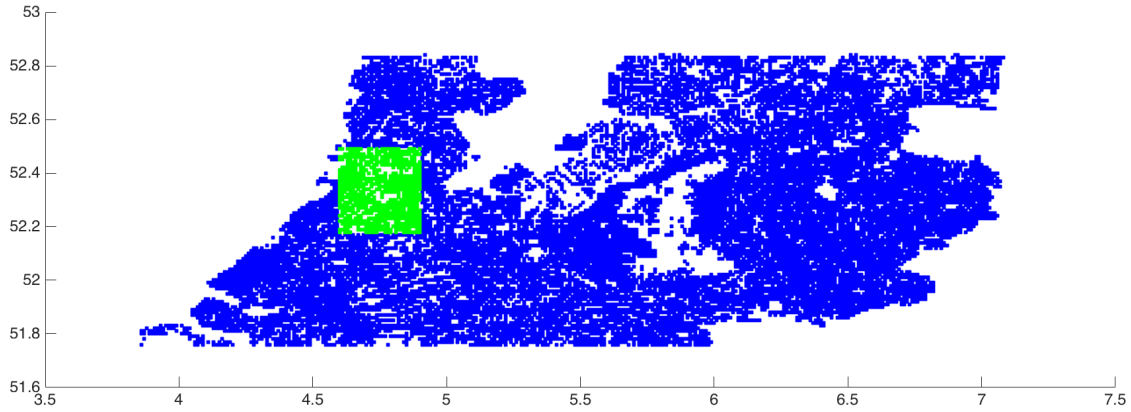

Figure 7.1: Noise grid with latitude and longitude coordinates: Blue dots indicate population points, green dots indicate the scope for which the runway allocation model calculates and optimizes noise.

Table 7.2: Scenario time segments.

Scenario	Time start	Time end	
Scenario 1	Full day run	06:00	00:00
	Morning run	06:00	12:00
	Afternoon run	12:00	18:00
	Evening run	18:00	00:00
Scenario 2	Full day run	06:00	00:00
	Morning run	06:00	12:00
	Afternoon run	12:00	18:00
	Evening run	18:00	00:00

7.3 Scenarios

The model will try to optimize fuel burn during the arrival, departure and taxi-phase of aircraft operating on Schiphol Airport. This is done by smartly and flexibly allocating aircraft on runways, resulting in shorter flight routes and potentially reduced delay. The fuel burn is compared to the currently applied situation in which aircraft follow a strict runway preference list, focusing on reducing noise exposure on surroundings. In order to display the workings of the Runway Allocation model several scenarios are tested. Two scenario days of Airport Schiphol operations are discussed in which a reference scenario is run in tandem with the scenario as computed by the allocation tool. Parameters remain unchanged, consequently a comparison can be made between both conventional and optimization methods. First the set-up of variables and parameters is explained. Thereafter two scenarios are elaborated on which are split up in several time-of-day segments. In the subsequent chapter further discussion and conclusions are given with respect to these scenarios.

7.3.1 Set-up

The scenarios, as will be explained further on in this chapter, obtain their characteristics through variables and parameters. Each scenario has its unique set of variables. By testing different variable settings, the workings of the model are highlighted. By using a reference scenario for both set-ups, potential gain in fuel consumption, noise exposure, emissions and runway allocation can be analyzed. The case study test set-up is split up in time segments as indicated in Table 7.2. Furthermore, it will be observed that there are several runs performed per scenario. For every scenario 41 simulations are done in order to establish a Pareto front. This will be further discussed in the subsequent sections.

7.3.2 Scenario 1

The first scenario which will be discussed is based on actual data of operations at Amsterdam Airport Schiphol. Full day operations and aircraft data has been collected for June 18th, 2013. The data specifics in terms of parameters and runway configuration will be explained in the following section. In the section on the reference scenario, the actual departure and landing times are used as input for the runway allocation tool together with actual runways used.

7.3.2.1 Scenario Parameters

Parameters are important as they characterize the scenario. Ideally they reflect reality. In the scenarios treated in this study assumptions are made in defining the parameters. As seen in Table 7.3 local conditions as wind and visibility are given constant values, although in reality these may fluctuate during the day. It is noted that the runway indicators in the runway distribution graphs are not given in alphabetical order. This is due to the fact that the model has been build firstly for arrivals only, in a later stage also departure runways were added. This results in runways R18L and R36L being shown last in the runway distribution graphs for the given scenarios.

Table 7.3: Scenario 1: Parameters

Parameter	Value	Dimension
Wind Direction	North-North-East (NNE)	[-]
Average wind speed	2.8	m/s
Maximum hourly average wind speed	4.0	m/s
Maximum gust speed	7.0	m/s
Minimum visibility	7.0	km
Average cloud cover	3	Oktas [10]
Runway configuration	All runways in operation	[-]
Time window	06:00 – 00:00	Time
Maintenance	No maintenance	[-]
Time-based separation	ICAO separation standards	sec
Number of flights in schedule	1201	Flights

7.3.2.2 Reference Scenario

In order to find comparative improvements when the runway allocation model is used, a reference scenario is in place. This scenario has as input the actual arrival and departure times of aircraft. Information on the actual assigned runway is provided. As seen in the previous section, the parameters indicate low wind speed levels. Resultantly, the runway configuration is in this case independent of wind. No runways are prohibited in their operations and aircraft can potentially operate on every runway. An overview of the actual runway allocation as processed through the runway allocation tool is found in Appendix F. In reality allocation preferences may occasionally change during the day. This could indicate changes in wind direction, and changes in aircraft intensity leading to more runways in operation to address demand. In Figure 7.2 the actual morning peak tracks of approaching and departing aircraft is illustrated.

[10] Oktas indicate the amount of cloud cover varying from 0 for clear sky to 8 for a completely clouded sky.

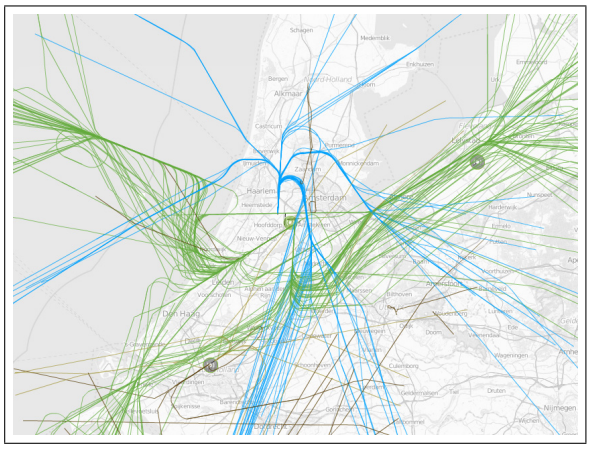

Figure 7.2: Actual morning peak on June 18th 2013, in- and outbound flights have different color [57].

7.3.2.3 Scenario 1: Full day operations

In this section it is tested how the model behaves using the parameter settings from Table 7.3. For a full day of operations at Amsterdam Airport Schiphol allocation is performed through optimization by the Runway Allocation tool. The model is ran for the given set of parameters, including 1201 flights operating at Schiphol airport. The full day scenario is run multiple times with different alpha and beta weightings, indicating different preferences for optimization with respect to fuel or noise. By weighted sum normalization, a Pareto frontier is created. The specifics of a Pareto front are discussed in Section 5.5.2

In order to indicate how the different weighting factors have influence, two figures of noise grids are plotted. The first, Figure 7.3, shows the locations for which the noise limit is exceeded for fuel only optimized settings ($\alpha = 1,\ \beta = 0$). This noise limit is set according to the official AAS regulations. In comparison, Figure 7.4 indicates the noise exposure for noise only optimization ($\alpha = 0,\ \beta = 1$). It is clear from these figures that significant reduction of noise exposure is possible by optimizing for noise.

The difference in exceeding noise limits is due to a different allocation of runways. All things equal, a different distribution over runways and segments shows that allocation can have crucial impact. A closer look on the resulting allocation distribution is given in Figure 7.5 for the fuel optimized case. The noise optimized case is displayed in Figure 7.6. For this latter case, a clear preference is given for runway R36R for arrivals and R36L for departures. Operations on these runways lead to less people annoyed by noise, due to the lower population density of areas which are being exposed.

An optimization either completely focused on fuel or on noise has been shown. If the weighting factors are further adjusted, different outcomes are anticipated. This multi-objective optimization works

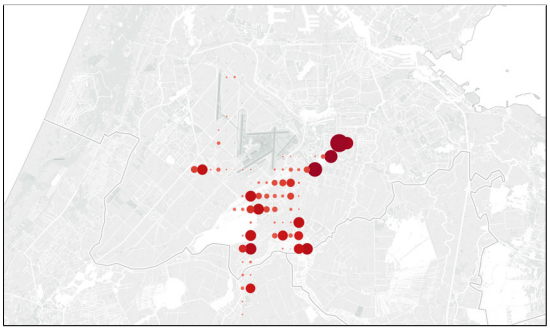

Figure 7.3: Noise grid for fuel optimized simulation with exposed population density indicated by the marker size, 24223 houses exposed.

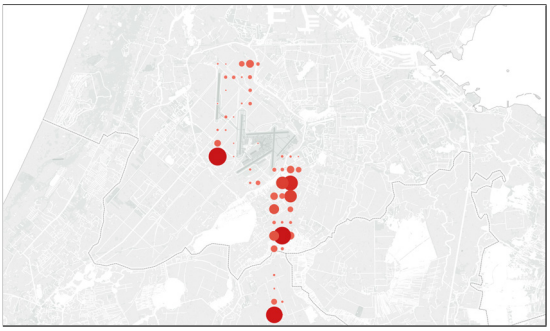

Figure 7.4: Noise grid for noise optimized simulation with exposed population density indicated by the marker size, 6076 houses exposed.

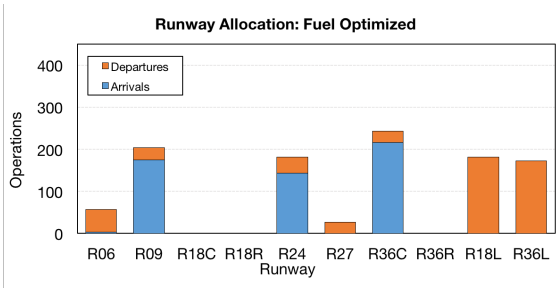

Figure 7.5: Runway distribution for a fuel optimized schedule.

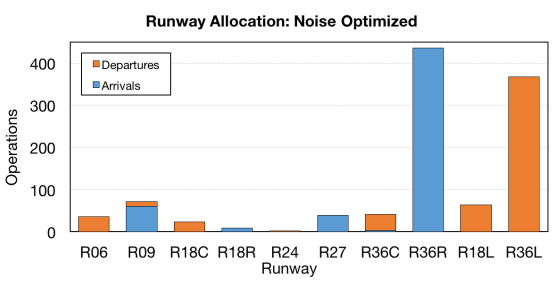

Figure 7.6: Runway distribution for a noise optimized schedule.

as a trade-off between fuel and noise. As previously discussed, the optimized locations lie at the edge of the feasible area. So called Pareto points are indicated in Figure 7.7. From this graph it is observed that indeed a curve exists for the optimal values, indicating the Pareto front. Both locations for optimized fuel and noise are found along the extremes.

A close-up, as seen in Figure 7.8, shows the location of the Pareto points. It is important to note that not all optimal solutions resulted from the optimization proved to be on the optimal curve. A selection is made based on identifying if a point has a better solution for either fuel or noise in comparison to its peer points. The orange dotted line indicates the currently applied annual average day limit for 12,800 houses exposed to the given L_{den} noise limit. The green dotted line indicates the houses exposed for the reference simulation. It lies above the orange dotted line, showing that the annual average limit is slightly crossed under the actual runway allocation. This is compensated for If on other days the limit value is not exceeding the annual average limit. The vertical grey dotted line indicate the actual fuel usage for the reference scenario. As observed, the more is optimized for noise, the more allocation assignments lie above the noise limit. In other words, optimizing for fuel comes at a cost of noise exposure.

In Figure 7.9 the emissions outcomes for different optimization settings are visualized. The noise and fuel optimal case is displayed. Also a multi-objective optimization is shown. This optimization corresponds to a chosen optimal point indicated by the red marker in the Pareto graph. The point is selected by taking the most optimal value for fuel, which lies below the actual limit line. Emissions for noise optimization are highest, whereas optimization for fuel leads to the lowest emission as seen in the figure.

Figure 7.10 indicates the delay occurring under the different optimization settings. What is observed is that a fuel reduced schedule not necessarily has to have the lowest delay. The algorithm makes a trade-off in which it is possible to give certain flights preference on runways, while other flights might be delayed by this decision. Delay can therefore have a positive impact on fuel usage. In other words, an aircraft can 'wait' for a beneficial runway to become available; fuel is saved if the new runway assigned leads to a shorter flight route or taxi phase.

It was observed in the Pareto front that some points lie within the limit's allowable exposure. Further analyzing of the scenario is done by selecting the value which is multi-optimized for fuel and noise, and lies below the limit. This multi-objective value (red marker) is now compared to the reference scenario. Figure 7.11 shows allocation for the optimized scenarios, whereas Figure 7.12 shows the actual allocation. It is indicated that outstanding improvements in fuel usage are possible by optimization through the runway allocation model. While simultaneously maintaining a satisfying noise exposure level. A gain in fuel efficiency of 9.2% is seen in Figure 7.13. Distinct emission savings are visualized in Figure 7.14.

In Figure 7.15 the exposure to the environment is displayed. The red dots indicate where the noise limit is exceeded. The size of the markers indicate the population density at the locations where noise limit is exceeded. The new optimized exposure to the environment is found in Figure 7.16, where exposure and population density are visualized. It is observed that the optimized map has a lower noise exposure than the reference scenario exposure. Next to fuel and emission savings, evidently the noise exposure rate is lower when using the optimized allocation model.

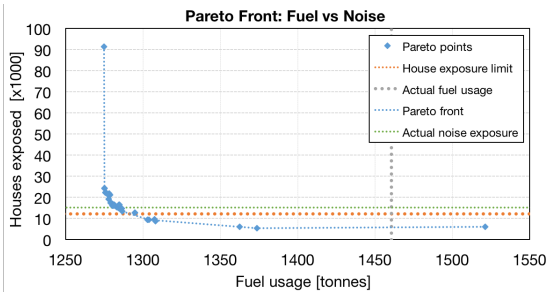

Figure 7.7: Pareto front indicating a set of optimal solutions. The grey dotted line indicates fuel use for the actual reference scenario.

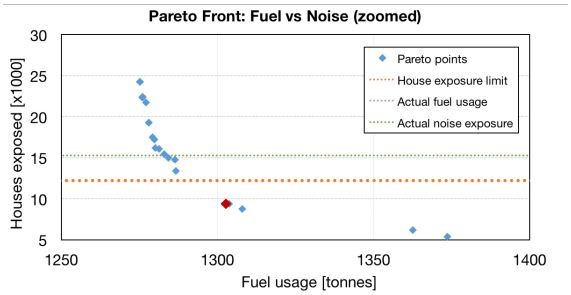

Figure 7.8: Pareto front zoomed-in, the red marker indicates the selected multi-objective solution.

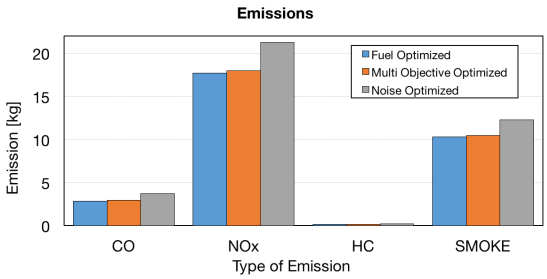

Figure 7.9: Emissions for the different optimization settings.

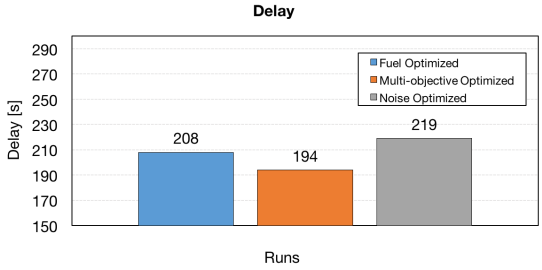

Figure 7.10: Delay for the different optimization settings.

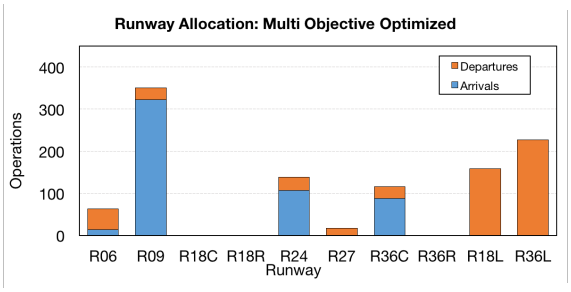

Figure 7.11: Runway distribution for a multi-objective optimization.

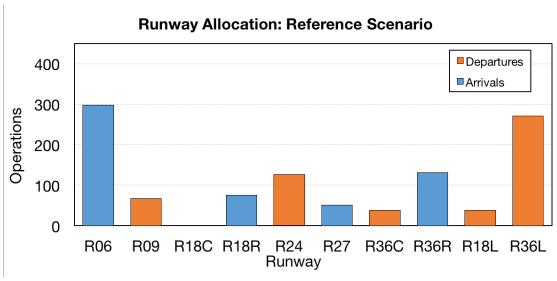

Figure 7.12: Actual full day runway allocation during June 18th 2013.

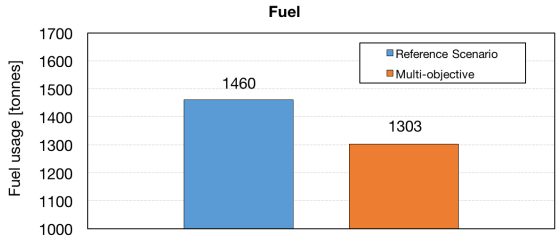

Figure 7.13: Fuel usage for Multi-objective optimization and Reference Scenario indicating a 9.2% increase in fuel efficiency.

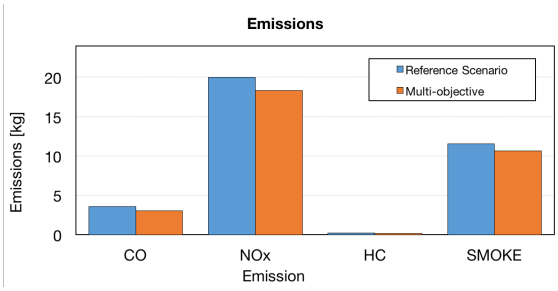

Figure 7.14: Emissions for Multi-objective optimization and Reference Scenario.

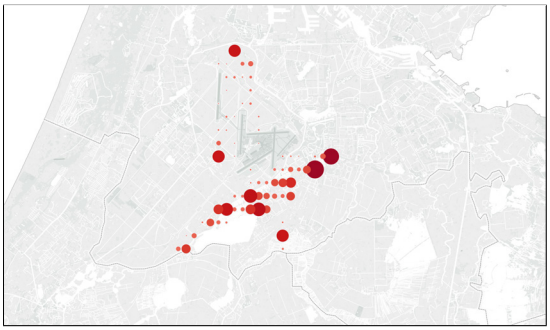

Figure 7.15: Noise grid for reference simulation with exposed population density indicated by the marker size, 15,274 houses exposed.

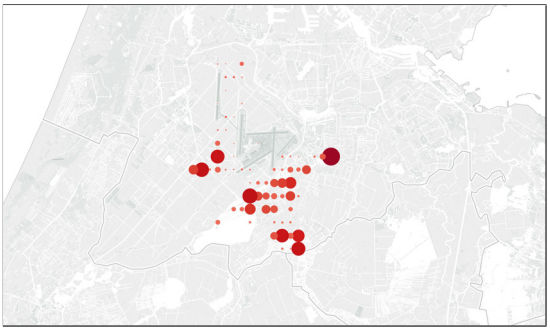

Figure 7.16: Noise grid for multi-objective simulation with exposed population density indicated by the marker size, 9,348 houses exposed.

7.3.2.4 Scenario 1: Morning operations

In order to test how the algorithm makes decisions in assigning runways this section focuses on the morning run. Other time of day segments will be discussed. Peak moments and air traffic density may vary during the day. During a busy day it may be possible that flexibility is heavily restricted by a high demand of flights. By comparing day segments it can be assessed in which situation flexible allocation is most profitable. The allocation as performed by the Runway Allocation Model is compared to the reference scenario. Furthermore, different optimization runs are explained. From the zoomed-in Pareto front, an optimal value may be identified having a beneficial trade-off between noise and fuel. This value, indicated by the red marker, is investigated further in terms of feasibility. The green dotted line indicates the number of houses exposed to the noise limit for the reference scenario. The difference in fuel usage for the reference scenario and optimized scenario is significant as seen from the fuel bars in the figures 7.19. This difference corresponds to a fuel efficiency increase of 5.19%. While emission remains fairly constant, as observed in Figure 7.20, some increases are noted for CO emissions.

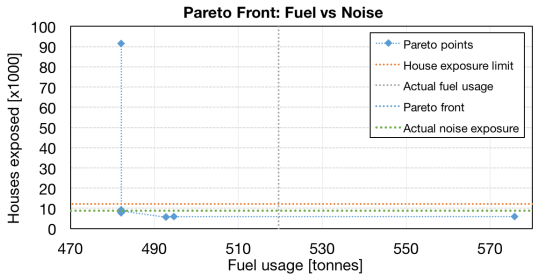

Figure 7.17: Pareto front for Scenario 1: Morning run.

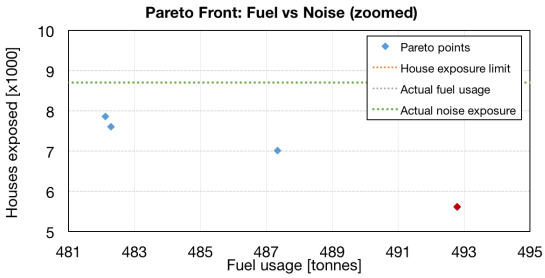

Figure 7.18: Pareto front zoomed for Scenario 1: Morning run.

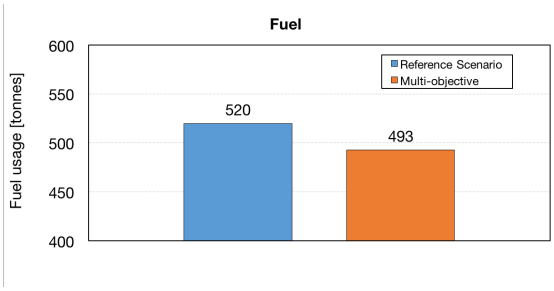

Figure 7.19: Fuel efficiency increase of 5.19% for the optimized scenario.

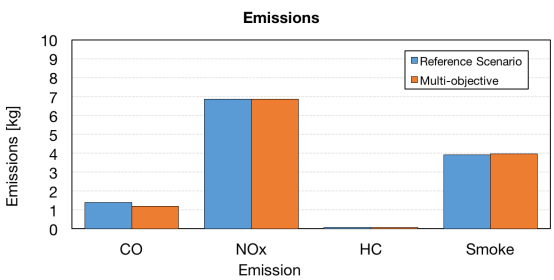

Figure 7.20: Emission savings for the optimized scenario.

7.3.2.5 Scenario 1: Afternoon operations

Here afternoon operations at Amsterdam Airport are simulated. The real reference scenario is used to compare with results using the flexible runway allocation approach. From the multi-objective optimization for several runs, a Pareto front is established. This is visualized in Figure 7.21. Further analysis in done for a selected multi-objective setting. Fuel and emission reductions for this setting are found in Figures 7.23 and 7.24, respectively. This results in a 9.01% increase in fuel efficiency, as compared to the reference scenario.

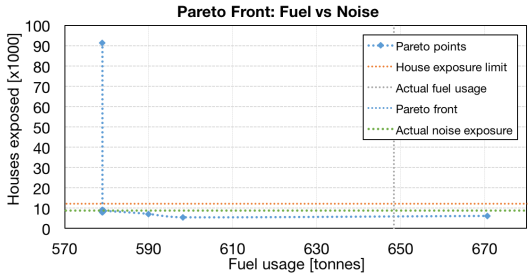

Figure 7.21: Pareto front for Scenario 1: Afternoon run.

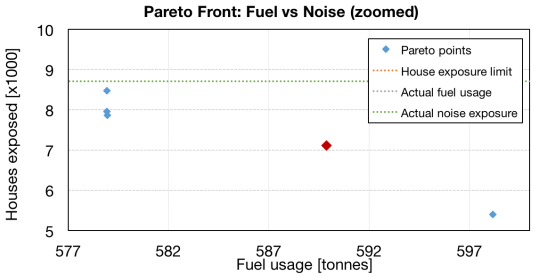

Figure 7.22: Pareto front zoomed for Scenario 1: Afternoon run.

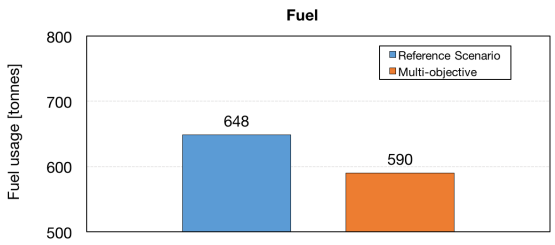

Figure 7.23: Fuel efficiency increase of 9.01% for the optimized scenario.

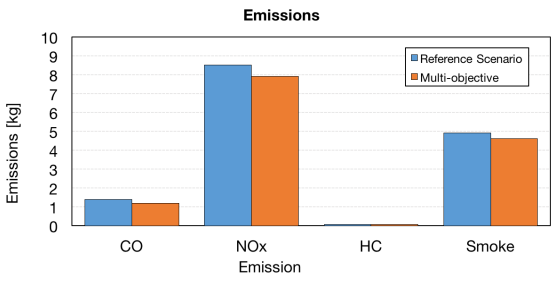

Figure 7.24: Emission savings for the optimized scenario.

7.3.2.6 Scenario 1: Evening operations

Evening operations at Amsterdam Airport have been computed. The real reference scenario is used to compare with results using the flexible runway allocation approach. As indicate by Figure 7.26, again a clear Pareto front is identified. Locations along this curve show optimal results for a range of weightings. For the selected Pareto point indicated by the red marker, fuel and noise costs are compared with the reference scenario. As indicated by the green dotted line, the noise exposure levels for both reference and optimized settings are comparable. An significant increase in fuel efficiency is drawn from Figure 7.27. Indicating a 4.44% gain in fuel reduction. Emission savings are evidently increasing, as is shown in Figure 7.28.

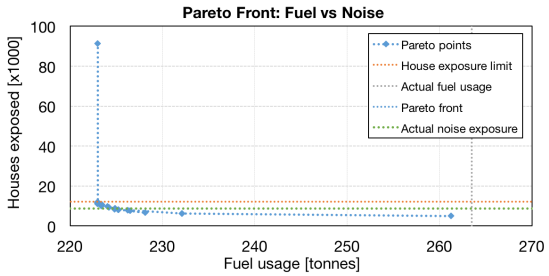

Figure 7.25: Pareto front for Scenario 1: Evening run.

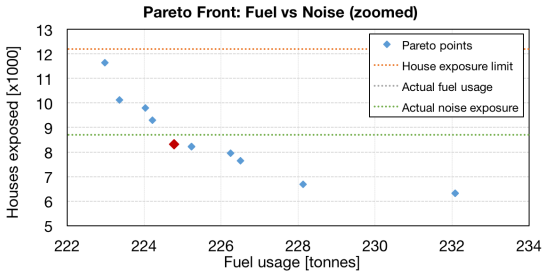

Figure 7.26: Pareto front zoomed for Scenario 1: Evening run.

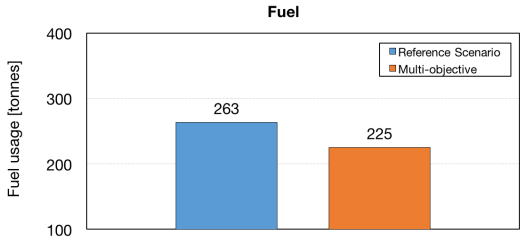

Figure 7.27: Fuel saving of 4.44% for the optimized scenario.

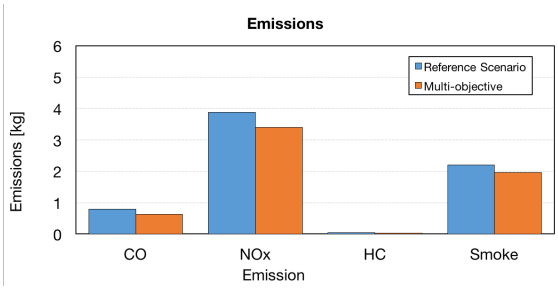

Figure 7.28: Emission savings for the optimized scenario.

7.3.3 Scenario 2

Scenario 2 is established with the same time segments as for Scenario 1. Actual data is used for June 21th 2013 operations, as they occurred at AAS. This scenario is selected since different parameters are used. Different wind and visibility settings lead to a change in runway availability. This will be explained further under Scenario Parameters.

7.3.3.1 Scenario Parameters

The major changes in Scenario 2 with respect to Scenario 1 are due to local conditions. Changes in weather lead to a restricted availability of AAS runways. The parameters are displayed in Table 7.4. Note the different wind speeds and reduced visibility due to bad weather conditions.

Table 7.4: Scenario 2: Parameters

Parameter	Value	Dimension
Wind Direction	South-West (SW)	[-]
Average wind speed	6.6	m/s
Maximum hourly average wind speed	10.0	m/s
Maximum gust speed	15.0	m/s
Minimum visibility	0.3	km
Average cloud cover	8	Oktas [11]
Runway configuration	Restrictions in place	[-]
Time window	06:00 – 00:00	Time
Maintenance	No maintenance	[-]
No operations	R06 R09 R36C R36R R36L	[-]
Time-based separation	ICAO separation standards	sec
Number of flights in schedule	1116	Flights

7.3.3.2 Reference Scenario

The reference scenario indicates the actual runway allocation as it occurred on June 21th 2013. In order to find improvements when flexible allocation is performed, this scenario will function as reference. Percentage gains in fuel efficiency, noise and emissions can now be identified. Due to bad weather conditions not all runways are operative. This reduces flexibility; flights can only be assigned to certain runways. The most prominent reason is that aircraft cannot land or take-off at certain tail-wind speeds and direction components. Noise abatement should not be the determining factor in runway allocation in the case of cross-wind exceeding 15 kt, or when tail wind exceeds 5 kt as indicated by ICAO [58]. The runways at AAS which are excluded of operation due to the weather conditions in this scenario are the following; no arrivals and departures on R06, R09, R36C, R36R, R36L.

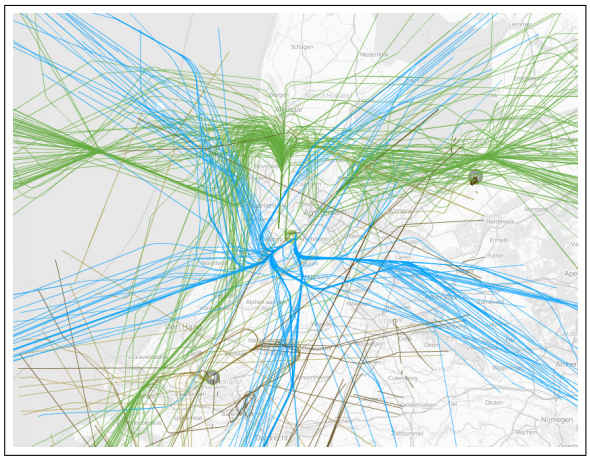

Figure 7.29: Actual Morning Peak on June 21th 2013 [57].

7.3.3.3 Scenario 2: Full day operations

In this section it is tested how the model behaves using the parameter settings from Table 7.4 for a full day of operations at AAS. The model takes into account all 1116 flights operating at Schiphol Airport. Several runs have been performed with different weighting settings using the same method as in Scenario 1.

In the figures 7.30 and 7.31 the noise exposure is indicated for a fuel and a noise optimized schedule. In Figure 7.32 it is observed how the model allocates runways under the alpha and beta settings of 1 and 0. This indicates a total preference for fuel is performed by the model. In figure 7.33, the alpha en beta settings are adjusted to find an optimum allocation for noise. It is clear from these figures that significant discrepancies are observed between the two allocations options.

The full day scenario is run multiple times with different alpha and beta weightings, indicating different preferences for optimization for fuel or noise. By weighted sum normalization, a Pareto frontier is created similar to Scenario 1. It is observed from figure 7.34 that a clear curve exists, which indicates the optimal noise versus fuel trade-off. The orange dotted line indicates the total limit of houses which, under current regulations, may not be exceeded on an annual basis. THe green dotted line shows the number of houses exposed to the noise limit under the actual reference scenario. The grey line indicates to fuel usage for the reference scenario.

An interesting finding is extracted from Figure 7.35; the fuel usage line for the reference scenario lies significantly closer towards the fuel usage found for fuel optimization. In other words, the potential of fuel optimization is smaller for Scenario 2. Reason for this is the reduced flexibility, due to restrictions on several runways. This will be further discussed by analyzing a single multi-objective optimization, which is indicated by the red marker in the figure. This value is selected to lie close to the green dotted line, indicating the noise limit for the reference scenario.

[11] Oktas indicate the amount of cloud cover varying from 0 for clear sky to 8 completely clouded.

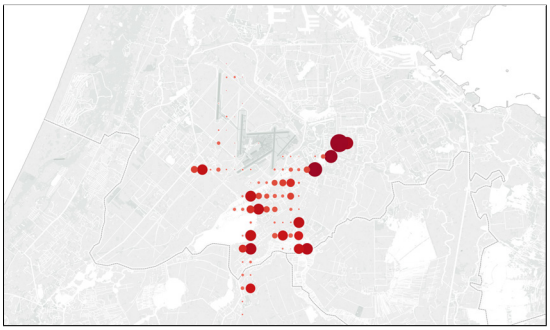

Figure 7.30: Noise grid for fuel optimized simulation with exposed population density indicated by the marker size, 28,822 houses exposed.

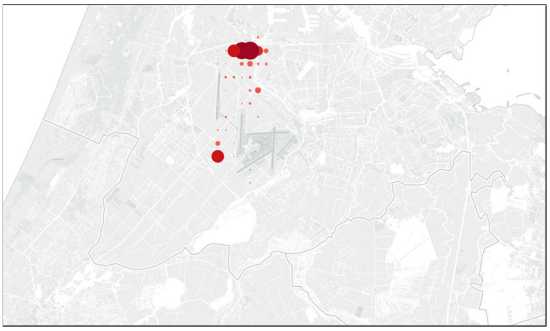

Figure 7.31: Noise grid for noise optimized simulation with exposed population density indicated by the marker size, 14,729 houses exposed.

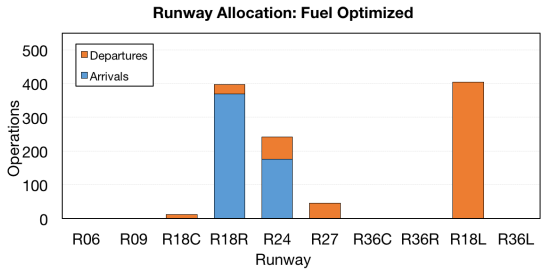

Figure 7.32: Runway distribution for a fuel optimized schedule.

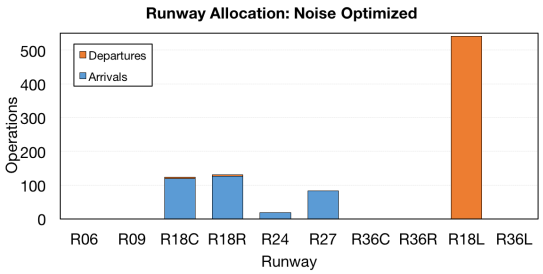

Figure 7.33: Runway distribution for a noise optimized schedule.

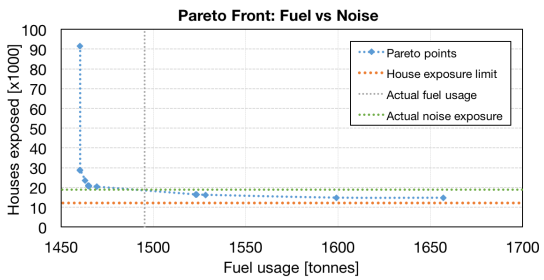

Figure 7.34: Pareto front.

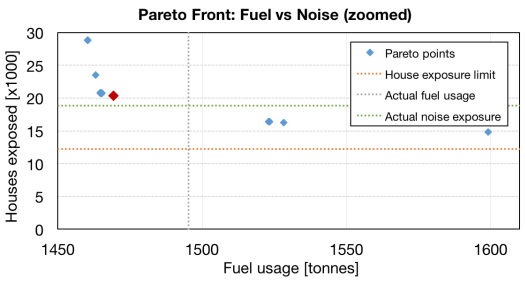

Figure 7.35: Pareto front zoomed.

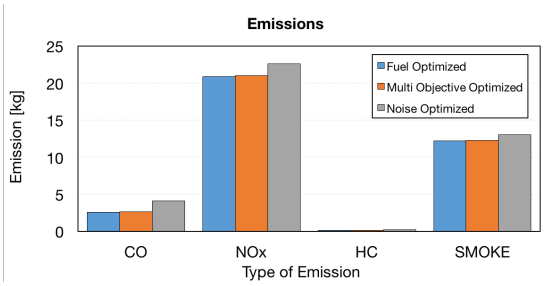

Figure 7.36: Emissions for fuel, noise and multi-objective optimized operations.

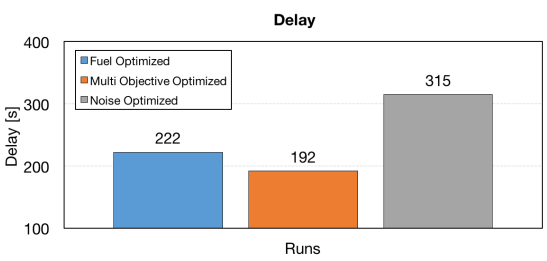

Figure 7.37: Delay for fuel, noise and multi-objective optimization.

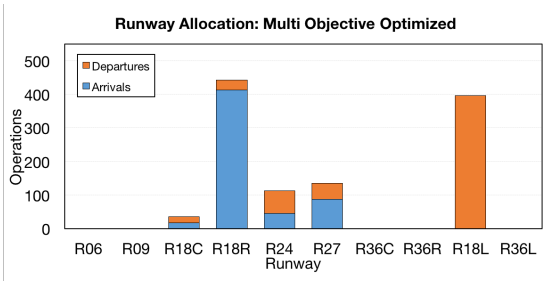

Figure 7.38: Runway allocation for the multi-objective optimized scenario.

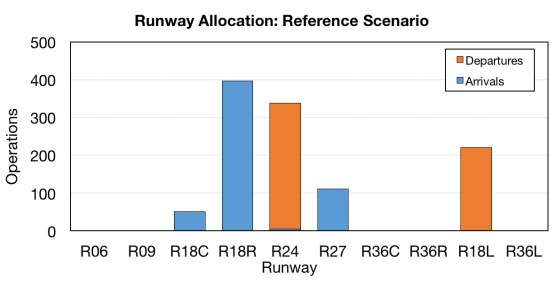

Figure 7.39: Actual runway allocation during June 21th 2013.

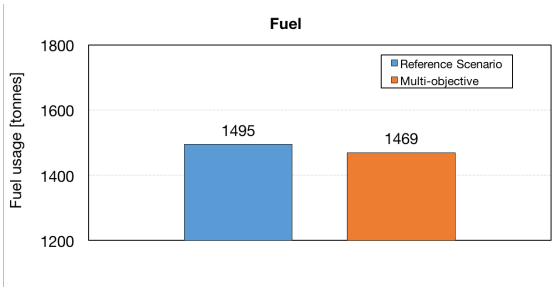

Figure 7.40: Fuel usage for Multi-objective optimization and Reference Scenario, indicating a fuel saving of 1.74%.

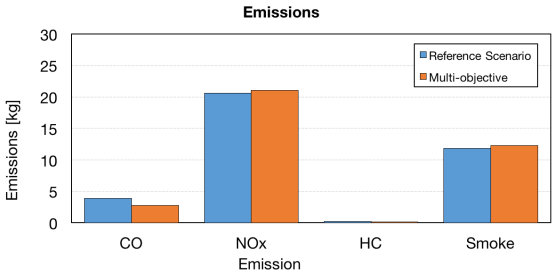

Figure 7.41: Emissions for Multi-objective optimization and Reference Scenario.

Multi-objective optimization establishes a trade-off between fuel and noise. Several optimizing runs are compared for emissions and delay in figures 7.36 and 7.37, respectively. Clearly optimization for fuel relates to a reduction in emissions due to fuel savings. In terms of delay, the model displays a significance reduction in delay time when optimizing for fuel. For scenario 2 the multi-objective solution of one of the Pareto points is compared to the reference scenario. Figure 7.38 indicates the runway allocation for the optimized method. This is compared to Figure 7.39 which indicates the reference scenario actual runway utilization. Interestingly, it is observed that there is not much difference in the fuel consumption, as shown in Figure 7.40. This corresponds to a 1.74% reduction in fuel use.

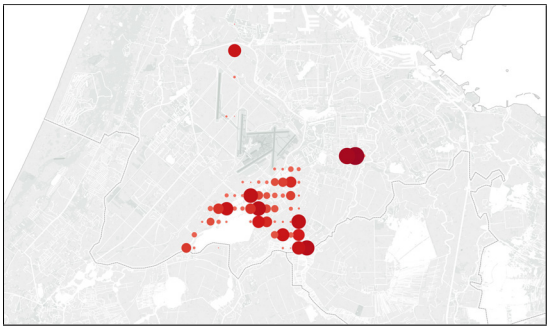

Figure 7.42: Noise grid for reference scenario with exposed population density indicated by the marker size, 18,839 houses exposed.

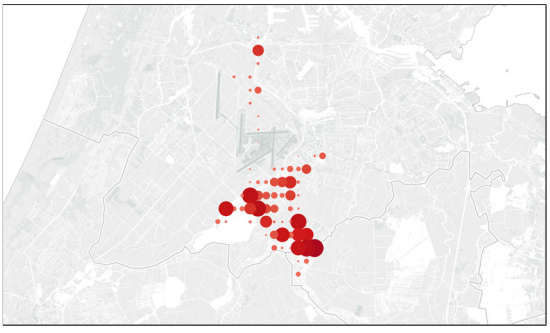

Figure 7.43: Noise grid for multi-objective simulation with exposed population density indicated by the marker size, 20,345 houses exposed.

When comparing emissions in Figure 7.41 an increase in NOx and Smoke is found using optimization. CO is lower when optimization is performed. The difference lie in the fact that CO emissions are high during taxi-phase. The optimization as performed by the allocation tool evidently reduces the taxiing time. In terms of noise exposure Figure 7.42 indicates the noise exposure for the reference scenario.

Figure 7.43 indicates the exposure on the surroundings under the multi-objetive case, where population density is indicated by marker size. Under the given settings, the exposed population is slightly higher for the multi-objective optimized case.

7.3.3.4 Scenario 2: Morning operations

The morning run is simulated by the runway allocation model for both optimized and reference scenarios. The results of the set of optimization runs is displayed in Figure 7.44. The Pareto curve can be clearly identified. If a closer look is taken, in Figure 7.45 it can be identified that the orange dotted line, which represents the L_{den} noise limit, is crossed. The reason no solutions are found which lie below this limit, is due to weather conditions imposing restrictions on runways. Operations at Schiphol Airport may occasionally cross the limit, as long as the average annual value remains under this limit. Another factor which is of influence is the demand for runways during the morning peak, which reduces flexibility further. In these day segments scenarios a time averaging factor is applied. This accounts for the shorter time span when accounting for the L_{den} limit.

For the multi-objective case an optimal location, shown by the red marker, is picked close to the actual noise limit line, indicate by the green dotted line. Locations which have a lower fuel usage come at the cost of noise exposure, hence an optimal point is taken which has a reasonable noise exposure. In terms of fuel use it is seen that an optimized schedule does not provide significant possibilities for fuel reduction; 0.6%. This is visualized in Figure 7.46, where a multi-objective point is analyzed. Reductions in emissions are evident from Figure 7.47. NOx and Smoke emissions are higher for the optimized case, whereas a small reduction in CO is observed.

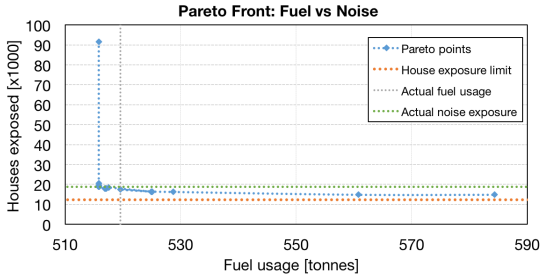

Figure 7.44: Pareto front for Scenario 2: Morning run.

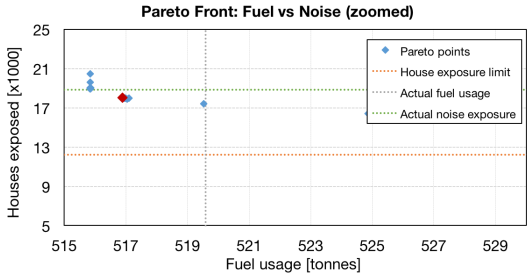

Figure 7.45: Pareto front zoomed for Scenario 2: Morning run.

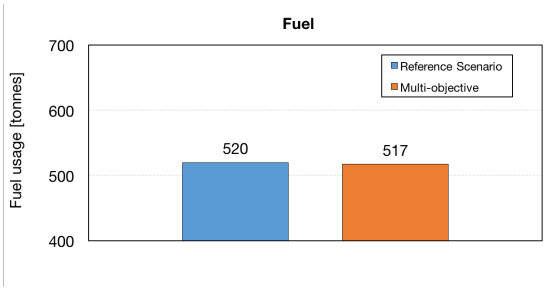

Figure 7.46: Fuel usage for Multi-objective optimization and Reference Scenario indicating 0.6% savings in fuel.

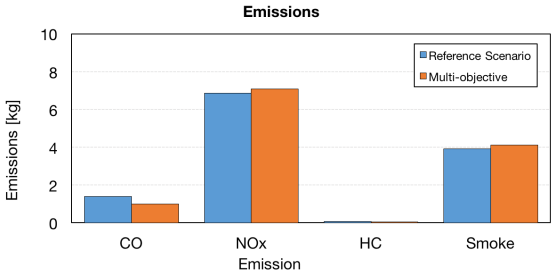

Figure 7.47: Emissions for Multi-objective optimization and Reference Scenario.

7.3.3.5 Scenario 2: Afternoon operations

The afternoon schedule results are depicted in Figure 7.48 for several optimization runs. It is observed that fuel savings may be possible with respect to the reference scenario. By taking a closer look in Figure 7.49 it is seen that fuel usage optimization is more profitable. Only small gains are possible. Reason for

this is the runway restriction due to local conditions. The results for a selected multi-objective run are found in Figure 7.50. A reduction of 1.95% is found for fuel usage.

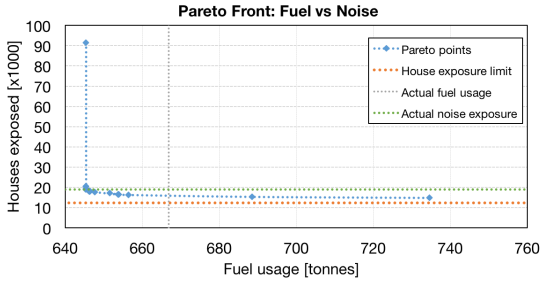

Figure 7.48: Pareto front for Scenario 2: Afternoon run.

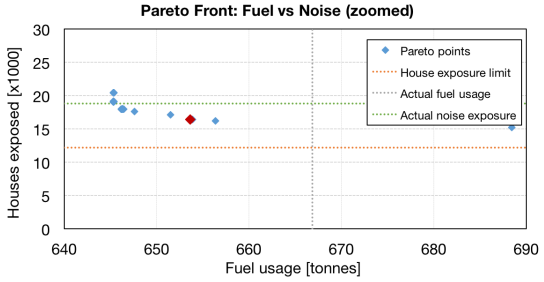

Figure 7.49: Pareto front zoomed for Scenario 2: Afternoon run.

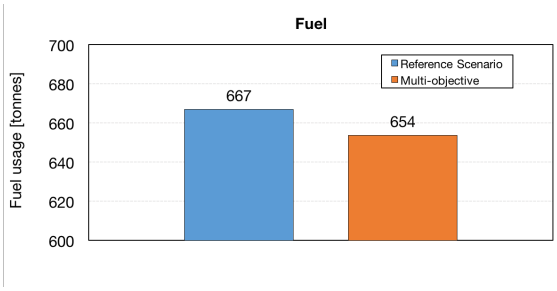

Figure 7.50: Fuel usage for Multi-objective optimization and Reference Scenario indicating 1.95% savings in fuel.

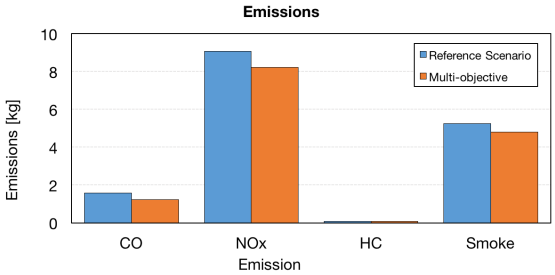

Figure 7.51: Emissions for Multi-objective optimization and Reference Scenario.

7.3.3.6 Scenario 2: Evening operations

The evening run is simulated for aircraft operations at Schiphol Airport from 18.00h until 00:00h. Here fuel penalties apply to operations during the evening and night. The set of Pareto points in Figure 7.52 show the results for different weighted optimization settings. It is observed that, again, the actual fuel usage indicated by the grey dotted line, lies closer towards the most optimum fuel location. This shows that potential savings in fuel are of smaller proportions in comparison with scenario 1. The fuel savings are 1.92% for a selected multi-objective optimization, as shown in Figure 7.54.

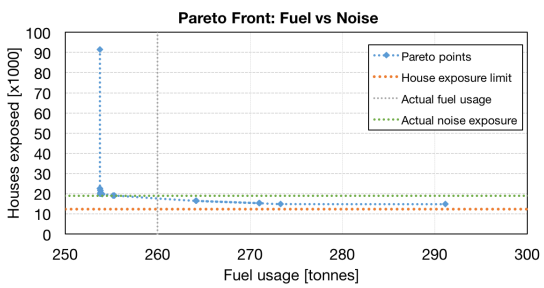

Figure 7.52: Pareto front for Scenario 1: Evening run.

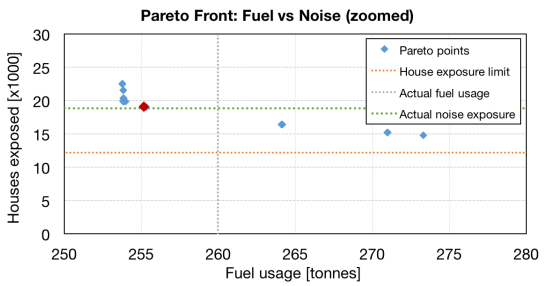

Figure 7.53: Pareto front zoomed for Scenario 1: Evening run.

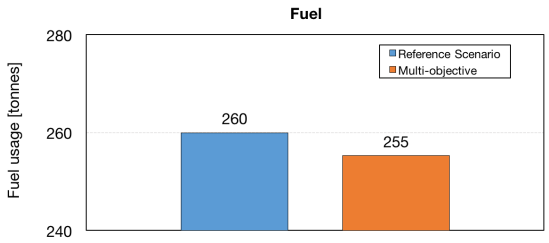

Figure 7.54: Fuel usage for Multi-objective optimization and Reference Scenario, indicating fuel saving of 1.92%.

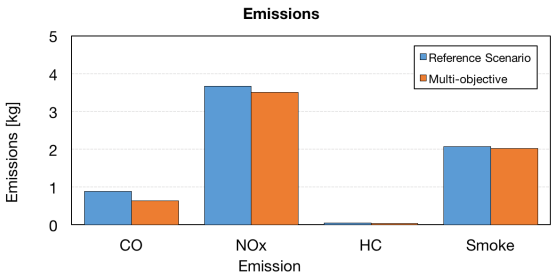

Figure 7.55: Emissions for Multi-objective optimization and Reference Scenario.

7.3.4 Scenario 3: Annual operations

The aforementioned scenarios have indicated operations for a single day. In Scenario 1 local conditions did not have influence on runway availability. In Scenario 2 wind- and visibility conditions restricted several runways. This led to a decrease in flexibility and allocation possibilities. Ideally, the model could be tested for all possible scenario. It is interesting to show how the model would perform on a full year of operations. To this end annual operations are discussed. Since only two scenarios are evaluated for this case study, assumptions are in place.

In figure 7.56 wind speeds are shown for a full year at Amsterdam Airport Schiphol [59]. In Figure 7.57 the wind directions are visualized. From these figure it is extracted that an average wind speed lies between 4-6 m/s and mostly comes from the south-west direction. For scenarios 1 and 2 this limit is 2.8 m/s and 6.6 m/s, respectively. Scenario 1 thereby represents a low wind scenario, resulting in no runway restrictions. Fuel and emission savings were shown to have potential of approximately 157 ton fuel or 9.2% efficiency increase for the optimized segments. In Scenario 2 it was seen that several restrictions were in place, limiting flexibility to a large extend. The main reason for these restrictions were due to operations on runways with tailwind or crosswinds. Savings in fuel of 27 ton or 1.74% on a daily basis were possible.

On an annual basis it is concluded from the graph that some restrictions are in place most of the time varying from low restrictions to heavy restrictions. Around 40% of the time an average wind of 5 m/s is observed from the graph, indicating low restrictions. Heavy restrictions, like Scenario 2, are present 40% of the time, whereas no restrictions are present 20% of the time. These are only indications and deserve further analysis for different wind speeds and directions. The projected savings have been established using the following relations, where x_l is daily fuel saving for low restricted scenarios, x_m is the daily fuel saving for a medium restricted scenario, x_h is daily fuel saving under heavily restricted scenarios.

$$\text{Annual projected savings:} \quad 365 \cdot (x_l \cdot 20\% + x_m \cdot 40\% + x_h \cdot 40\%) \quad [kg] \tag{7.1}$$

Under the aforementioned assumptions, it can be shown that fuel and emissions savings on annual basis are between 1% tot 9%. Annually this may indicate values of around 4% - 6% or 15,000-30,000 tons kerosene in potential fuel and related emission savings through flexible allocation, while maintaining a favorable noise exposure level to the surroundings.

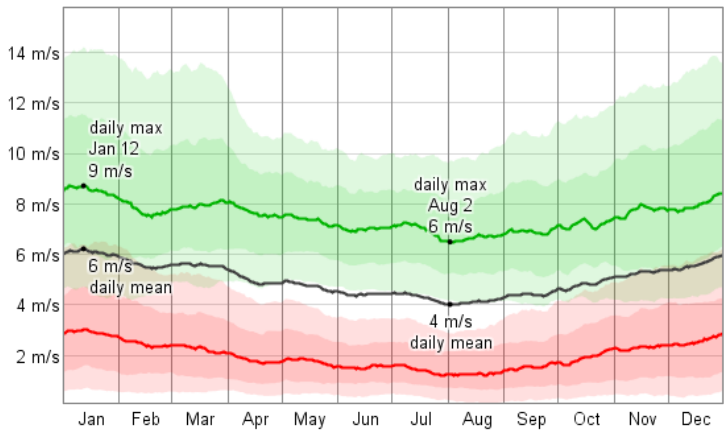

Figure 7.56: Annual average wind speeds and average maximum windspeeds at Schiphol in 2013 [59].

Figure 7.57: Annual wind directions at Schiphol in 2013 [59].

7.3.5 Scenario Results

Two scenarios have been elaborately discussed in the previous sections. By applying optimization through the runway allocation tool, scenarios can be optimized for fuel and noise. By selecting appropriate α and β weights a trade-off can be visualized. The resulting Pareto front is shown for the different scenarios and the different time of day segments.

The full day simulation of Scenario 1 shows significant changes in noise exposure to the environment for an optimization towards fuel or noise. Different distribution of aircraft over the runways can result in increase or decrease of noise levels at population points. It has been seen that noise population density plays a role in assigning runways. In the Pareto front, the optimal values for fuel and noise are indicated. A clear curve exists on which optimal points lie. In the scenarios a selected optimal point was further discussed. This multi-objective solution is compared to a reference scenario. The key findings of analyses of both scenarios are given below.

- **Optimization:** Key findings indicate that a decrease in fuel usage comes at the cost of houses exposed to a given noise limit. Due to the curving feature of the Pareto front, beneficial values for the weightings are existent with respect to the currently used reference scenario.

- **Delay:** It has been shown that optimization has influence on delay. For a fuel optimized case, often delay is reduced to a minimum in order to put aircraft on the ground as early as possible, hence reducing total fuel consumption. Nevertheless, in some cases it may be possible for the optimization to select a longer total delay duration. Reason behind this, is that an aircraft can hold for a beneficial runway become available, hence reducing total flying/taxing time.

- **Emissions:** A linear relation between fuel and emission is assumed. This linear relation is set-up per flight segment. Aircraft have different emissions under different segments; even under shorter

total time a relative longer taxiing time may therefore potentially have the effect of increasing CO emissions.

- **Scenario 1:** For the full day simulation in Scenario 1 a potential fuel efficiency increase for the selected multi-objective optimization corresponds to a saving of 157 ton kerosene (9.2%) in fuel consumption. Next to this full day scenario, the time of day segmented runs indicated a lower potential increase. The fuel savings for the morning run are 27 ton (5.19%), the afternoon run shows 58 ton (9.01%) fuel decrease and the evening run displays a 38 ton (4.44%) fuel reduction. The reason for the total fuel savings of cumulative time segments to be smaller then the total of the full day run, is due to increased flexibility of a full day's run. Since the model is able to optimize for a longer time span, more flexibility is obtainable. It is thereby possible to mitigate the noise penalty factors which are apparent in the evening run. By compensation, aircraft in that time segment can be assigned a more profitable runway when full day optimization is performed.

- **Scenario 2:** It is shown in Scenario 2 that several runway restrictions are existent. Due to deteriorated weather conditions, flight operations are restricted to fewer runways. It is noted that these restrictions have impact on the potential of fuel savings by the runway allocation tool. Still some increase in efficiency are observed for the selected multi-objective optimization; ranging from 1 to 2%. For the full day scenario fuel savings are around 26 ton (1.74%). Morning operations are relatively lower due to high runway demand; 3 ton (0.6%). Afternoon operations indicate 13 ton (1.95%) potential savings. Finally, evening operations show 5 ton (1.92%) in fuel savings. In comparison with Scenario 1 potential gains are lower due to reduced flexibility since fewer runways are available. Improvement in the range of 1 to 2% on the selected segments in aviation terms still bears significant potential.

- **Time segments:** When comparing the different time segments for both scenarios, it is observed that the potential savings for both morning segments are lowest. It can be established that the morning peak has high runway demand. Due to this high demand, maximum capacity is reached sooner. This results in lower flexibility. The afternoon segment is for both scenarios the most profitable. This is due to a reduction in demand of runways, leading to increased flexibility. For the evening simulation it is found that due to a higher demand, flexibility is lower as holds for the morning simulations. Due to penalizing factors for the evening and night period a different assignment is found when comparing a full day scenario to the evening scenario.

- **Annual operations:** By looking at potential annual gains, savings in fuel and emission might be beneficial if the runway allocation model is utilized. Preferably more simulations with different settings have to be researched. The two discussed scenarios give an indication of the potential the flexible allocation might have. The annual efficiency increase in fuel and emission savings can be established to be approximately 4% - 6% or 15,000 - 30,000 tons kerosene under given assumptions.

In the next section the verification and validation is done for the runway allocation model. Additionally, a closer look will be given on the actual allocation trade-offs and separation of aircraft over the runways. Additionally, the noise to fuel ratio will be discussed further.

Chapter 8

Synthesis

This section will synthesize the results from the previous chapter. It will first be explained how verification and validation is done in Section 8.1 and Section 8.2, respectively. In Section 8.3 a more detailed overview of actual allocation as processed by the runway allocation model is reviewed. Finally, results of the established Pareto front will be discussed, in which the noise to fuel ratio proves to be interesting.

8.1 Verification

By verification of the runway allocation model, it is checked if the model behaves according to a reasonable expected outcome. This is done by checking individual code blocks of the runway allocation model and verify whether results are as anticipated. These checks are done for each individual methodology within the runway allocation model; runway dependencies, fuel computations, noise computations, emission computations and the linear programming model itself. In order to verify the results of the model, hand calculations are performed for all computations and compared with the model's results. This has been done for fuel, noise, emission and dependency matrices. Several test-cases have been set-up in order to test different settings. These test cases included only 2 runways, a limited set of flights and limited restrictions. By starting with a simplified case and thereafter step-wise expanding to a full model, results have been verified at every incremental addition towards a complete model. Additional verification is done using the reference scenario. For this scenario, the actual flight data and runway distribution is known. By comparing scenario 1 and 2 full day simulations with their reference scenarios, it can be identified that the model's result for optimization is reasonably as was expected.

8.2 Validation

Validation is done by checking if the output of the model conforms to an anticipated actual result. It is checked if the solutions are correct with respect to reality. By comparing to actual existing data an indication is given on the feasibility of the design. By checking results with official measurements at so-called *handhavingspunten*, the simulated data is compared to actual data. Additionally, experts of Schiphol group and pilots have been consulted in order to validate and suggest improvements with respect to methodologies and output.

An overview of the results for validating noise exposure levels simulated by the full day run of Scenario 1, is found in Appendix D.1. The locations correspond to a selection of *handhavingspunten*, as indicated in Figure 8.1. An overview of the complete map with locations is added to the appendix. The results of validation by comparing measurement points prove that indeed noise levels are comparable to the actual real data. In other words, the expected results are within a reasonable range; the model is positively validated. Notwithstanding, it is noted that some of the measuring points exceed the noise limit as defined by the real boundary values. The main reason behind this is that the official regulations imply calculation of noise levels on a yearly basis. The established L_{den} boundary value is based on

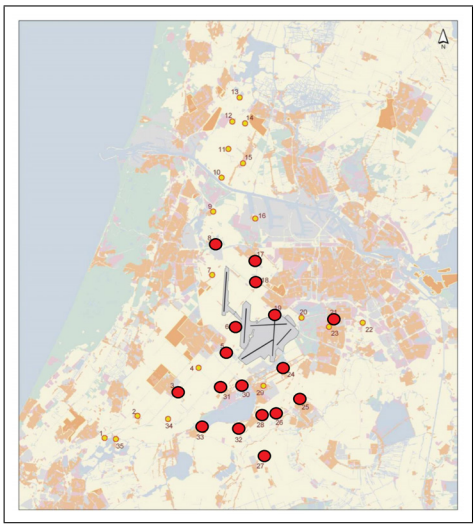

Figure 8.1: Selected validation *Handhavings*- locations at AAS indicated by red markers [60].

averaged yearly movements. Since the simulation is done only for one full day, it can be assumed that these occasional infringements are allowed if on other days they are compensated for. Throughout the year different runways will be allocated, resulting in different noise loads to the environment.

Noise coefficients have been computed using the Integrated Noise Model. This model has been extensively tested by the FAA and used within academics and the aviation industry. The results of the model are thereby assumed to indicate a reasonable approximation of reality. For the runway allocation model, the noise coefficients have been computed twice; for the Medium MTOW category and for the Heavy category. This was done using a Boeing 737-800 and 777-200ER, respectively. The results for these computations were positively checked to see if they correspond to actual flight data and if their mutual relation is of expected proportions.

Validation for the computation of fuel coefficients has been done by comparing several sources. Aircraft performance and fuel flow were evaluated using BADA. The results were compared to the ICAO Aircraft Engine Emission Databank, in order to validate the obtained results for fuel flow. Additionally, fuel flow results were obtained through INM, in which multiple runs for different segments indicated similar fuel flow levels as found trough the other collected sources.

8.3 Results

In this section a thorough look is given on the case study scenarios of the previous section. The actual assignment of aircraft on runways is reviewed for the reference scenario and the optimized scenario. The different trade-offs which the model makes when optimizing are highlighted. Furthermore, different Pareto fronts are compared. The noise to fuel ratio will be investigated further.

8.3.1 Runway Allocation

In order to take a closer look at the actual allocation performed by the model, this section will go into detail by comparing the reference scenario runway distribution against the optimized distribution. Figure 8.2 indicates the runway schedule as actually occurred on June 21th 2013 at AAS, as compiled by the runway allocation model. It uses the AAS standard preference list procedures. Figure 8.3 shows the allocation when optimization is performed by the runway allocation tool. The optimization corresponds to previously discussed scenario for full day operations. Traffic is visualized starting from 06.30h until 08:00h. Several characteristics are discussed below. In the legend it is shown that symbols are indicating Arrivals and Departures, displayed by the direction of the triangle indicators. Furthermore, the size of

the indicator displays the MTOW category. Here heavy aircraft are identified by a larger marker.

Figure 8.2: Runway allocation schedule by Preference List for actual flights on June 21th 2013. MTOW class is identified by the indicator size.

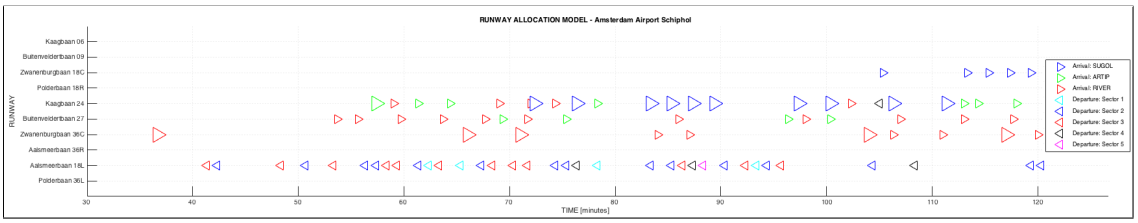

Figure 8.3: Runway allocation using the Runway Allocation mode. MTOW class is identified by the indicator size.

- **Optimization:** Optimization for this example is performed with the following weighting settings: $\alpha = 0.175$ and $\beta = 0.825$, indicating a relative preference for noise optimization.

- **Restricted runways:** Runway restrictions are in place in this example as discussed in Section 7.3.3.1. This is readily observed since no operations occur at the restricted runways. Using the GUI of the runway allocation model these restrictions can be inserted into the scenarios.

- **Separation regulations:** Regulations resulting from Schiphol Aiport's separation standards are observed from the model. Consecutive aircraft are sufficiently spaced in order to address these time based and distance based regulations.

- **Runway dependencies:** Next to separation standards, the runway dependencies imply that not every operations is possible. The model tries to find an optimal solution while addressing these various dependency constraints.

- **WTC grouping:** The optimized model tries to find an optimal set of consecutive aircraft in order to reduce delay. The Wake Vortex Category of an aircraft is of impact, since different separation regulations are in place for a different set of consecutive aircraft.

- **Mixed mode:** If the time windows allows for enough time spacing, mixed mode operations are allowed in this example. Although mixed mode operations increase workload for ATC and increase potential risks, it still is a interesting approach in order to reduce fuel consumption and potentially noise levels. An example is indicated by a black triangle in Figure 8.3 for an operation on the Kaagbaan (24) observed at the x-axis at time $t = 106$ [s].

- **Time to Runway:** An arriving aircraft gets allocated a runway at the IAF location. From this location it can then proceed towards the allocated runway. A different runway leads to a change in time to runway. This is observed by looking at the first Heavy MTOW aircraft in Figure 8.3, indicated by the large red indicator at time $t = 37$. In comparison, the same aircraft is assigned at a different runway at a later time in Figure 8.2 at time $t = 51$. The time to runway differs

between both figures. By a shorter flying time net fuel consumption is reduced.

- **Delay:** Trade-off by the optimization model can have impact on delay. The model can choose for an aircraft to delay for the following time steps; $d = \{0, 20, 40, 60\}$. It might occur that an aircraft is intentionally delayed, if a more beneficial runway becomes available after the time of delay.

- **Risks:** It is noted that although all major dependencies and regulations are addressed for, actual operations at AAS might be bounded to additional constraints. These constraint might be applicable to the increased risk when workload for ATC is intensified. Other constraints might be existent by ground restrictions of taxiing aircraft when they cross a runway. These factors have not been implemented in the simulation model.

8.3.2 Noise to Fuel Ratio

In this section further analysis is done on the Pareto fronts established in the different scenarios of Chapter 7. It is researched if an optimal ratio between noise and fuel can be distilled from the curvature of the Pareto front.

Defining a ratio is only possible if normalization is applied since the dimensions of both numerator and denominator should be identical or otherwise dimensionless. The selected normalization method is selected to be the Weighted Sum Method. Noise and fuel are now both dimensionless and can therefore be compared. From Figure 8.4 it can be observed that multiple Pareto fronts are collected in one figure. Analyzing the ratio between noise and fuel, which gives a beneficial solution for multi-objective optimization, shows interesting results. The following formula is established for this ratio:

$$\text{Noise to Fuel Ratio:} \quad \frac{N_{houses}}{F_{fuel}} \tag{8.1}$$

An optimal solution will always consist of a trade-off between fuel and noise. In both academics and industry, a discussion about which trade-off is most satisfactory is an interesting one when multiple stakeholders are involved. Using the previously defined ratio it is possible to quantify this trade-off. It gives an handle for further discussions on the topic of runway allocation. An indication of the most optimal settings is given in Figure 8.4 by the selected quadrangle. It can be viewed from the ratio and curvature of the Pareto front, solutions exists were a small step in noise increase can lead to significant decrease in fuel consumption. The opposite also holds if noise is optimized further; when noise exposure is decreased, fuel consumption will grow. From analyzing the ratios between noise and fuel, it is come to a conclusion that a range of weighting settings provide results which are both satisfactory for fuel and noise with respect to current reference scenarios. Different scenarios show the same range in ratios to be given interesting results. The range in ratios is the following, in which the boundaries indicate the different α-weighting factors:

$$\text{Optimal Noise to Fuel Ratio Range:} \quad \alpha_1 < \frac{N_{houses}}{F_{fuel}} < \alpha_2 \tag{8.2}$$

$$\text{where:} \quad \alpha_1 = 0.07 \tag{8.3}$$

$$\alpha_2 = 0.09 \tag{8.4}$$

Flexibility does potentially improve the runway schedule's fuel and noise performance. Currently a preference list is used which leaves ample room for flexibility. It is shown that flexibility through optimization has significant effect in potential fuel, emission and noise savings. It can be observed that certain optimization settings indicate an optimal noise to fuel ratio range. The established ratio is subject to discussion, but gives an interesting look on the potential savings in airport operations using optimization.

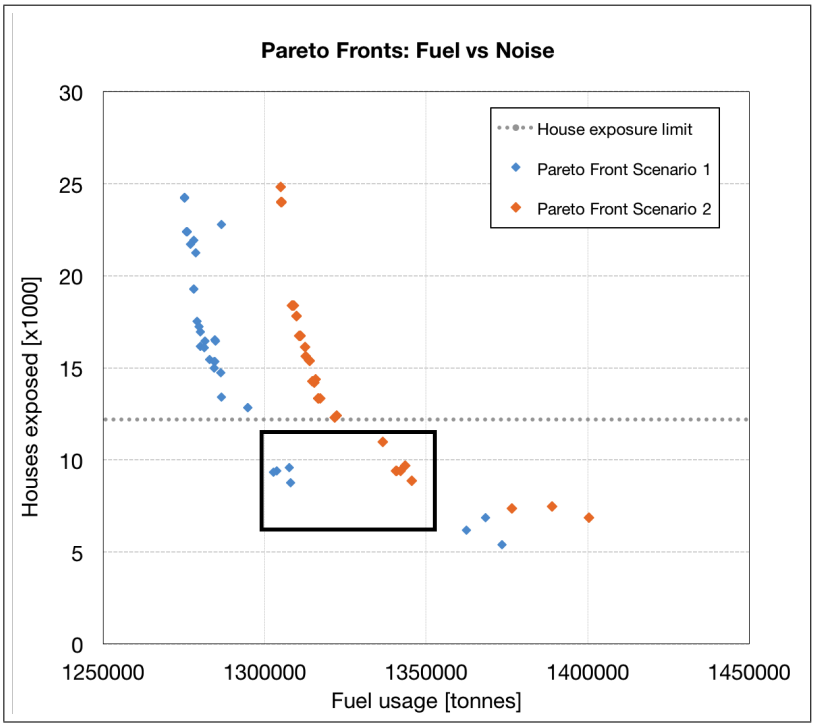

Figure 8.4: Noise to Fuel Ratio; the selected square indicates the range of optimum settings.

Chapter 9

Conclusions and Recommendations

In this chapter conclusions are given on the performed study regarding flexible arrival and departure runway allocation. Section 9.1 shows the general conclusion from this research. Limitations with respect to the developed allocation model are discussed in Section 9.2. Finally, recommendations and suggestions for future research possibilities are given in Section 9.3.

9.1 General Conclusion

The main goal of this research is to research if fuel burn can significantly be reduced using flexible arrival and departure runway allocation. This is done by addressing a predefined set of variables and rules, accounting for noise annoyance, runway capacity and the current and future demand of flights. It can be concluded from this research that flexible allocation indeed can have significant beneficial impact on fuel usage. Optimization through flexible runway allocation is tested for the Amsterdam Airport Schiphol case study. Conclusions which result from this study are explained in more detail in this section.

The first main conclusion is that fuel usage can be significantly reduced by flexible runway allocation. Under the assumption of a linear relation between fuel usage and emissions, emissions can additionally be reduced. In order to test the potential fuel and emission savings of flexible runway allocation, an optimization tool has been developed. In order to make a comparison, both reference scenarios and optimized scenarios are evaluated. Two scenarios have been established; one scenario for low wind levels resulting in all runways available and one scenario in which operations are restricted by local conditions. For a full day simulation of a low wind scenario a potential fuel increase for multi-objective optimization corresponds to a saving of 157 ton kerosene (9.2%) in fuel consumption. It is shown that for a scenario in which local conditions have their effect on runway availability, savings are equally possible. Due to deteriorated weather conditions, flight operations are restricted to fewer runways. It is noted that these restrictions have impact on the potential of fuel savings by the runway allocation tool. Still some increase in efficiency is observed for the selected multi-objective optimization. For the full day scenario with runway restrictions fuel savings are around 26 ton (1.74%). In both scenarios the noise exposure to the environment is within desirable noise regulation limits.

Secondly, it can be concluded that flexibility and accompanied savings in fuel, noise and emissions, are depended of the time of day and the accompanied peaks in runway demand. Several time of day segmented runs are researched to this end. These are split up in morning, afternoon and evening segments. For the scenario 1 case study with no runway restrictions potential fuel efficiency increase is found. The fuel savings for the morning run are 27 ton (5.19%), the afternoon run shows 58 ton (9.01%) fuel usage decrease and the evening run displays a 38 ton (4.44%) fuel reduction. Even for the scenario 2 case in which several runways are restricted, potential savings are found for the various time of day segments. Morning operations are relatively lower due to high runway demand; 3 ton (0.6%). Afternoon operations indicate 13 ton (1.95%) potential savings. Finally, evening operations show 5

ton (1.92%) in fuel savings. In comparison with Scenario 1 potential efficiency gains are lower due to reduced flexibility since fewer runways are available. The reason for the total fuel savings of cumulative time segments to be smaller then the total of the full day run, is due to increased flexibility of a full day's run. Since the model is able to optimize for a longer time span, more flexibility is obtainable. It is thereby possible to mitigate the noise penalty factors which are apparent in the evening run. By compensation, aircraft in that time segment can be assigned a more profitable runway when full day optimization is performed.

When comparing the different time segments for both scenarios, it is observed that the potential savings for both morning segments are lowest. It can be established that the morning peak has high runway demand. Due to this high demand, capacity is restrained and results in lower flexibility. The afternoon segment is for both scenarios the most profitable. This is due to a reduction in demand of runways, leading to increased flexibility. For the evening simulation it is found that due to a higher demand, flexibility is lower as holds for the morning simulations. Due to penalty factors a different assignment is found when comparing a full day scenario to the evening scenario.

Delaying of aircraft deliberately can have a positive effect on flexibility. Results show that optimization has influence on delay. For a fuel optimized case, often delay is reduced to a minimum in order to put aircraft on the ground as early as possible, hence reducing total fuel consumption. Nevertheless, in some cases it may be possible for the optimization to select a longer total delay duration. Reason behind this, is that an aircraft can hold for a beneficial runway to become available, hence reducing total flight/taxiing time. Runway flexibility is thereby increased.

It can be concluded that annual savings in terms of fuel and emission by flexible runway allocation have significant potential. By looking at potential annual gains, savings in fuel and emissions might be beneficial if the runway allocation model is utilized. Preferably more simulations with different settings have to be researched. The two discussed scenarios give an indication of the potential that flexible allocation might have. The annual efficiency increase in fuel and emission savings can be established to be approximately 4% - 6% or 15,000 - 30,000 tons kerosene under the given assumptions.

A range of optimal noise to fuel ratios exists for multi-objective optimization. From comparison of several scenarios it can be observed that certain optimization settings indicate an optimal noise to fuel ratio range. The established ratio is subject to discussion, but gives an interesting look on the potential savings in airport operations using allocation optimization. A range of optimal α-weights lies approximately between 0.07 and 0.09, which has improved fuel, noise and emission rates with respect to reference scenarios.

In conclusion, using the developed runway allocation tool to flexibly allocate arrival and departure runways can have significant impact on both fuel and emissions savings. Depending on the flexibility of available runways, mainly restricted by separation- and noise regulations, runway demand, local conditions and maintenance, savings are possible. For scenarios where there is plenty of room for flexibility, savings are evident. For restricted scenarios potential savings exist, although to a lesser extend. Due to the level of runway demand, afternoon operations have most flexibility and potential for savings. Annual savings can amount to significant fuel and emission reduction.

9.2 Limitations

Here an overview is given of the limitations of the runway allocation model. The limitations indicate current restrictions and shortcomings of the model. To overcome these limitation, suggestions for areas of further improvement are discussed in more detail in this section.

- An important limitation in the runway allocation tool lies in the establishment of the runway dependencies. Currently, the runway dependencies are in binary format indicating runway availability

on a 20 second interval. A smaller interval will represent reality more accordingly. Additionally the runway dependencies do not consider a closing and opening case of consecutive aircraft on the same common approach path with different approach speeds. Further implementing separation regulations for consecutive aircraft of different MTOW classes is desirable.

- In this research only two runway configurations have been researched for the Amsterdam Airport case. Ideally, a large number of scenarios could be simulated in order to more accurately represent annual operations at airports. The scenarios should be ran with different parameters, thereby representing various weather conditions and runway configurations.

- Certain model parameters have been simplified with respect to reality in this study which is a limitation with respect to actual operations. Fuel computations can be based on a broader set of input variables; windspeed, aircraft speed, aircraft type etc. hence increasing the complexity of the model. Several methods exist in order to compute emissions using a more dynamic method, e.g. Boeing 2 method. Furthermore, unique aircraft weights due to stage length properties can be incorporated.

- In terms of the used noise regulations only exposure to houses has been evaluated. Noise hindrance of individuals and severe sleep disturbances have not been considered. Notwithstanding, they pose additional constraints on the runway's fuel and noise performance. From the results of the runway allocation model it is possible to compute these noise hindrances afterwards using a dose-response relation. It is not possible to optimize for these values using the optimization tool.

- Segment computations for fuel calculations have been done by measurements of AIP charts. Actual flight data could be used in order to obtain more accuracy in these segment computations. Fuel flow and total fuel consumption are taken constant per segment, which is a limitation.

- Other limitations are the assumption of only taking two aircraft as representative for the Medium and Heavy MTOW class. Implementing more MTOW classes and aircraft types would improve the model. Only one type of procedure (IACO-A) has been applied for departures. For arrivals an approximation of step wise descent has been applied. This could be further improved to incorporate more procedures.

- Computation time can be improved in order to compute more scenarios within a limited time frame. This would also add to the potential of having real time flight schedules as live input.

9.3 Recommendations

This section will elaborate on recommendations for further research. Both the fields of academics as well as the aviation industry might gain from future research on the topic of flexible runway allocation. Several suggestions are listed below:

- Further research can be readily performed using the runway allocation model. Due to its generic characteristics, input parameters can be changed. A suggestion for further research is to study different arrival and departure procedures. The case study in this report uses ICAO-A as procedure for departing aircraft. Implementing other procedures might lead to interesting results in terms of noise reduction. Procedures for arrivals, such as step-wise descent and Continuous Descent Approach, can be further researched on their effect on noise and fuel. Additionally, runway tracks and possible Initial-Approach Fixes (e.g. a potential fourth IAF for Schiphol Airport) can be added to the simulation.

- The developed model can be further expanded by incorporating trajectory allocation. In this study flight segments were of fixed length. Several studies focus on arrival or departure trajectory optimization, which might be an excellent addition to the studies done for this research. Trajectory

allocation in combination with runway allocation will prove a strong tool in order to further reduce fuel, noise and emissions. This will further increase the flexibility of the runway allocation model.

- Optimization is done for fuel and noise only, while considering a linear relation with emissions. The relation can be further analyzed, and even optimization for emissions could be added to the objective function. This would make it is possible to specifically optimize for certain types of emissions. This also holds for delay, if it is preferred to keep delay to a minimum. Additionally, risks can be evaluated and brought into the objective function.

- The capacity model can be implemented in currently used methods for determining and allocating runways. The addition of a real time flight schedule input might be useful in order to allocate aircraft as soon as they enter the specified airspace. Probability factors within scheduling will then play a role, which indicates an interesting research area and improvement.

- Dynamic stage length has not been included in this study. This indicates the difference in aircraft weight depending on the origin or destination. Different fuel weight (i.e. an heavier aircraft) might lead to increased fuel consumption and thereby a different trade-off in optimization. Additionally, studies can further research the possibilities of implementing variable airspeed of aircraft. The common approach path will then play a role in determining runway dependencies.

- The model can be expanded by implementing aircraft specific characteristics for a large set of aircraft, hence increasing fleet mix characteristics. This research assumed only two types of aircraft MTOW classes, whereas a more realistic allocation model could include a wide variety of aircraft types. For future research, the impact of WTC grouping can then be simulated more accurately. Additionally, the effect on noise and fuel of old aircraft versus a new fleet can be researched.

- The developed optimization method chosen for this research was Mixed-Integer Linear Programming. This method was selected after careful trade-off from a variety of optimization algorithm methods. Research can be performed into other optimization techniques such as genetic algorithm, simulated annealing, dynamic search or a combination of these.

- This study has not researched the fields of taxi- and apron capacity and ground restrictions. It is recommended to implement these in order to give a broader scope of runway capacity as it occurs at airports.

- It is recommended to further investigate the potential risks of flexible arrival and departure allocation. Not only should runway dependencies factors be further validated, also the human aspect of e.g. ATC workload should be researched. An interesting research area arises if hard- and software are indeed able to flexibly allocate aircraft to runways; to what extend is human interaction desirable.

- In terms of industry recommendations this model can be used and expanded to perform research on a new flexible preference list for assigning aircraft. Since a pure flexible allocation schedule will increase ATC workload, a semi-flexible preference list can be established for time of day segments with each having specific flights origins and destination combinations and runway demand. The currently used preference list can thereby be significantly improved to reduce fuel and emissions, while maintaining desirably noise exposure to the environment.

Appendix A

Procedures

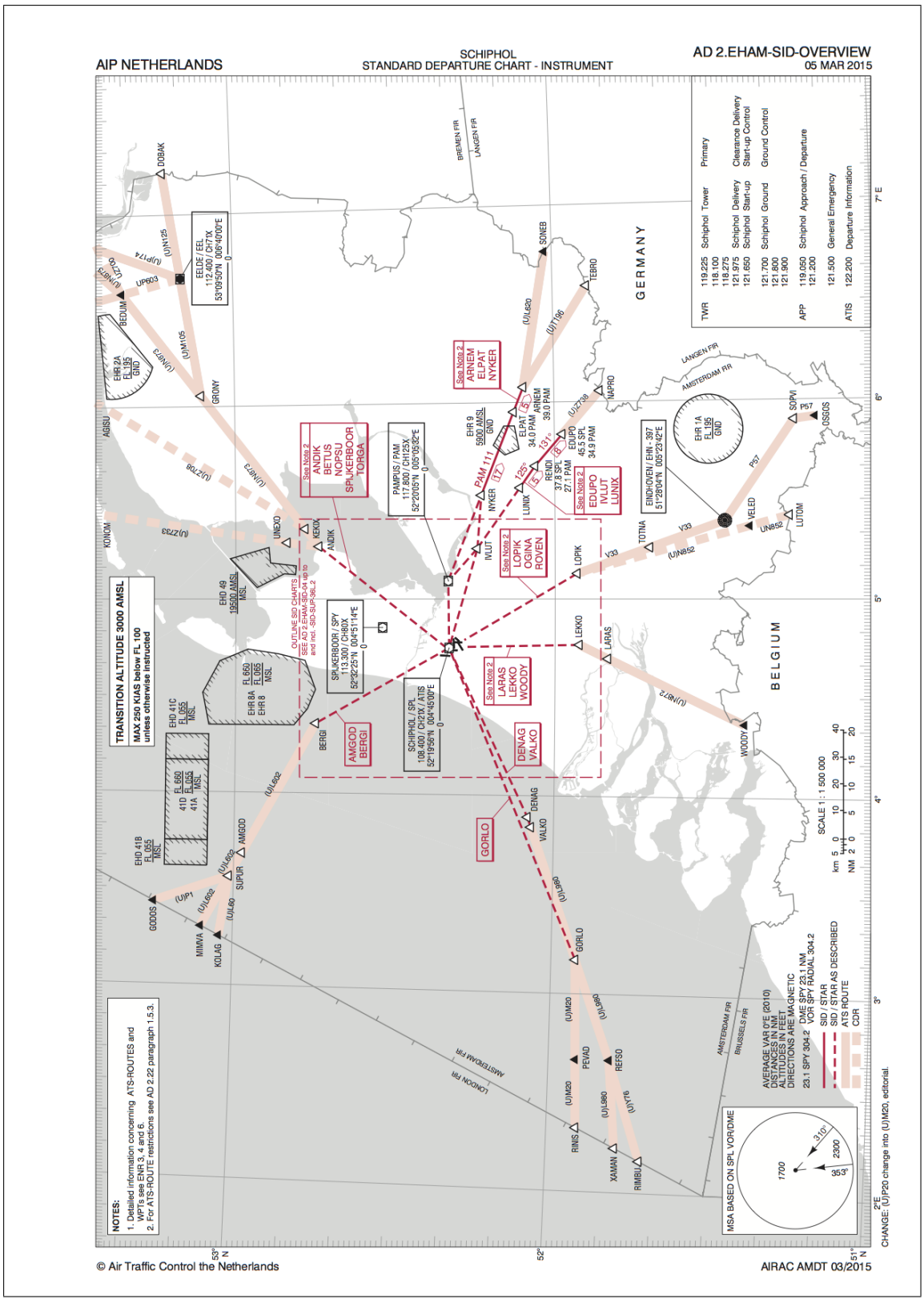

Figure A.1: SID AAS [14].

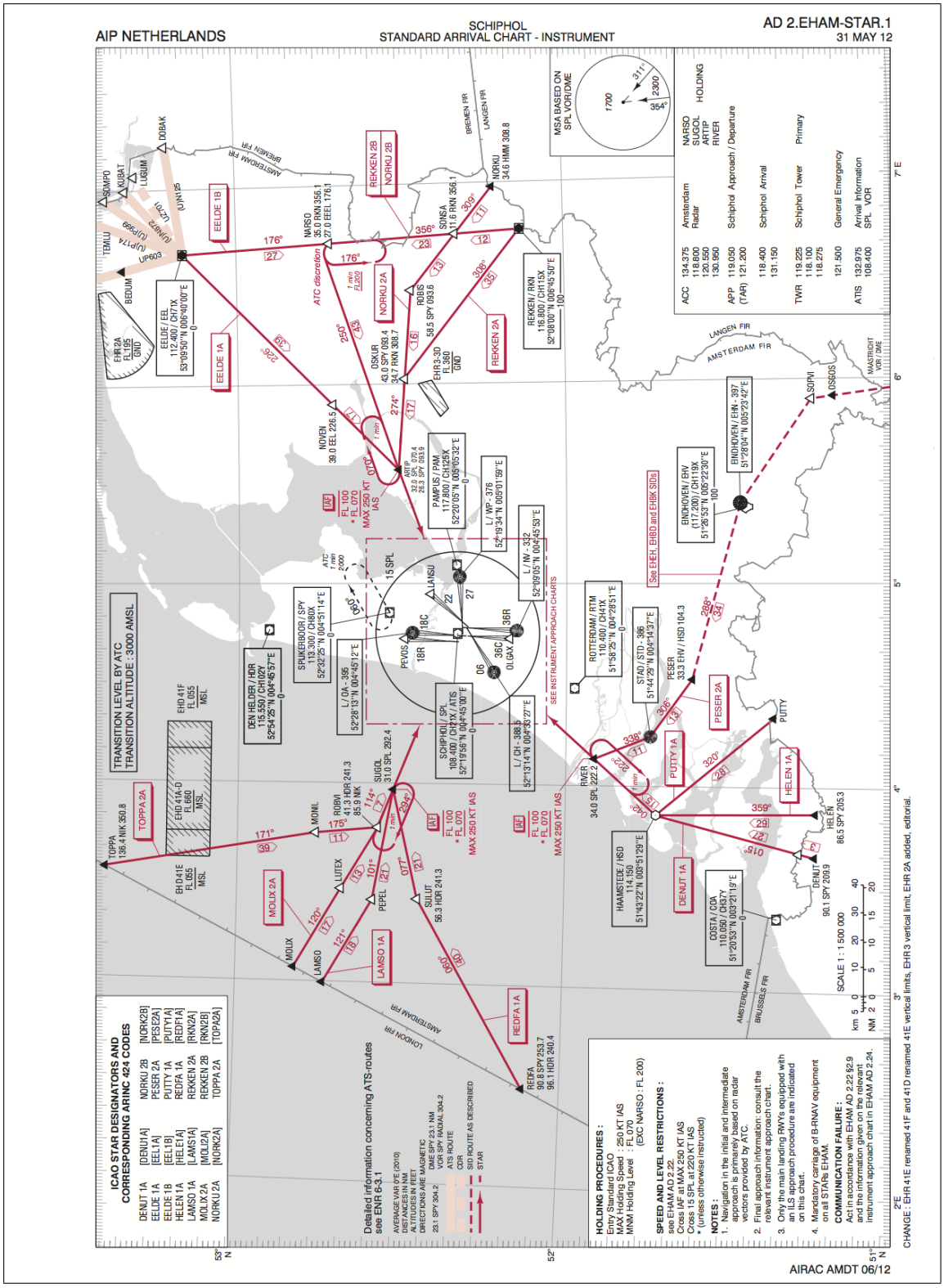

Figure A.2: STAR AAS [14].

Appendix B

Airports

Figure B.1: Converging/diverging runways: Chicago O'Hare Airport (ORD)

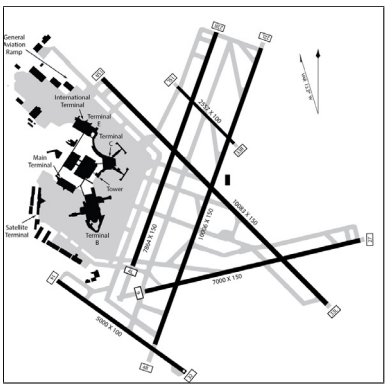

Figure B.2: Converging and intersecting runways: Boston Logan Airport (BOS)

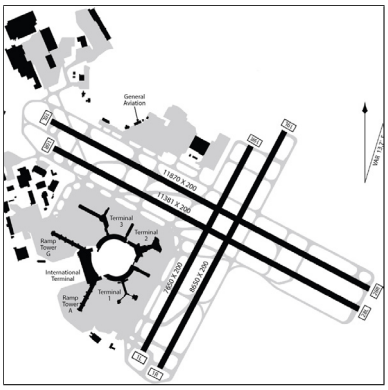

Figure B.3: Intersecting runways: San Franscico Airport (SFO)

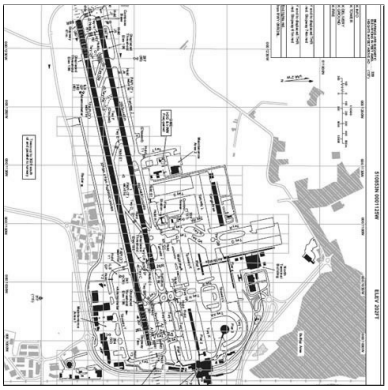

Figure B.4: Operated as single runway: London Gatwick Airport (LGW)

Appendix C

Scheduling

C.1 Flight Schedule

Table C.1: AAS Flight Schedule (arrivals excerpt).

FLID	TIME	ACTYPE	ORIGIN	GATE	RWY	IAF
DL0049	07:00	332	BOM	E17	18R	ARTIP
KL0438	07:00	332	BAH	E22	18R	ARTIP
KL0590	07:00	333	ACC	G03	18R	RIVER
KL0736	07:00	744	CUR	E20	18R	SUGOL
KL0571	07:05	772	DAR	E19	18R	ARTIP
SQ324	07:10	772	SIN	G07	18R	ARTIP
KL1340	07:10	73W	BLL	C10	18R	ARTIP
KL1852	07:15	F70	DUS	B65	18C	ARTIP
KL0836	07:15	77W	DPS	F07	18R	ARTIP
KL1776	07:15	73W	HAM	C08	18R	ARTIP
KL1750	07:15	F70	BRE	B20	18R	ARTIP
KL1720	07:15	F70	BRU	A45	18R	RIVER
UA946	07:15	763	IAD	E04	18R	SUGOL
KL1900	07:20	E90	HAJ	B32	18C	ARTIP
KL1880	07:20	F70	NUE	B63	18R	ARTIP
KL1866	07:20	E90	STR	B51	18R	ARTIP
KL1818	07:20	73H	TXL	C05	18R	ARTIP
KL1124	07:25	73W	CPH	C11	18R	ARTIP
KL1736	07:25	F70	LUX	B36	18R	RIVER
KL0642	07:25	772	JFK	D47	18R	SUGOL
KL1196	07:30	73H	SVG	D04	18C	ARTIP
KL0662	07:30	74E	IAH	F05	18R	SUGOL
KL0714	07:30	744	PBM	E22	18R	SUGOL
KL0410	07:35	332	ALA	D57	18C	ARTIP
KL0652	07:35	74E	IAD	F04	18R	SUGOL
DL0034	07:35	76W	EWR	E06	18R	SUGOL
LH3334	07:40	CR9	HAM	B94	18C	ARTIP
KL1206	07:40	E90	KRS	B28	18C	ARTIP
UA964	07:45	763	EWR	E02	18R	SUGOL
KL1332	07:50	E90	AAL	A43	18C	ARTIP
EZS1041	07:50	319	BSL	H01	18C	RIVER
3O2125	07:50	32S	CMN	G02	18R	RIVER
KL1314	07:50	E90	BOD	B16	18R	RIVER
KL0672	07:50	M11	YUL	F08	18R	SUGOL
KL1152	07:50	E90	GOT	B53	22	ARTIP
KL1212	07:55	F70	TRF	B71	22	ARTIP
CAI509	08:00	73H	AYT	D12	22	ARTIP
KL1300	08:05	E90	TLS	B55	18R	RIVER
AF5482	08:05	ER4	SXB	B73	18R	RIVER
DL0619	08:05	333	DTW	E24	18R	SUGOL
KL1382	08:05	73H	KBP	D46	22	ARTIP
KL0554	08:05	772	CAI	F05	22	ARTIP
KL1178	08:05	F70	LPI	B74	22	ARTIP
KL1362	08:05	73W	WAW	C06	22	ARTIP
KL1582	08:05	E90	BLQ	A46	22	RIVER
KL1184	08:10	73W	BGO	B23	18R	ARTIP
KL1502	08:10	F70	NWI	A49	18R	SUGOL

C.2 Time to Runway

Table C.2: Time to Runway overview. SECTOR indicates an outbound flight, hence the time represents the time to runway from the AIBT. All values are expressed in seconds.

Runway		R06	R09	R18C	R18R	R24	R27	R36C	R36R	R18L	R36L
IAF	SUGOL	709	467	747	777	1040	1032	747	823	0	0
	ARTIP	1177	935	735	766	503	495	831	792	0	0
	RIVER	636	623	1202	1261	1177	1170	438	514	0	0
SECTOR	ANDIK	278	240	371	714	180	376	240	269	376	714
	NYKER	278	240	371	714	180	376	240	269	376	714
	LEKKO	278	240	371	714	180	376	240	269	376	714
	VALKO	278	240	371	714	180	376	240	269	376	714
	BERGI	278	240	371	714	180	376	240	269	376	714

C.3 Time to Taxi

Table C.3: Time to taxi, empirically determined. All values are expressed in seconds.

Runway		R06	R09	R18C	R18R	R24	R27	R36C	R36R	R18L	R36L
IAF	SUGOL	60	52	80	154	39	81	52	58	0	0
	ARTIP	60	52	80	154	39	81	52	58	0	0
	RIVER	60	52	80	154	39	81	52	58	0	0
SECTOR	ANDIK	60	52	80	154	39	81	52	58	81	154
	NYKER	60	52	80	154	39	81	52	58	81	154
	LEKKO	60	52	80	154	39	81	52	58	81	154
	VALKO	60	52	80	154	39	81	52	58	81	154
	BERGI	60	52	80	154	39	81	52	58	81	154

C.4 Speed Limits

Table C.4: Example of speed limits from AIP charts for AAS [14].

Speed limit	Kts indicated airspeed
Aircraft at distance of more than 4 NM to runway threshold	160
Aircraft within 15 NM of SPL DME (unless otherwise stated by ATC)	220
Aircraft below 10,000 ft (after crossing IAF)	250

Appendix D

Handhavingspunten

Table D.1: Validation using *Handhavingspunten* [60].

Location	**Limit value** L_{den} [dbA]	**Simulated value** L_{den} [dBA]	**Percentage** [%]
Point 5	57,92	57,98	101,4
Point 6	57,4	60,55	206,5
Point 17	57,15	58,29	130,0
Point 18	61,25	56,86	36,4
Point 19	53,9	52,21	67,8
Point 21	57,47	47,69	10,5
Point 23	56,71	47,69	12,5
Point 24	57,56	60,68	205,1
Point 25	57,91	52,02	25,8
Point 26	55,43	57,34	155,2
Point 27	56,19	54,78	72,3
Point 28	55,51	54,26	75,0
Point 29	57,04	55,41	68,7
Point 30	57,54	50,59	20,2
Point 31	58,78	45,1	4,3
Point 32	56,99	41,82	3,0
Point 33	56,77	40,28	2,2

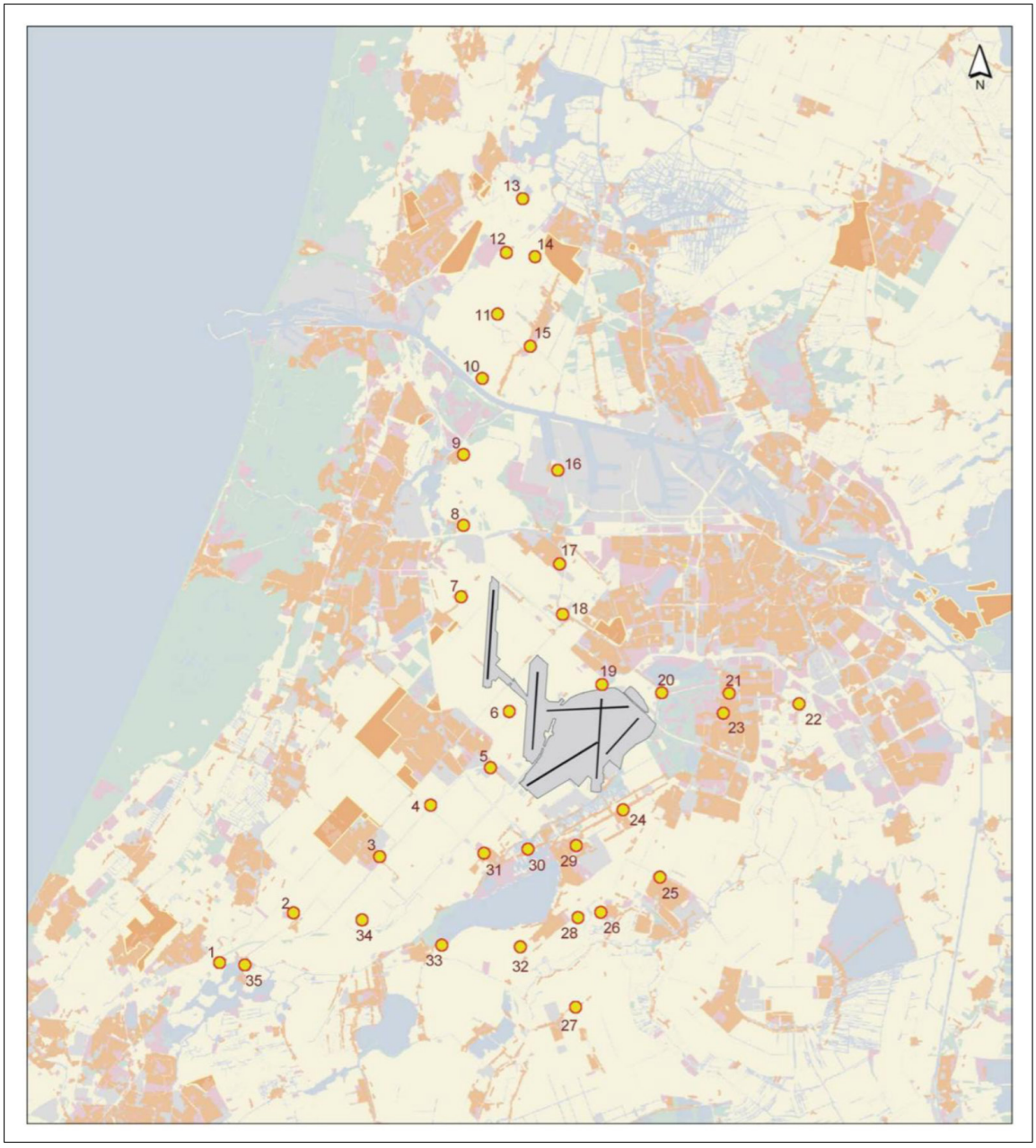

Figure D.1: Handhavingspunten AAS [60].

Appendix E

Fuel Flow

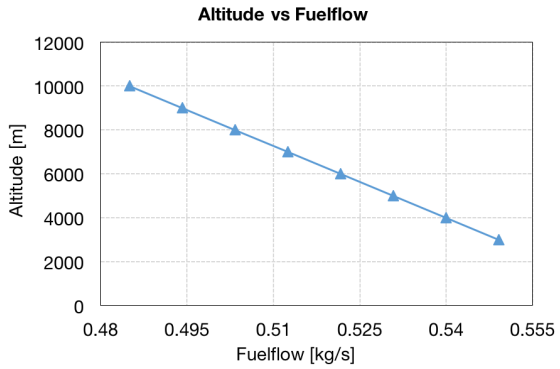

Figure E.1: Fuel flow Boeing 777-200ER Initial phase (1).

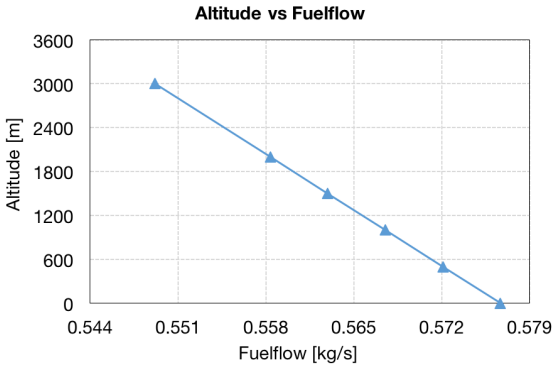

Figure E.2: Fuel flow 777-200ER Final phase (2).

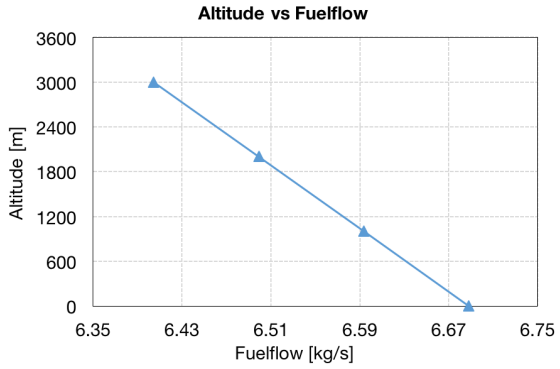

Figure E.3: Fuel flow 777-200ER Take-Off (5).

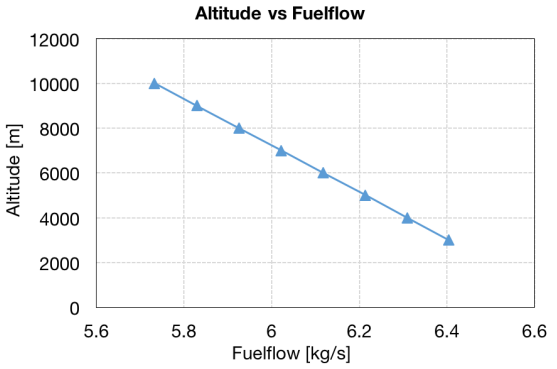

Figure E.4: Fuel flow 777-200ER Climb-Out (6).

Appendix F

Runway Allocation

F.1 Scenario 1: Morning Run

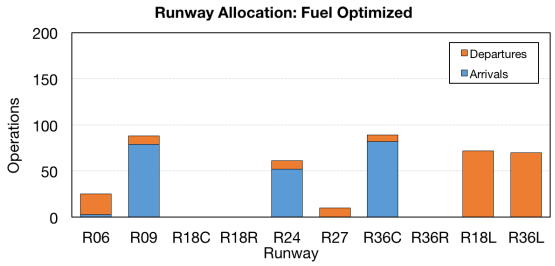

Figure F.1: Runway allocation for a fuel optimized schedule.

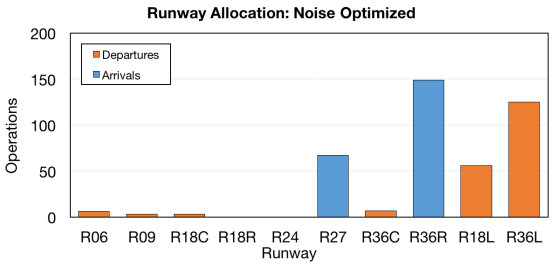

Figure F.2: Runway allocation for a noise optimized schedule.

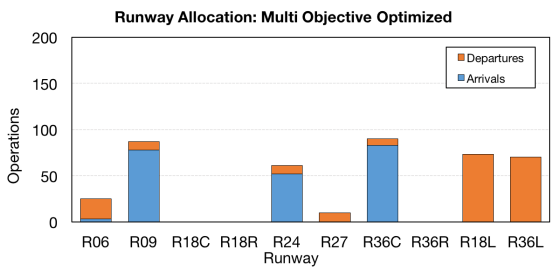

Figure F.3: Runway allocation for a multi-objective optimized schedule.

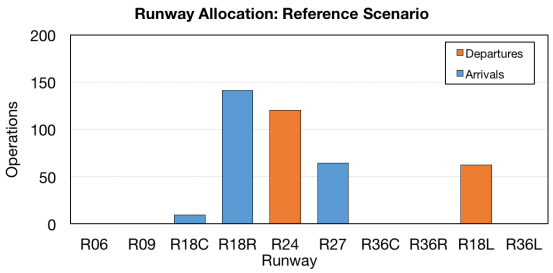

Figure F.4: Runway allocation for the reference scenario.

F.2 Scenario 1: Afternoon run

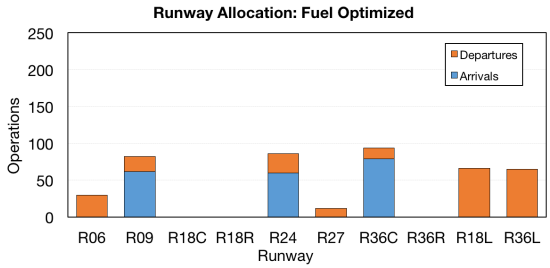

Figure F.5: Runway allocation for a fuel optimized schedule.

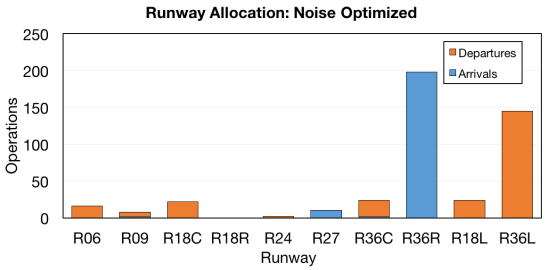

Figure F.6: Runway allocation for a noise optimized schedule.

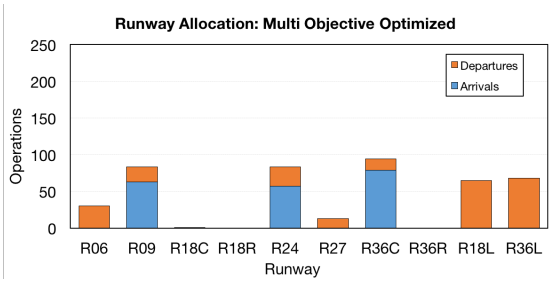

Figure F.7: Runway allocation for a multi-objective optimized schedule.

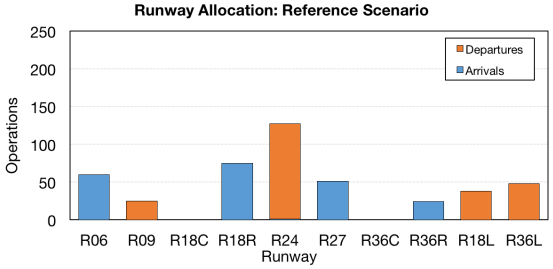

Figure F.8: Runway allocation for the reference scenario.

F.3 Scenario 1: Evening run

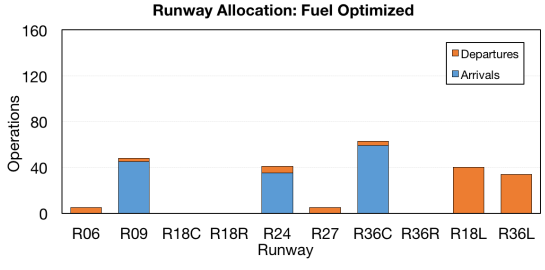

Figure F.9: Runway allocation for a fuel optimized schedule.

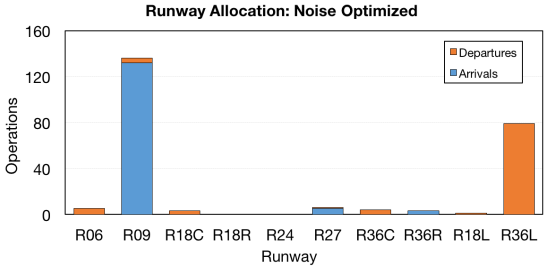

Figure F.10: Runway allocation for a noise optimized schedule.

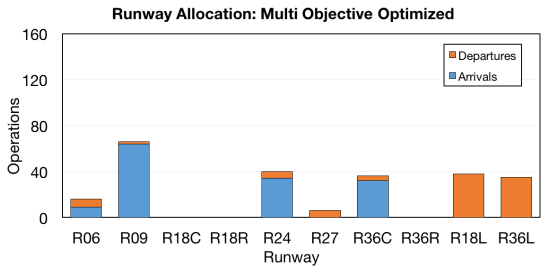

Figure F.11: Runway allocation for a multi-objective optimized schedule.

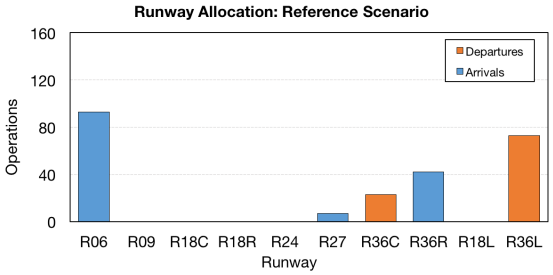

Figure F.12: Runway allocation for the reference scenario.

F.4 Scenario 2: Morning run

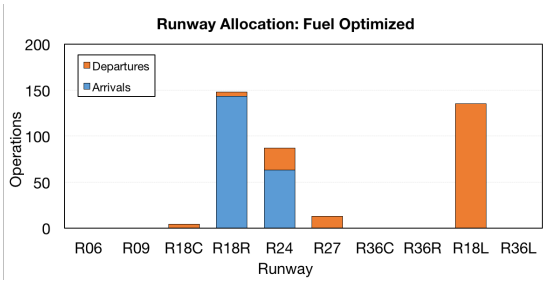

Figure F.13: Runway allocation for a fuel optimized schedule.

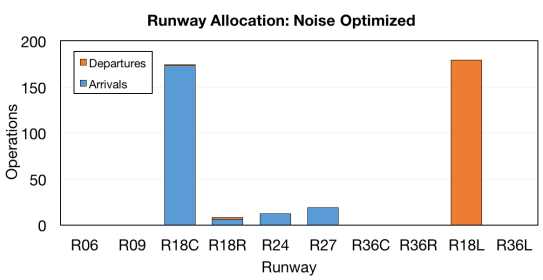

Figure F.14: Runway allocation for a noise optimized schedule.

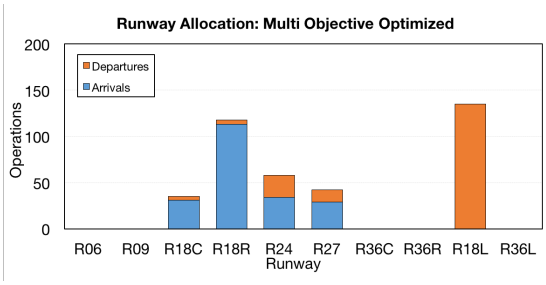

Figure F.15: Runway allocation for a multi-objective optimized schedule.

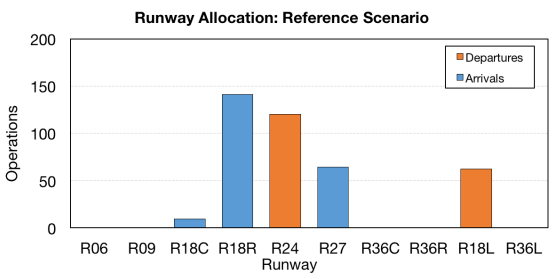

Figure F.16: Runway allocation for the reference scenario.

F.5 Scenario 2: Afternoon run

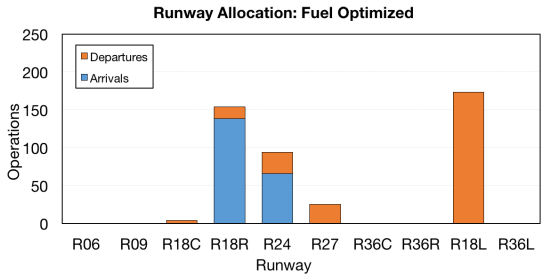

Figure F.17: Runway allocation for a fuel optimized schedule.

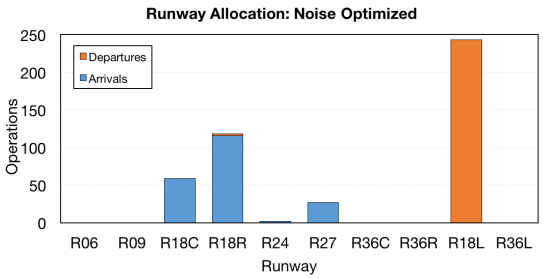

Figure F.18: Runway allocation for a noise optimized schedule.

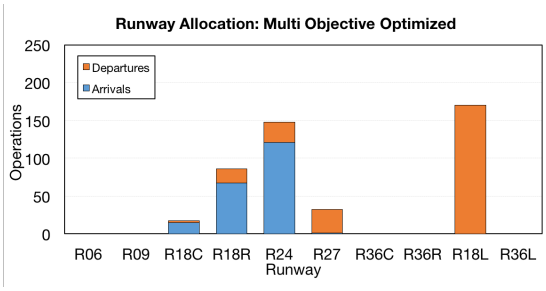

Figure F.19: Runway allocation for a multi-objective optimized schedule.

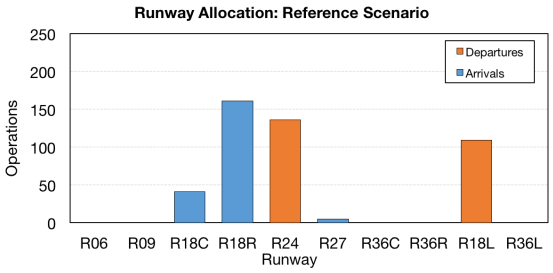

Figure F.20: Runway allocation for the reference scenario.

F.6 Scenario 2: Evening run

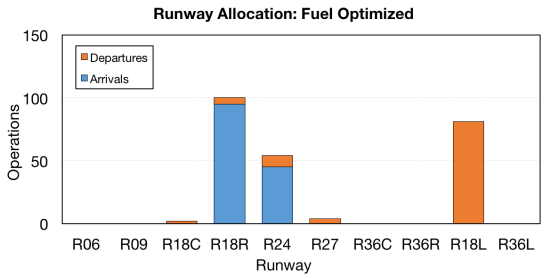

Figure F.21: Runway allocation for a fuel optimized schedule.

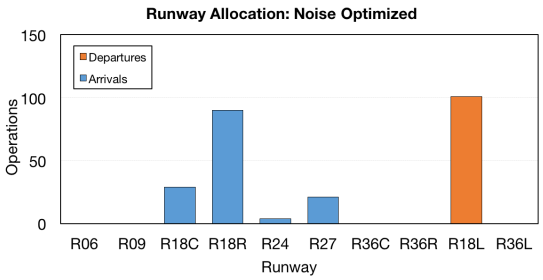

Figure F.22: Runway allocation for a noise optimized schedule.

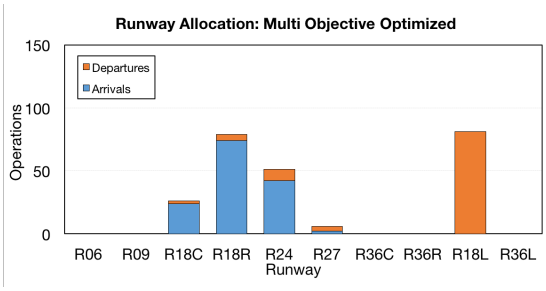

Figure F.23: Runway allocation for a multi-objective optimized schedule.

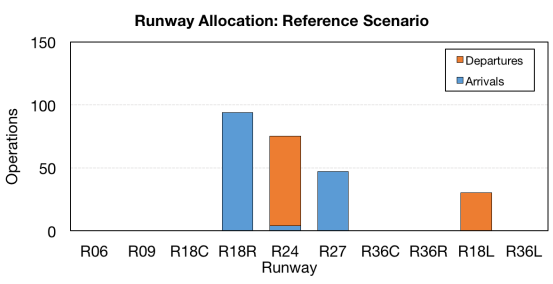

Figure F.24: Runway allocation for the reference scenario.

Appendix G

Noise Grids

G.1 Scenario 1

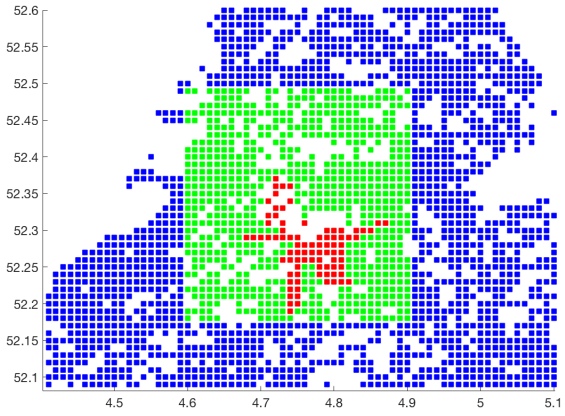

Figure G.1: Noise Grid Scenario 1: Full Day, fuel optimized.

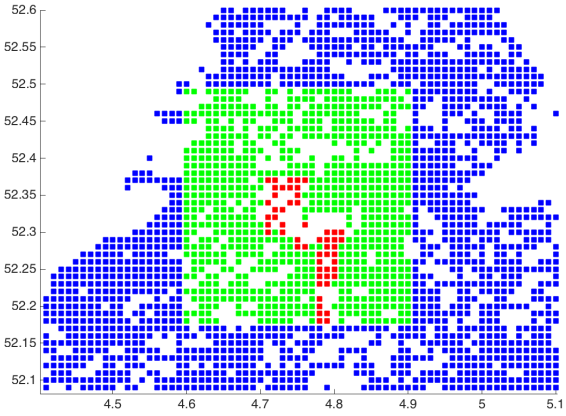

Figure G.2: Noise Grid Scenario 1: Full Day, noise optimized.

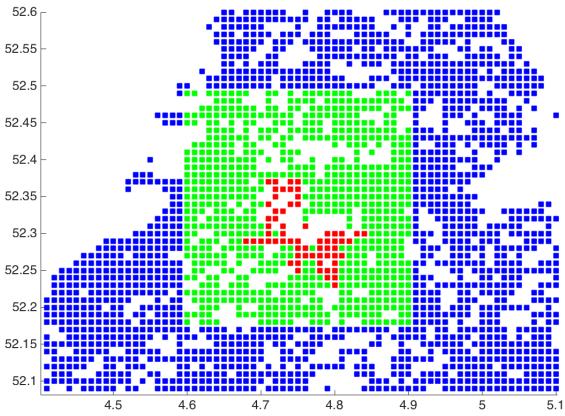

Figure G.3: Noise Grid Scenario 1: Full Day, multi-objective optimized.

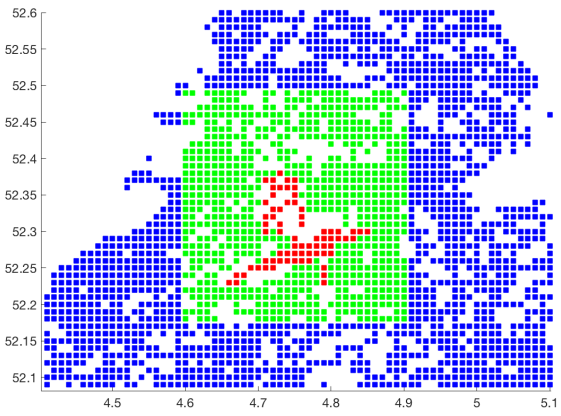

Figure G.4: Noise Grid Scenario 1: Full day, Reference Scenario.

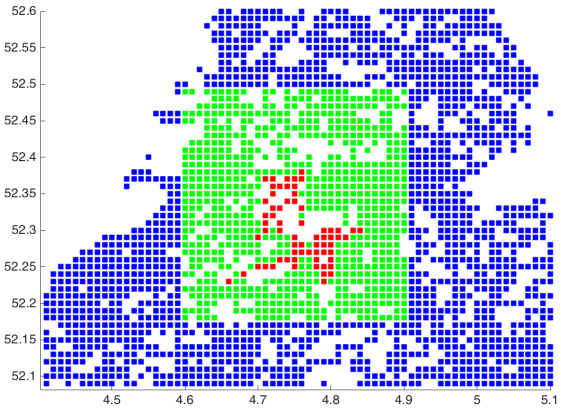

Figure G.5: Noise Grid Scenario 1: Morning, multi-objective optimized.

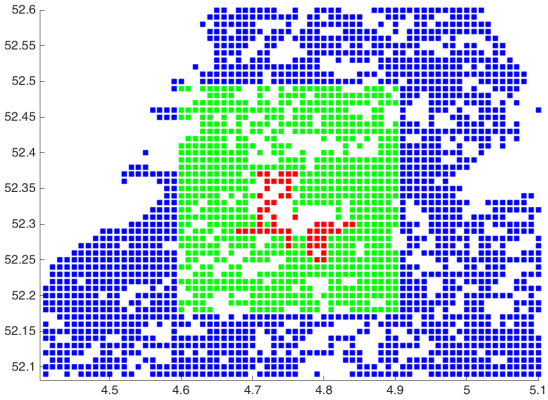

Figure G.6: Noise Grid Scenario 1: Afternoon, multi-objective optimized.

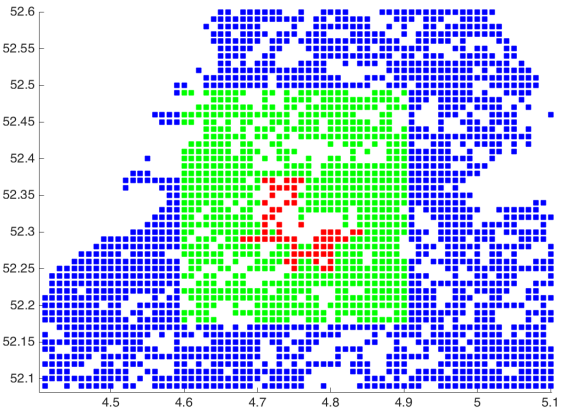

Figure G.7: Noise Grid Scenario 1: Evening, multi-objective optimized.

G.2 Scenario 2

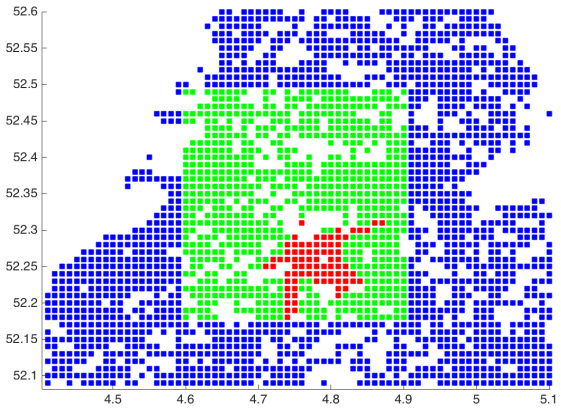

Figure G.8: Noise Grid Scenario 2: Full Day, fuel optimized.

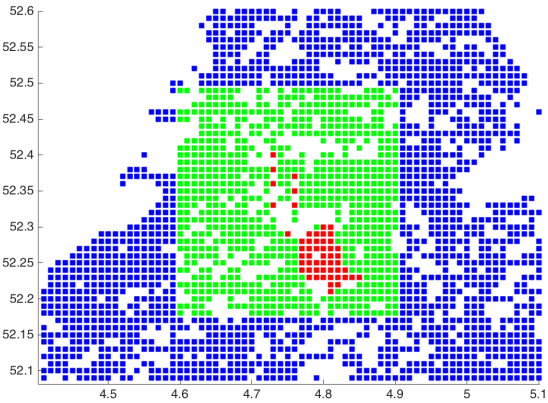

Figure G.9: Noise Grid Scenario 2: Full Day, noise optimized.

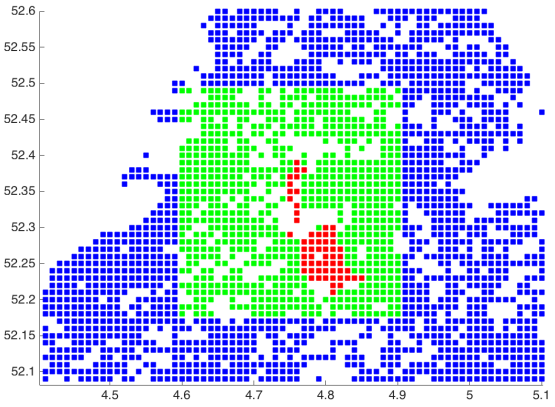

Figure G.10: Noise Grid Scenario 2: Full Day, multi-objective optimized.

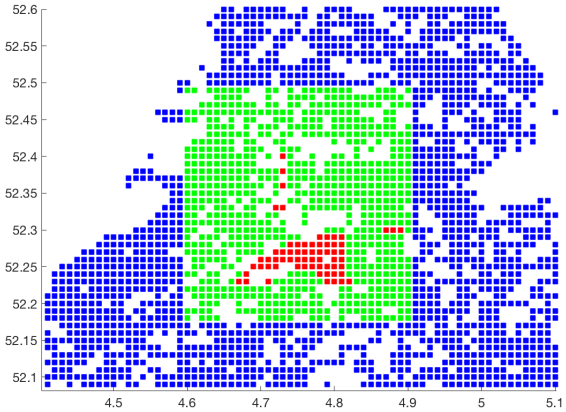

Figure G.11: Noise Grid Scenario 2: Full day, Reference scenario.

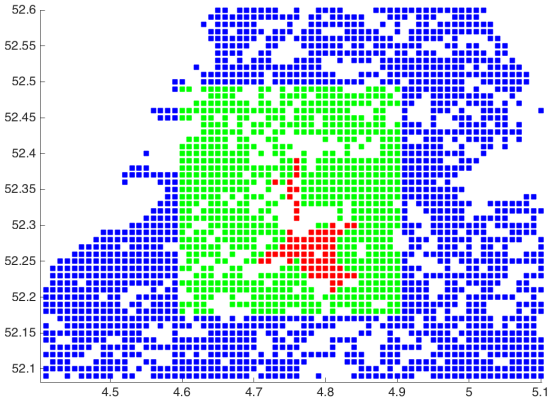

Figure G.12: Noise Grid Scenario 2: Morning, multi-objective optimized.

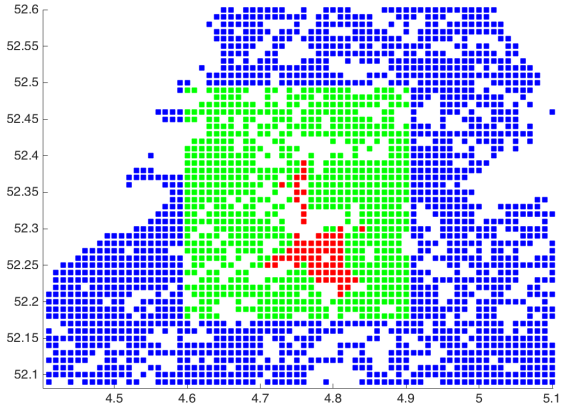

Figure G.13: Noise Grid Scenario 2: Afternoon, multi-objective optimized.

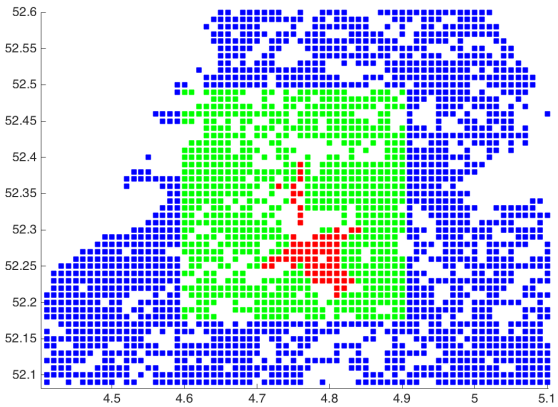

Figure G.14: Noise Grid Scenario 2: Evening, multi-objective optimized.

Appendix H

Runway Dependency Matrices

R06 - Medium - Arrival

nr	1	2	3	4	5	6	7	8	9	10	11	12	13	Dependency
Time	-120	-100	-80	-60	-40	-20	0	20	40	60	80	100	120	
Steps	-6	-5	-4	-3	-2	-1	0	1	2	3	4	5	6	
R06	0	0	0	0	0	1	1	1	1	1	0	0	0	ROT
R09	0	0	0	0	0	0	0	0	0	0	0	0	0	
R18C	0	0	0	0	1	1	1	0	0	0	0	0	0	Missed Approach
R18R	0	0	0	0	0	0	0	0	0	0	0	0	0	
R24	0	0	0	1	1	1	1	1	1	1	1	0	0	Opposite
R27	0	0	0	0	0	0	0	0	0	0	0	0	0	
R36C	0	0	0	0	1	1	1	1	1	0	0	0	0	Intersecting
R36R	0	0	0	0	0	0	1	1	1	1	0	0	0	Missed Approach
R18L	0	0	0	0	0	0	1	1	1	1	0	0	0	Missed Approach
R36L	0	0	0	0	0	0	0	0	0	0	0	0	0	

R06 Heavy Arrival

nr	1	2	3	4	5	6	7	8	9	10	11	12	13	
Time	-120	-100	-80	-60	-40	-20	0	20	40	60	80	100	120	
Steps	-6	-5	-4	-3	-2	-1	0	1	2	3	4	5	6	
R06	0	0	0	0	0	1	1	1	1	1	0	0	0	ROT
R09	0	0	0	0	0	0	0	0	0	0	0	0	0	
R18C	0	0	0	0	1	1	1	0	0	0	0	0	0	Missed Approach
R18R	0	0	0	0	0	0	0	0	0	0	0	0	0	
R24	0	0	0	1	1	1	1	1	1	1	1	1	0	Opposite
R27	0	0	0	0	0	0	0	0	0	0	0	0	0	
R36C	0	0	0	0	1	1	1	1	1	0	0	0	0	Intersecting
R36R	0	0	0	0	0	0	1	1	1	1	0	0	0	Missed Approach
R18L	0	0	0	0	0	0	1	1	1	1	0	0	0	Missed Approach
R36L	0	0	0	0	0	0	0	0	0	0	0	0	0	

R06 Medium Departure

nr	1	2	3	4	5	6	7	8	9	10	11	12	13	Dependency
Time	-120	-100	-80	-60	-40	-20	0	20	40	60	80	100	120	
Steps	-6	-5	-4	-3	-2	-1	0	1	2	3	4	5	6	
R06	0	0	0	0	0	1	1	1	1	1	0	0	0	ROT
R09	0	0	0	0	0	0	0	0	0	0	0	0	0	
R18C	0	0	0	0	1	1	1	0	0	0	0	0	0	Missed Approach
R18R	0	0	0	0	0	0	0	0	0	0	0	0	0	
R24	0	0	0	1	1	1	1	1	1	1	1	1	0	Opposite
R27	0	0	0	0	0	0	0	0	0	0	0	0	0	
R36C	0	0	0	0	1	1	1	1	1	0	0	0	0	Intersecting
R36R	0	0	0	0	0	0	1	1	1	1	0	0	0	Missed Approach
R18L	0	0	0	0	0	0	1	1	1	1	0	0	0	Missed Approach
R36L	0	0	0	0	0	0	0	0	0	0	0	0	0	

R06 Heavy Departure

nr	1	2	3	4	5	6	7	8	9	10	11	12	13	
Time	-120	-100	-80	-60	-40	-20	0	20	40	60	80	100	120	
Steps	-6	-5	-4	-3	-2	-1	0	1	2	3	4	5	6	
R06	0	0	0	0	0	1	1	1	1	1	1	0	0	ROT
R09	0	0	0	0	0	0	0	0	0	0	0	0	0	
R18C	0	0	0	0	1	1	1	0	0	0	0	0	0	Missed Approach
R18R	0	0	0	0	0	0	0	0	0	0	0	0	0	
R24	0	0	0	1	1	1	1	1	1	1	1	1	0	Mixed Mode
R27	0	0	0	0	0	0	0	0	0	0	0	0	0	
R36C	0	0	0	0	1	1	1	1	1	0	0	0	0	Intersecting
R36R	0	0	0	0	0	0	1	1	1	1	0	0	0	Missed Approach
R18L	0	0	0	0	0	0	1	1	1	1	0	0	0	Missed Approach
R36L	0	0	0	0	0	0	0	0	0	0	0	0	0	

R09 Medium Arrival

nr	1	2	3	4	5	6	7	8	9	10	11	12	13	Dependency
Time	-120	-100	-80	-60	-40	-20	0	20	40	60	80	100	120	
Steps	-6	-5	-4	-3	-2	-1	0	1	2	3	4	5	6	
R06	0	0	0	0	0	0	0	0	0	0	0	0	0	
R09	0	0	0	0	1	1	1	1	1	1	0	0	0	ROT
R18C	0	0	0	0	1	1	1	1	0	0	0	0	0	Intersecting
R18R	0	0	0	1	1	1	1	0	0	0	0	0	0	Missed Approach 18R
R24	0	0	0	0	0	0	0	0	0	0	0	0	0	
R27	0	0	0	0	0	0	1	1	1	1	1	0	0	Opposite
R36C	0	0	0	0	1	1	1	1	0	0	0	0	0	Intersecting
R36R	0	0	0	0	0	0	1	1	1	0	0	0	0	Intersecting
R18L	0	0	0	0	0	0	1	1	1	0	0	0	0	Intersecting
R36L	0	0	0	0	1	1	0	0	0	0	0	0	0	Jet Blast

R09 Heavy Arrival

nr	1	2	3	4	5	6	7	8	9	10	11	12	13	
Time	-120	-100	-80	-60	-40	-20	0	20	40	60	80	100	120	
Steps	-6	-5	-4	-3	-2	-1	0	1	2	3	4	5	6	
R06	0	0	0	0	0	0	0	0	0	0	0	0	0	
R09	0	0	1	1	1	1	1	1	1	1	1	0	0	ROT
R18C	0	0	0	0	1	1	1	1	0	0	0	0	0	Intersecting
R18R	0	0	0	1	1	1	1	0	0	0	0	0	0	
R24	0	0	0	0	0	0	0	0	0	0	0	0	0	
R27	0	0	0	0	0	0	1	1	1	1	1	0	0	Opposite
R36C	0	0	0	0	1	1	1	1	0	0	0	0	0	Intersecting
R36R	0	0	0	0	0	0	1	1	1	0	0	0	0	Intersecting
R18L	0	0	0	0	0	0	1	1	1	0	0	0	0	Intersecting
R36L	0	0	0	0	1	1	0	0	0	0	0	0	0	

R09 Medium Departure

nr	1	2	3	4	5	6	7	8	9	10	11	12	13	Dependency
Time	-120	-100	-80	-60	-40	-20	0	20	40	60	80	100	120	
Steps	-6	-5	-4	-3	-2	-1	0	1	2	3	4	5	6	
R06	0	0	0	0	0	0	0	0	0	0	0	0	0	
R09	0	0	0	0	1	1	1	1	1	1	0	0	0	ROT
R18C	0	0	0	0	1	1	1	1	0	0	0	0	0	Intersecting
R18R	0	0	0	1	1	1	1	0	0	0	0	0	0	Missed Approach 18R
R24	0	0	0	0	0	0	0	0	0	0	0	0	0	
R27	0	0	0	0	0	0	1	1	1	1	1	0	0	Opposite
R36C	0	0	0	0	1	1	1	1	0	0	0	0	0	Intersecting
R36R	0	0	0	0	0	0	1	1	1	0	0	0	0	Intersecting
R18L	0	0	0	0	0	0	1	1	1	0	0	0	0	Intersecting
R36L	0	0	0	0	1	1	0	0	0	0	0	0	0	Jet Blast

R09 Heavy Departure

nr	1	2	3	4	5	6	7	8	9	10	11	12	13	
Time	-120	-100	-80	-60	-40	-20	0	20	40	60	80	100	120	
Steps	-6	-5	-4	-3	-2	-1	0	1	2	3	4	5	6	
R06	0	0	0	0	0	0	0	0	0	0	0	0	0	
R09	0	0	1	1	1	1	1	1	1	1	0	0	0	ROT
R18C	0	0	0	0	1	1	1	1	0	0	0	0	0	Intersecting
R18R	0	0	0	1	1	1	1	0	0	0	0	0	0	
R24	0	0	0	0	0	0	0	0	0	0	0	0	0	
R27	0	0	0	0	0	0	1	1	1	1	1	1	0	Opposite
R36C	0	0	0	0	1	1	1	1	0	0	0	0	0	Intersecting
R36R	0	0	0	0	0	0	1	1	1	0	0	0	0	Intersecting
R18L	0	0	0	0	0	0	1	1	1	0	0	0	0	Intersecting
R36L	0	0	0	0	1	1	0	0	0	0	0	0	0	

R18C Medium Arrival

nr	1	2	3	4	5	6	7	8	9	10	11	12	13	Dependency
Time	-120	-100	-80	-60	-40	-20	0	20	40	60	80	100	120	
Steps	-6	-5	-4	-3	-2	-1	0	1	2	3	4	5	6	
R06	0	0	0	0	0	0	1	1	1	1	0	0	0	Missed Approach
R09	0	0	0	0	0	1	1	1	1	0	0	0	0	Intersecting
R18C	0	0	0	0	0	0	1	1	1	1	1	0	0	ROT
R18R	0	0	0	0	0	0	0	0	0	0	0	0	0	
R24	0	0	0	0	0	0	1	1	1	1	0	0	0	Missed Approach
R27	0	0	0	0	0	1	1	1	1	1	0	0	0	
R36C	0	0	0	0	0	0	1	1	1	1	1	1	0	Opposite
R36R	0	0	0	0	0	0	0	0	0	0	0	0	0	
R18L	0	0	0	0	0	0	0	0	0	0	0	0	0	
R36L	0	0	0	0	0	0	0	0	0	0	0	0	0	

R18C Heavy Arrival

nr	1	2	3	4	5	6	7	8	9	10	11	12	13	
Time	-120	-100	-80	-60	-40	-20	0	20	40	60	80	100	120	
Steps	-6	-5	-4	-3	-2	-1	0	1	2	3	4	5	6	
R06	0	0	0	0	0	0	1	1	1	1	0	0	0	Missed Approach
R09	0	0	0	0	0	1	1	1	1	0	0	0	0	Intersecting
R18C	0	0	0	0	0	0	1	1	1	1	1	0	0	ROT
R18R	0	0	0	0	0	0	0	0	0	0	0	0	0	
R24	0	0	0	0	0	0	1	1	1	1	0	0	0	Missed Approach
R27	0	0	0	0	0	1	1	1	1	1	0	0	0	
R36C	0	0	0	0	0	0	1	1	1	1	1	1	1	Opposite
R36R	0	0	0	0	0	0	0	0	0	0	0	0	0	
R18L	0	0	0	0	0	0	0	0	0	0	0	0	0	
R36L	0	0	0	0	0	0	0	0	0	0	0	0	0	

R18C Medium Departure

nr	1	2	3	4	5	6	7	8	9	10	11	12	13	Dependency
Time	-120	-100	-80	-60	-40	-20	0	20	40	60	80	100	120	
Steps	-6	-5	-4	-3	-2	-1	0	1	2	3	4	5	6	
R06	0	0	0	0	0	0	1	1	1	1	0	0	0	Missed Approach
R09	0	0	0	0	0	1	1	1	1	0	0	0	0	Intersecting
R18C	0	0	0	0	0	0	1	1	1	1	0	0	0	ROT
R18R	0	0	0	0	0	0	0	0	0	0	0	0	0	
R24	0	0	0	0	0	0	1	1	1	1	0	0	0	Missed Approach
R27	0	0	0	0	0	1	1	1	1	1	0	0	0	
R36C	0	0	0	0	0	0	1	1	1	1	1	1	0	Opposite
R36R	0	0	0	0	0	0	0	0	0	0	0	0	0	
R18L	0	0	0	0	0	0	0	0	0	0	0	0	0	
R36L	0	0	0	0	0	0	0	0	0	0	0	0	0	

R18C Heavy Deparure

nr	1	2	3	4	5	6	7	8	9	10	11	12	13	
Time	-120	-100	-80	-60	-40	-20	0	20	40	60	80	100	120	
Steps	-6	-5	-4	-3	-2	-1	0	1	2	3	4	5	6	
R06	0	0	0	0	0	0	1	1	1	1	0	0	0	Missed Approach
R09	0	0	0	0	0	1	1	1	1	0	0	0	0	Intersecting
R18C	0	0	0	0	0	0	1	1	1	1	1	0	0	ROT
R18R	0	0	0	0	0	0	0	0	0	0	0	0	0	
R24	0	0	0	0	0	0	1	1	1	1	0	0	0	Missed Approach
R27	0	0	0	0	0	1	1	1	1	1	0	0	0	
R36C	0	0	0	0	0	0	1	1	1	1	1	1	1	Opposite
R36R	0	0	0	0	0	0	0	0	0	0	0	0	0	
R18L	0	0	0	0	0	0	0	0	0	0	0	0	0	
R36L	0	0	0	0	0	0	0	0	0	0	0	0	0	

R18L Medium Arrival

nr	1	2	3	4	5	6	7	8	9	10	11	12	13	Dependency
Time	-120	-100	-80	-60	-40	-20	0	20	40	60	80	100	120	
Steps	-6	-5	-4	-3	-2	-1	0	1	2	3	4	5	6	
R06	0	0	0	0	0	1	1	1	1	0	0	0	0	Missed Approach
R09	0	0	0	0	0	1	1	1	1	1	0	0	0	Intersecting
R18C	0	0	0	0	0	0	0	0	0	0	0	0	0	
R18R	0	0	0	0	0	0	0	0	0	0	0	0	0	
R24	0	0	0	0	1	1	1	1	1	0	0	0	0	Intersecting
R27	0	0	0	0	0	1	1	1	1	1	0	0	0	Intersecting
R36C	0	0	0	0	0	0	1	1	1	1	1	1	0	Opposite
R36R	0	0	0	0	0	0	0	0	0	0	0	0	0	
R18L	0	0	0	0	0	0	1	1	1	1	1	0	0	ROT
R36L	0	0	0	0	0	0	0	0	0	0	0	0	0	

R18L Medium Arrival

nr	1	2	3	4	5	6	7	8	9	10	11	12	13	
Time	-120	-100	-80	-60	-40	-20	0	20	40	60	80	100	120	
Steps	-6	-5	-4	-3	-2	-1	0	1	2	3	4	5	6	
R06	0	0	0	0	0	1	1	1	1	0	0	0	0	Missed Approach
R09	0	0	0	0	0	1	1	1	1	1	0	0	0	Intersecting
R18C	0	0	0	0	0	0	0	0	0	0	0	0	0	
R18R	0	0	0	0	0	0	0	0	0	0	0	0	0	
R24	0	0	0	0	1	1	1	1	1	0	0	0	0	Intersecting
R27	0	0	0	0	0	1	1	1	1	1	0	0	0	Intersecting
R36C	0	0	0	0	0	0	1	1	1	1	1	1	1	Opposite
R36R	0	0	0	0	0	0	0	0	0	0	0	0	0	
R18L	0	0	0	0	0	0	1	1	1	1	1	1	0	ROT
R36L	0	0	0	0	0	0	0	0	0	0	0	0	0	

R18L Medium Departure

nr	1	2	3	4	5	6	7	8	9	10	11	12	13	Dependency
Time	-120	-100	-80	-60	-40	-20	0	20	40	60	80	100	120	
Steps	-6	-5	-4	-3	-2	-1	0	1	2	3	4	5	6	
R06	0	0	0	0	0	1	1	1	1	0	0	0	0	Missed Approach
R09	0	0	0	0	0	1	1	1	1	1	0	0	0	Intersecting
R18C	0	0	0	0	0	0	0	0	0	0	0	0	0	
R18R	0	0	0	0	0	0	0	0	0	0	0	0	0	
R24	0	0	0	0	1	1	1	1	1	0	0	0	0	Intersecting
R27	0	0	0	0	0	1	1	1	1	1	0	0	0	Intersecting
R36C	0	0	0	0	0	0	1	1	1	1	1	1	0	Opposite
R36R	0	0	0	0	0	0	0	0	0	0	0	0	0	
R18L	0	0	0	0	0	0	1	1	1	1	1	0	0	ROT
R36L	0	0	0	0	0	0	0	0	0	0	0	0	0	

R18L Heavy Departure

nr	1	2	3	4	5	6	7	8	9	10	11	12	13	
Time	-120	-100	-80	-60	-40	-20	0	20	40	60	80	100	120	
Steps	-6	-5	-4	-3	-2	-1	0	1	2	3	4	5	6	
R06	0	0	0	0	0	1	1	1	1	0	0	0	0	Missed Approach
R09	0	0	0	0	0	1	1	1	1	1	0	0	0	Intersecting
R18C	0	0	0	0	0	0	0	0	0	0	0	0	0	
R18R	0	0	0	0	0	0	0	0	0	0	0	0	0	
R24	0	0	0	0	1	1	1	1	1	0	0	0	0	Intersecting
R27	0	0	0	0	0	1	1	1	1	1	0	0	0	Intersecting
R36C	0	0	0	0	0	0	1	1	1	1	1	1	1	Opposite
R36R	0	0	0	0	0	0	0	0	0	0	0	0	0	
R18L	0	0	0	0	0	0	1	1	1	1	1	1	0	ROT
R36L	0	0	0	0	0	0	0	0	0	0	0	0	0	

R18R Medium Arrival

nr	1	2	3	4	5	6	7	8	9	10	11	12	13	Dependency
Time	-120	-100	-80	-60	-40	-20	0	20	40	60	80	100	120	
Steps	-6	-5	-4	-3	-2	-1	0	1	2	3	4	5	6	
R06	0	0	0	0	0	0	0	0	0	0	0	0	0	
R09	0	0	0	0	0	1	1	1	1	0	0	0	0	Intersecting
R18C	0	0	0	0	0	0	0	0	0	0	0	0	0	
R18R	0	0	0	0	0	0	1	1	1	1	1	0	0	ROT
R24	0	0	0	0	0	0	0	0	0	0	0	0	0	
R27	0	0	0	0	0	0	1	1	1	1	0	0	0	Missed Approach
R36C	0	0	0	0	0	0	0	0	0	0	0	0	0	
R36R	0	0	0	0	0	0	0	0	0	0	0	0	0	
R18L	0	0	0	0	0	0	0	0	0	0	0	0	0	
R36L	0	0	0	0	0	0	1	1	1	1	1	1	0	Mixed Mode

R18R Heavy Arrival

nr	1	2	3	4	5	6	7	8	9	10	11	12	13	
Time	-120	-100	-80	-60	-40	-20	0	20	40	60	80	100	120	
Steps	-6	-5	-4	-3	-2	-1	0	1	2	3	4	5	6	
R06	0	0	0	0	0	0	0	0	0	0	0	0	0	
R09	0	0	0	0	0	1	1	1	1	0	0	0	0	Intersecting
R18C	0	0	0	0	0	0	0	0	0	0	0	0	0	
R18R	0	0	0	0	0	0	1	1	1	1	1	0	0	ROT
R24	0	0	0	0	0	0	0	0	0	0	0	0	0	
R27	0	0	0	0	0	0	1	1	1	1	0	0	0	Missed Approach
R36C	0	0	0	0	0	0	0	0	0	0	0	0	0	
R36R	0	0	0	0	0	0	0	0	0	0	0	0	0	
R18L	0	0	0	0	0	0	0	0	0	0	0	0	0	
R36L	0	0	0	0	0	0	1	1	1	1	1	1	1	Opposite

R18R Medium Departure

nr	1	2	3	4	5	6	7	8	9	10	11	12	13	Dependency
Time	-120	-100	-80	-60	-40	-20	0	20	40	60	80	100	120	
Steps	-6	-5	-4	-3	-2	-1	0	1	2	3	4	5	6	
R06	0	0	0	0	0	0	0	0	0	0	0	0	0	
R09	0	0	0	0	0	1	1	1	1	0	0	0	0	Intersecting
R18C	0	0	0	0	0	0	0	0	0	0	0	0	0	
R18R	0	0	0	0	0	0	1	1	1	1	1	0	0	ROT
R24	0	0	0	0	0	0	0	0	0	0	0	0	0	
R27	0	0	0	0	0	0	1	1	1	1	0	0	0	Missed Approach
R36C	0	0	0	0	0	0	0	0	0	0	0	0	0	
R36R	0	0	0	0	0	0	0	0	0	0	0	0	0	
R18L	0	0	0	0	0	0	0	0	0	0	0	0	0	
R36L	0	0	0	0	0	0	1	1	1	1	1	1	0	Opposite

R18R Heavy Departure

nr	1	2	3	4	5	6	7	8	9	10	11	12	13	
Time	-120	-100	-80	-60	-40	-20	0	20	40	60	80	100	120	
Steps	-6	-5	-4	-3	-2	-1	0	1	2	3	4	5	6	
R06	0	0	0	0	0	0	0	0	0	0	0	0	0	
R09	0	0	0	0	0	1	1	1	1	0	0	0	0	Intersecting
R18C	0	0	0	0	0	0	0	0	0	0	0	0	0	
R18R	0	0	0	0	0	0	1	1	1	1	1	0	0	ROT
R24	0	0	0	0	0	0	0	0	0	0	0	0	0	
R27	0	0	0	0	0	0	1	1	1	1	0	0	0	Missed Approach
R36C	0	0	0	0	0	0	0	0	0	0	0	0	0	
R36R	0	0	0	0	0	0	0	0	0	0	0	0	0	
R18L	0	0	0	0	0	0	0	0	0	0	0	0	0	
R36L	0	0	0	0	0	0	1	1	1	1	1	1	1	Opposite

R24 Medium Arrival

nr	1	2	3	4	5	6	7	8	9	10	11	12	13	Dependency
Time	-120	-100	-80	-60	-40	-20	0	20	40	60	80	100	120	
Steps	-6	-5	-4	-3	-2	-1	0	1	2	3	4	5	6	
R06	0	0	0	0	0	0	1	1	1	1	1	1	0	Opposite
R09	0	0	0	0	0	0	0	0	0	0	0	0	0	
R18C	0	0	0	0	1	1	1	1	1	0	0	0	0	Missed Approach
R18R	0	0	0	0	0	0	0	0	0	0	0	0	0	
R24	0	0	0	0	0	0	1	1	1	1	1	0	0	ROT
R27	0	0	0	0	0	0	0	0	0	0	0	0	0	
R36C	0	0	0	0	1	1	1	1	1	0	0	0	0	Missed Approach
R36R	0	0	0	0	1	1	1	1	1	0	0	0	0	Jet Blast
R18L	0	0	0	0	1	1	1	1	1	0	0	0	0	Jet Blast
R36L	0	0	0	0	0	0	0	0	0	0	0	0	0	

R24 Heavy Arrival

nr	1	2	3	4	5	6	7	8	9	10	11	12	13	
Time	-120	-100	-80	-60	-40	-20	0	20	40	60	80	100	120	
Steps	-6	-5	-4	-3	-2	-1	0	1	2	3	4	5	6	
R06	0	0	0	0	0	0	1	1	1	1	1	1	1	Opposite
R09	0	0	0	0	0	0	0	0	0	0	0	0	0	
R18C	0	0	0	0	1	1	1	1	1	0	0	0	0	Missed Approach
R18R	0	0	0	0	0	0	0	0	0	0	0	0	0	
R24	0	0	0	0	0	0	1	1	1	1	1	1	0	ROT
R27	0	0	0	0	0	0	0	0	0	0	0	0	0	
R36C	0	0	0	0	1	1	1	1	1	0	0	0	0	Missed Approach
R36R	0	0	0	0	1	1	1	1	1	0	0	0	0	Jet Blast
R18L	0	0	0	0	1	1	1	1	1	0	0	0	0	Jet Blast
R36L	0	0	0	0	0	0	0	0	0	0	0	0	0	

R24 Medium Departure

nr	1	2	3	4	5	6	7	8	9	10	11	12	13	Dependency
Time	-120	-100	-80	-60	-40	-20	0	20	40	60	80	100	120	
Steps	-6	-5	-4	-3	-2	-1	0	1	2	3	4	5	6	
R06	0	0	0	0	0	0	1	1	1	1	1	1	0	Opposite
R09	0	0	0	0	0	0	0	0	0	0	0	0	0	
R18C	0	0	0	0	1	1	1	1	1	0	0	0	0	Missed Approach
R18R	0	0	0	0	0	0	0	0	0	0	0	0	0	
R24	0	0	0	0	0	0	1	1	1	1	1	0	0	ROT
R27	0	0	0	0	0	0	0	0	0	0	0	0	0	
R36C	0	0	0	0	1	1	1	1	1	0	0	0	0	Missed Approach
R36R	0	0	0	0	1	1	1	1	1	0	0	0	0	Jet Blast
R18L	0	0	0	0	1	1	1	1	1	0	0	0	0	Jet Blast
R36L	0	0	0	0	0	0	0	0	0	0	0	0	0	

R24 Heavy Departure

nr	1	2	3	4	5	6	7	8	9	10	11	12	13	
Time	-120	-100	-80	-60	-40	-20	0	20	40	60	80	100	120	
Steps	-6	-5	-4	-3	-2	-1	0	1	2	3	4	5	6	
R06	0	0	0	0	0	0	1	1	1	1	1	1	1	Opposite
R09	0	0	0	0	0	0	0	0	0	0	0	0	0	
R18C	0	0	0	0	1	1	1	1	1	0	0	0	0	Missed Approach
R18R	0	0	0	0	0	0	0	0	0	0	0	0	0	
R24	0	0	0	0	0	0	1	1	1	1	1	1	0	ROT
R27	0	0	0	0	0	0	0	0	0	0	0	0	0	
R36C	0	0	0	0	1	1	1	1	1	0	0	0	0	Missed Approach
R36R	0	0	0	0	1	1	1	1	1	0	0	0	0	Jet Blast
R18L	0	0	0	0	1	1	1	1	1	0	0	0	0	Jet Blast
R36L	0	0	0	0	0	0	0	0	0	0	0	0	0	

R27 Medium Arrival

nr	1	2	3	4	5	6	7	8	9	10	11	12	13	Dependency
Time	-120	-100	-80	-60	-40	-20	0	20	40	60	80	100	120	
Steps	-6	-5	-4	-3	-2	-1	0	1	2	3	4	5	6	
R06	0	0	0	0	0	0	0	0	0	0	0	0	0	
R09	0	0	0	0	0	0	1	1	1	1	1	1	0	Opposite
R18C	0	0	0	0	0	0	0	1	1	1	1	0	0	Missed Approach
R18R	0	0	0	0	0	0	0	1	1	1	1	1	0	Missed Approach
R24	0	0	0	0	0	0	0	0	0	0	0	0	0	
R27	0	0	0	0	0	0	1	1	1	1	1	0	0	ROT
R36C	0	0	0	0	0	0	0	1	1	1	1	0	0	Missed Approach
R36R	0	0	0	0	0	0	0	0	0	0	0	0	0	
R18L	0	0	0	0	0	0	0	0	0	0	0	0	0	
R36L	0	0	0	0	0	0	0	1	1	1	1	1	0	Missed Approach

R27 Heavy Arrival

nr	1	2	3	4	5	6	7	8	9	10	11	12	13	
Time	-120	-100	-80	-60	-40	-20	0	20	40	60	80	100	120	
Steps	-6	-5	-4	-3	-2	-1	0	1	2	3	4	5	6	
R06	0	0	0	0	0	0	0	0	0	0	0	0	0	
R09	0	0	0	0	0	0	1	1	1	1	1	1	1	Opposite
R18C	0	0	0	0	0	0	0	1	1	1	1	0	0	Missed Approach
R18R	0	0	0	0	0	0	0	1	1	1	1	1	0	Missed Approach
R24	0	0	0	0	0	0	0	0	0	0	0	0	0	
R27	0	0	0	0	0	0	1	1	1	1	1	1	0	ROT
R36C	0	0	0	0	0	0	0	1	1	1	1	0	0	Missed Approach
R36R	0	0	0	0	0	0	0	0	0	0	0	0	0	
R18L	0	0	0	0	0	0	0	0	0	0	0	0	0	
R36L	0	0	0	0	0	0	0	1	1	1	1	1	0	Missed Approach

R27 Medium Departure

nr	1	2	3	4	5	6	7	8	9	10	11	12	13	Dependency
Time	-120	-100	-80	-60	-40	-20	0	20	40	60	80	100	120	
Steps	-6	-5	-4	-3	-2	-1	0	1	2	3	4	5	6	
R06	0	0	0	0	0	0	0	0	0	0	0	0	0	
R09	0	0	0	0	0	0	1	1	1	1	1	1	0	Opposite
R18C	0	0	0	0	0	0	0	1	1	1	1	0	0	Missed Approach
R18R	0	0	0	0	0	0	0	1	1	1	1	1	0	Missed Approach
R24	0	0	0	0	0	0	0	0	0	0	0	0	0	
R27	0	0	0	0	0	0	1	1	1	1	1	0	0	ROT
R36C	0	0	0	0	0	0	0	1	1	1	1	0	0	Missed Approach
R36R	0	0	0	0	0	0	0	0	0	0	0	0	0	
R18L	0	0	0	0	0	0	0	0	0	0	0	0	0	
R36L	0	0	0	0	0	0	0	1	1	1	1	1	0	Missed Approach

R27 Heavy Departure

nr	1	2	3	4	5	6	7	8	9	10	11	12	13	
Time	-120	-100	-80	-60	-40	-20	0	20	40	60	80	100	120	
Steps	-6	-5	-4	-3	-2	-1	0	1	2	3	4	5	6	
R06	0	0	0	0	0	0	0	0	0	0	0	0	0	
R09	0	0	0	0	0	0	1	1	1	1	1	1	1	Opposite
R18C	0	0	0	0	0	0	0	1	1	1	1	0	0	Missed Approach
R18R	0	0	0	0	0	0	0	1	1	1	1	1	0	Missed Approach
R24	0	0	0	0	0	0	0	0	0	0	0	0	0	
R27	0	0	0	0	0	0	1	1	1	1	1	1	0	ROT
R36C	0	0	0	0	0	0	0	1	1	1	1	0	0	Missed Approach
R36R	0	0	0	0	0	0	0	0	0	0	0	0	0	
R18L	0	0	0	0	0	0	0	0	0	0	0	0	0	
R36L	0	0	0	0	0	0	0	1	1	1	1	1	0	Missed Approach

R36C Medium Arrival

nr	1	2	3	4	5	6	7	8	9	10	11	12	13	Dependency
Time	-120	-100	-80	-60	-40	-20	0	20	40	60	80	100	120	
Steps	-6	-5	-4	-3	-2	-1	0	1	2	3	4	5	6	
R06	0	0	0	0	1	1	1	1	0	0	0	0	0	Missed Approach
R09	0	0	0	0	0	1	1	1	1	0	0	0	0	Intersecting
R18C	0	0	0	0	0	0	1	1	1	1	1	1	0	Opposite
R18R	0	0	0	0	0	0	0	0	0	0	0	0	0	
R24	0	0	0	0	1	1	1	1	0	0	0	0	0	Missed Approach
R27	0	0	0	0	0	0	1	1	1	1	1	0	0	Missed Approach
R36C	0	0	0	0	1	1	1	1	1	1	1	0	0	ROT
R36R	0	0	0	0	0	0	0	0	0	0	0	0	0	
R18L	0	0	0	0	0	0	0	0	0	0	0	0	0	
R36L	0	0	0	0	0	0	0	0	0	0	0	0	0	

R36C Heavy Arrival

nr	1	2	3	4	5	6	7	8	9	10	11	12	13	
Time	-120	-100	-80	-60	-40	-20	0	20	40	60	80	100	120	
Steps	-6	-5	-4	-3	-2	-1	0	1	2	3	4	5	6	
R06	0	0	0	0	1	1	1	1	0	0	0	0	0	Missed Approach
R09	0	0	0	0	0	1	1	1	1	0	0	0	0	Intersecting
R18C	0	0	0	0	0	0	1	1	1	1	1	1	1	Opposite
R18R	0	0	0	0	0	0	0	0	0	0	0	0	0	
R24	0	0	0	0	1	1	1	1	0	0	0	0	0	Missed Approach
R27	0	0	0	0	0	0	1	1	1	1	1	0	0	Missed Approach
R36C	0	0	0	0	1	1	1	1	1	1	1	0	0	ROT
R36R	0	0	0	0	0	0	0	0	0	0	0	0	0	
R18L	0	0	0	0	0	0	0	0	0	0	0	0	0	
R36L	0	0	0	0	0	0	0	0	0	0	0	0	0	

R36C Medium Departure

nr	1	2	3	4	5	6	7	8	9	10	11	12	13	Dependency
Time	-120	-100	-80	-60	-40	-20	0	20	40	60	80	100	120	
Steps	-6	-5	-4	-3	-2	-1	0	1	2	3	4	5	6	
R06	0	0	0	0	1	1	1	1	0	0	0	0	0	Missed Approach
R09	0	0	0	0	0	1	1	1	1	0	0	0	0	Intersecting
R18C	0	0	0	0	0	0	1	1	1	1	1	1	0	Opposite
R18R	0	0	0	0	0	0	0	0	0	0	0	0	0	
R24	0	0	0	0	1	1	1	1	0	0	0	0	0	Missed Approach
R27	0	0	0	0	0	0	1	1	1	1	1	0	0	Missed Approach
R36C	0	0	0	0	1	1	1	1	1	1	1	0	0	ROT
R36R	0	0	0	0	0	0	0	0	0	0	0	0	0	
R18L	0	0	0	0	0	0	0	0	0	0	0	0	0	
R36L	0	0	0	0	0	0	0	0	0	0	0	0	0	

R36C Heavy Departure

nr	1	2	3	4	5	6	7	8	9	10	11	12	13	
Time	-120	-100	-80	-60	-40	-20	0	20	40	60	80	100	120	
Steps	-6	-5	-4	-3	-2	-1	0	1	2	3	4	5	6	
R06	0	0	0	0	1	1	1	1	0	0	0	0	0	Missed Approach
R09	0	0	0	0	0	1	1	1	1	0	0	0	0	Intersecting
R18C	0	0	0	0	0	0	1	1	1	1	1	1	1	Opposite
R18R	0	0	0	0	0	0	0	0	0	0	0	0	0	
R24	0	0	0	0	1	1	1	1	0	0	0	0	0	Missed Approach
R27	0	0	0	0	0	0	1	1	1	1	1	0	0	Missed Approach
R36C	0	0	0	0	1	1	1	1	1	1	1	1	0	ROT
R36R	0	0	0	0	0	0	0	0	0	0	0	0	0	
R18L	0	0	0	0	0	0	0	0	0	0	0	0	0	
R36L	0	0	0	0	0	0	0	0	0	0	0	0	0	

R36L Medium Arrival

nr	1	2	3	4	5	6	7	8	9	10	11	12	13	Dependency
Time	-120	-100	-80	-60	-40	-20	0	20	40	60	80	100	120	
Steps	-6	-5	-4	-3	-2	-1	0	1	2	3	4	5	6	
R06	0	0	0	0	0	0	0	0	0	0	0	0	0	
R09	0	0	0	0	0	0	0	0	0	0	0	0	0	
R18C	0	0	0	0	0	0	0	0	0	0	0	0	0	
R18R	0	0	0	0	0	0	1	1	1	1	1	1	0	Opposite
R24	0	0	0	0	0	0	0	0	0	0	0	0	0	
R27	0	0	0	0	0	0	0	0	0	0	0	0	0	
R36C	0	0	0	0	0	0	0	0	0	0	0	0	0	
R36R	0	0	0	0	0	0	0	0	0	0	0	0	0	
R18L	0	0	0	0	0	0	0	0	0	0	0	0	0	
R36L	0	0	0	0	0	0	1	1	1	1	1	0	0	ROT

R36L Heavy Arrival

nr	1	2	3	4	5	6	7	8	9	10	11	12	13	Dependency
Time	-120	-100	-80	-60	-40	-20	0	20	40	60	80	100	120	
Steps	-6	-5	-4	-3	-2	-1	0	1	2	3	4	5	6	
R06	0	0	0	0	0	0	0	0	0	0	0	0	0	
R09	0	0	0	0	0	0	0	0	0	0	0	0	0	
R18C	0	0	0	0	0	0	0	0	0	0	0	0	0	
R18R	0	0	0	0	0	0	1	1	1	1	1	1	0	Opposite
R24	0	0	0	0	0	0	0	0	0	0	0	0	0	
R27	0	0	0	0	0	0	0	0	0	0	0	0	0	
R36C	0	0	0	0	0	0	0	0	0	0	0	0	0	
R36R	0	0	0	0	0	0	0	0	0	0	0	0	0	
R18L	0	0	0	0	0	0	0	0	0	0	0	0	0	
R36L	0	0	0	0	0	0	1	1	1	1	1	1	0	ROT

R36L Medium Departure

nr	1	2	3	4	5	6	7	8	9	10	11	12	13	Dependency
Time	-120	-100	-80	-60	-40	-20	0	20	40	60	80	100	120	
Steps	-6	-5	-4	-3	-2	-1	0	1	2	3	4	5	6	
R06	0	0	0	0	0	0	0	0	0	0	0	0	0	
R09	0	0	0	0	0	0	0	0	0	0	0	0	0	
R18C	0	0	0	0	0	0	0	0	0	0	0	0	0	
R18R	0	0	0	0	0	0	1	1	1	1	1	1	0	Opposite
R24	0	0	0	0	0	0	0	0	0	0	0	0	0	
R27	0	0	0	0	0	0	0	0	0	0	0	0	0	
R36C	0	0	0	0	0	0	0	0	0	0	0	0	0	
R36R	0	0	0	0	0	0	0	0	0	0	0	0	0	
R18L	0	0	0	0	0	0	0	0	0	0	0	0	0	
R36L	0	0	0	0	0	0	1	1	1	1	1	0	0	ROT

R36L Heavy Departure

nr	1	2	3	4	5	6	7	8	9	10	11	12	13	Dependency
Time	-120	-100	-80	-60	-40	-20	0	20	40	60	80	100	120	
Steps	-6	-5	-4	-3	-2	-1	0	1	2	3	4	5	6	
R06	0	0	0	0	0	0	0	0	0	0	0	0	0	
R09	0	0	0	0	0	0	0	0	0	0	0	0	0	
R18C	0	0	0	0	0	0	0	0	0	0	0	0	0	
R18R	0	0	0	0	0	0	1	1	1	1	1	1	0	Opposite
R24	0	0	0	0	0	0	0	0	0	0	0	0	0	
R27	0	0	0	0	0	0	0	0	0	0	0	0	0	
R36C	0	0	0	0	0	0	0	0	0	0	0	0	0	
R36R	0	0	0	0	0	0	0	0	0	0	0	0	0	
R18L	0	0	0	0	0	0	0	0	0	0	0	0	0	
R36L	0	0	0	0	0	0	1	1	1	1	1	1	0	ROT

R36R Medium Arrival

nr	1	2	3	4	5	6	7	8	9	10	11	12	13	Dependency
Time	-120	-100	-80	-60	-40	-20	0	20	40	60	80	100	120	
Steps	-6	-5	-4	-3	-2	-1	0	1	2	3	4	5	6	
R06	0	0	0	0	0	1	1	1	1	0	0	0	0	Missed Approach
R09	0	0	0	0	0	0	0	1	1	1	1	0	0	Intersecting
R18C	0	0	0	0	0	0	0	0	0	0	0	0	0	
R18R	0	0	0	0	0	0	0	0	0	0	0	0	0	
R24	0	0	0	0	1	1	1	1	1	0	0	0	0	Intersecting
R27	0	0	0	0	0	0	0	1	1	1	1	0	0	Intersecting
R36C	0	0	0	0	0	0	1	1	1	1	1	0	0	ROT
R36R	0	0	0	0	0	0	0	0	0	0	0	0	0	
R18L	0	0	0	0	0	0	1	1	1	1	1	1	0	Mixed Mode
R36L	0	0	0	0	0	0	0	0	0	0	0	0	0	

R36R Heavy Arrival

nr	1	2	3	4	5	6	7	8	9	10	11	12	13	Dependency
Time	-120	-100	-80	-60	-40	-20	0	20	40	60	80	100	120	
Steps	-6	-5	-4	-3	-2	-1	0	1	2	3	4	5	6	
R06	0	0	0	0	0	1	1	1	1	0	0	0	0	Missed Approach
R09	0	0	0	0	0	0	0	1	1	1	1	0	0	Intersecting
R18C	0	0	0	0	0	0	0	0	0	0	0	0	0	
R18R	0	0	0	0	0	0	0	0	0	0	0	0	0	
R24	0	0	0	0	1	1	1	1	1	0	0	0	0	Intersecting
R27	0	0	0	0	0	0	0	1	1	1	1	0	0	Intersecting
R36C	0	0	0	0	0	0	1	1	1	1	1	1	0	ROT
R36R	0	0	0	0	0	0	0	0	0	0	0	0	0	
R18L	0	0	0	0	0	0	1	1	1	1	1	1	1	Opposite
R36L	0	0	0	0	0	0	0	0	0	0	0	0	0	

R36R Medium Departure

nr	1	2	3	4	5	6	7	8	9	10	11	12	13	Dependency
Time	-120	-100	-80	-60	-40	-20	0	20	40	60	80	100	120	
Steps	-6	-5	-4	-3	-2	-1	0	1	2	3	4	5	6	
R06	0	0	0	0	0	1	1	1	1	0	0	0	0	Missed Approach
R09	0	0	0	0	0	0	0	1	1	1	1	0	0	Intersecting
R18C	0	0	0	0	0	0	0	0	0	0	0	0	0	
R18R	0	0	0	0	0	0	0	0	0	0	0	0	0	
R24	0	0	0	0	1	1	1	1	1	0	0	0	0	Intersecting
R27	0	0	0	0	0	0	0	1	1	1	1	0	0	Intersecting
R36C	0	0	0	0	0	0	1	1	1	1	1	0	0	ROT
R36R	0	0	0	0	0	0	0	0	0	0	0	0	0	
R18L	0	0	0	0	0	0	1	1	1	1	1	1	0	Opposite
R36L	0	0	0	0	0	0	0	0	0	0	0	0	0	

R36R Heavy Departure

nr	1	2	3	4	5	6	7	8	9	10	11	12	13	Dependency
Time	-120	-100	-80	-60	-40	-20	0	20	40	60	80	100	120	
Steps	-6	-5	-4	-3	-2	-1	0	1	2	3	4	5	6	
R06	0	0	0	0	0	1	1	1	1	0	0	0	0	Missed Approach
R09	0	0	0	0	0	0	0	1	1	1	1	0	0	Intersecting
R18C	0	0	0	0	0	0	0	0	0	0	0	0	0	
R18R	0	0	0	0	0	0	0	0	0	0	0	0	0	
R24	0	0	0	0	1	1	1	1	1	0	0	0	0	Intersecting
R27	0	0	0	0	0	0	0	1	1	1	1	0	0	Intersecting
R36C	0	0	0	0	0	0	1	1	1	1	1	1	0	ROT
R36R	0	0	0	0	0	0	0	0	0	0	0	0	0	
R18L	0	0	0	0	0	0	1	1	1	1	1	1	1	Opposite
R36L	0	0	0	0	0	0	0	0	0	0	0	0	0	

Bibliography

[1] Federal Aviation Administration. *Procedures for Determination of Airport Capacities*. 1973.

[2] Mirkovic. *Airfield Modelling - State of the Art*. Faculty of Transport adn Traffic Engineering, University of Belgrade, 2009.

[3] M. Janic. *An application of the Methodology for Assessment of the Sustainability of Air Transport System*. OTB Research Institute for the Build Environment TU Delft, 2003.

[4] Schiphol Group. *Gebruiksprognose 2015*. 2014.

[5] J.G. Delsen. *MSc Thesis Kick-off Document*. Delft University of Technology, 2015.

[6] J.G. Delsen. *Literature Study - Flexible Arrival and Departure Runway Allocation*. Delft University of Technology, 2015.

[7] Blumstein. *The landing capacity of a runway*. Operations Research 7, 1959.

[8] Stamatopoulos, Zografos, and Odoni. *A decision support system for airport strategic planning*. Transportation Research Part C 12, 2004.

[9] Klugt. *Calculating capacity of dependent runway configurations*. Delft University of Technology, 2012.

[10] Schiphol Group. *Schiphol Annual Report 2014*. 2014.

[11] LVNL. *Baanpreferentie*. `https://www.lvnl.nl/omgeving/route--en-baangebruik/baanpreferenties.html`. 2015.

[12] W.J Mansveld. *34 098 - Wijziging van de Wet luchtvaart in verband met de invoering van een nieuw normen- en handhavingstelsel voor de luchthaven Schiphol en enige andere wijzigingen*. Tweede Kamer de Staten-Generaal, 2014.

[13] LVNL. *Voorschriften Dienst Verkeersleiding*. 2012.

[14] AIS. *Integrated Aeronautical Information Package Netherlands (AIP)*. `https://www.ais-netherlands.nl`. 2015.

[15] Oldenziel. *Integral Optimisation of Standard Instrument Departures at Amsterdam Airport Schiphol*. Delft University of Technology, 2013.

[16] International Civil Aviation Organization. *Flight Procedures Doc 8168 OPS/611*. Aircraft Operations. Volume I: Flight Procedures, 2006.

[17] Kim et al. *Airport Cooperative Research*. Program, Tech. Rep., 2013.

[18] Schiphol Group. *Gebruiksprognose 2014*. 2013.

[19] Schiphol Group. *Gebruiksprognose 2016*. Schiphol Group, 2015.

[20] BAS. *Bijzonder Baangebruik*. `https://www.bezoekbas.nl`. 2015.

[21] ICAO. *Procedures for Air Navigation Services - Air Traffic Management (PANS-ATM, Doc 4444)*. International Civil Aviation Organization, 2007.

[22] LVNL. *Runway Incursion Alerting System Schiphol (RIASS)*. `http://www.lvnl.nl/overons/veiligheid/runway-incursion-alerting-system-schiphol-riass.html`. 2015.

[23] Ashford and Wright. *Airport Engineering*. Wiley, 1992.

[24] Idris et al. *Observations of Departure Pocesses at Logan Airport to Suport the Development of Departure Planning Tools*. The 2nd USA Europe Air Traffic Management RD Seminar Orlando USA, 1998.

[25] Idris et al. *Identification of Flow Constraint and Control Points in Departure Operations at Airport Systems*. AIAA Guidance Navigation, Control Conference, and Exhibit Boston USA, 1998.

[26] M. Janic. *Expansion of Airport Capacity: Case of London Heathrow Airport*. Transportation Research Records, 1888, 2004.

[27] Odoni. *Airfield Capacity*. Massachusetts Institute of Technology, 2002.

[28] Hockaday and Kanafani. *Developments in Airport Capacity Analysis*. Transportation Research Vol. 8 pp 171-180, 1974.

[29] M. Janic. *Airport Analysis, Planning and Design: Demand, Capacity and Congestion*. Nova Science Publishers, 2009.

[30] Federal Aviation Administration. *Airport Capacity and Delay*. 1983.

[31] Gilbo. *Airport Capacity: Representation, Estimation, Optimization*. IEEE Transactions on Control Systems Technology Vol. 1, 1993.

[32] Paul Roling. *Lecture 3 - Airside Capacity*. AE4446 Airport Design, Operations, Air Transport, and Operations , Delft University of Technology, 2015.

[33] M. Janic. *Modelling the capacity of closely-spaced parallel runways using innovative approach procedures*. Transportation Research Part C, 2008.

[34] Transport Research Board. *Airport Cooperative Research Program Report 79*. `http://onlinepubs.trb.org/onlinepubs/acrp/acrp_rpt_079.pdf`. 2012.

[35] LVNL. *Seperation of Aircraft*. `http://www.lvnl.nl/en/about-us/safety/separation-of-aircraft.html`. 2015.

[36] Federal Aviation Administration. *Aircraft Wake Turbulence*. Advisory Circular, 2014.

[37] EUROCONTROL. *Wake Vortex*. `http://www.eurocontrol.int/articles/wake-vortex`. 2015.

[38] Veerbeek and Brouwer. *Noise measurement analysis during a noise abatement departure procedure trial*. National Aerospace Laboratory NLR, 2012.

[39] Visser and Wijnen. *Optimization of Noise Abatement Departure Trajectories*. Journal of Aircraft 38, 2011.

[40] Chandrasekar and Hwang. *Algorithm for Optimal Arrival and Departure Sequencing and Runway Assignment*. American Institute of Aeronautics and Astronautics Inc, 2014.

[41] Ed Gordijn. *Berekening geluidsbelasting Schiphol en de invloed van het weer*. `http://www.knmi.nl/klimaatmaatwerk/meteo_geluid/Gordijn.pdf`. 2009.

[42] Paul Roling. *Airport surface traffic planning optimization: a case study of Amsterdam Airport Schiphol*. American Institute of Aeronautics and Astronautics Inc, 2009.

[43] Scott. *Stock Illustration and Design*. `http://www.norebbo.com`. 2016.

[44] Harshad Khadilkar and Hamsa Balakrishnan. *Estimation of Aircraft Taxi-out Fuel Burn using Flight Data Recorder Archives*. Massachusetts Institute of Technology, 2011.

[45] Prof. dr. D.G. Simons. *Introduction to Aircraft Noise*. Delft University of Technology, 2015.

[46] International Organization for Standardization. *ISO 226:2003 revision*. International Organization for Standardization, 2003.

[47] European Civil Aviation Conference. *Report on Standard Method of Computing Noise Contours around Civil Airports*. International Civil Aviation Organization, 2015.

[48] Federal Aviation Administration. *Integrated Noise Model (INM) Version 7.0 Technical Manual*. U.S. Department of Transportation, 2008.

[49] International Civil Aviation Organization. *ICAO Engine Exhaust Emissions Databank*. ICAO, Doc 9646- AN/943., 1995.

[50] John Wang. *Encyclopedia of Business Analytics and Optimization*. Montclair State University, USA, 2014.

[51] Katta G. Murty. *Operations Research and Management Science Handbook*. Taylor and Francis Group, 2008.

[52] Centraal Bureau voor Statistiek. *Regionale kerncijfers Nederland*. `http://statline.cbs.nl/StatWeb/publication/?VW=T&DM=SLNL&PA=70072ned&D1=0-118&D2=0,12&D3=14-15&HD=100914-1525&HDR=T&STB=G1,G2`. 2015.

[53] Branca Fierro and Spletzer. *On-line Optimization-based Coordination of Multiple Unmanned Vehicles*. IEEE Int. Conf. on Networking, Sensing and Control, Tucson, Arizona, 2005.

[54] H. Mausser. *Normalization and Other Topics in MultiObjective Optimization*. Proceedings of the Fields–MITACS Industrial Problems Workshop, 2006.

[55] Wilfried Jakob and Christian Blume. *Pareto Optimization or Cascaded Weighted Sum: A Comparison of Concepts*. MDPI - Open Acces algorithms, 2014.

[56] Smith de Araujo Poldi. *A Genetic Algorithm for the One-Dimensional Cutting Stock Problem with Setups*. Pesquisa Operational. vol.34 no.2, 2014.

[57] Casper Flights. *Vliegverkeer InZicht*. `http://inzicht.bezoekbas.nl`. 2016.

[58] International Civil Aviation Organization. *Procedure for Air Navigation Services*. ANS-OPS Doc 8168-OPS/611, 2006.

[59] WeatherSpark. *Average Weather for Amsterdam*. `https://weatherspark.com/averages/28802/Amsterdam-Noord-Holland-The-Netherlands`. 2016.

[60] Inspectie Leefomgeving en Transport. *Handhavingsrapportage Schiphol 1 november 2014 - 1 mei 2015*. Ministerie van Infrastructuur en Milieu, 2015.